THE
PHYSICAL REVIEW
A Journal of Experimental and Theoretical Physics Established by E. L. Nichols in 1893
VOL. 58, No. 1 JULY 1, 1940 SECOND SERIES

Radioactive Products from Gases Produced in Uranium Fission*

G. N. GLASOE, *Columbia University, New York, New York*
J. STEIGMAN, *College of the City of New York, New York, New York*
Pupin Physics Laboratories, Columbia University
(Received May 13, 1940)

Some radioactive products from the gases produced in the fission of uranium by slow neutrons have been studied as to their chemical identity and characteristic half-life periods. Two Rb activities have been observed, one of which decays with a period of 15.4±0.2 minutes into an active Sr with a half-life of 51±2 days; the other decays with a period of 17.8±0.2 minutes into an apparently inactive end product. The parent of the 15.4-minute Rb is a gas with a half-life of a few minutes whereas the other Rb arises from the decay of a 175±10-minute Kr. Absorption in Al indicates the maximum β-particle energy for these active products to be 3.8 Mev for the 15.4-minute Rb and 4.6 Mev for the 17.8-minute Rb. In a similar manner, a Cs has been observed which decays with a 32±0.5-minute period into a Ba which is inactive or of very long or short period with no evidence of the 300-hour product reported by Hahn and Strassmann. Data have been obtained which indicate that this long period Ba arises from the decay of a product of a very short period gas. This 32-minute Cs results from the decay of a Xe with a half-life of 17±1 minutes. Absorption in Al indicates a maximum β-particle energy of 2.6 Mev for this Cs activity.

INTRODUCTION

INVESTIGATIONS by Hahn and Strassmann and by Heyn, Aten and Bakker on the identification of the elements resulting from the slow neutron fission of uranium have resulted in the assignment of some of the observed radioactive periods to isotopes of rubidium and caesium. The latter were presumed to result from the β-disintegration of radioactive krypton and xenon. The present investigation was undertaken to determine the periods of these active gases and to establish genetic relationships between them and their products. In a preliminary report[1] it was indicated that the decay of a short period gas resulted in an active product with a half-life of about 18 minutes. This was attributed to the Rb of the same period reported by others.[2] Further work indicated, however, that an active Rb with approximately the same period could be obtained under conditions which pointed to a gas of much longer half-life as the parent substance. This report deals with the differentiation of these Rb activities and with a study of the 32-minute Cs previously reported.[2]

EXPERIMENTAL PROCEDURE

A 2.5-liter saturated aqueous solution of uranium nitrate, backed with paraffin, was irradiated with neutrons produced by protons on Be in the cyclotron. The radioactive gases resulting from the uranium fission were removed from the solution with a stream of air broken up into

* Publication assisted by the Ernest Kempton Adams Fund for Physical Research of Columbia University.
[1] G. N. Glasoe and J. Steigman, Phys. Rev. **55**, 982 (1939).
[2] O. Hahn and F. Strassmann, Naturwiss. **27**, 529 (1939); F. A. Heyn, A. H. Aten and C. J. Bakker, Nature **143**, 516 (1939).

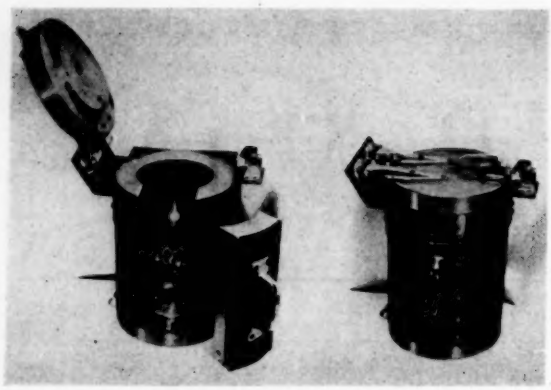

FIG. 1. Lead shield for Geiger-Müller counter.

small bubbles by means of a sintered glass disk or a perforated tube. In some instances the gases were collected after the irradiation. In other instances they were removed continuously during the neutron bombardment. This variation in procedure facilitated the differentiation of the products arising from the short period gases and those resulting from the decay of long period gases.

The products of the radioactive gases were concentrated and collected by a method first used by Rutherford[3] for obtaining the decay products of thoron. The procedure involves the collection of the positively charged recoil ions resulting from the disintegration of the active gas. To obtain the products of the long-lived gases the latter were collected in a metal vessel by water displacement and the recoil ions concentrated on a platinum wire made about 1000 volts negative with respect to the vessel. High activity of the products of the short period gases was obtained most satisfactorily by passing a continuous air stream through the solution, and into a metal cylinder containing the platinum wire, during the irradiation. Variation of the rate of the air flow provided a means of enhancing the activity of one product relative to others provided there was a sufficient difference between the periods of the active gases.

The chemical separation and identification of the decay products collected in the above manner was performed after the removal of the active deposit by immersing the platinum wire in hot water or some solution appropriate to the particular procedure. The chemical separations were carried out by following the standard method of adding inactive "carrier" salts of the elements in question. The active material was obtained either in the form of a precipitate or a residue resulting from the evaporation of a filtrate. After drying, the precipitate or residue was mounted on filter paper with cellophane tape and placed inside a brass tube which was then slipped over a Geiger-Müller counter. The counter tube[4] was made with a thin glass wall the inner surface of which was coated with chemically deposited silver to serve as the cathode. The GM counter was mounted in a thick lead shield as shown in Fig. 1 and connected to a scaling circuit with hard tubes, arranged so that scaling rates of 2, 4, 8, 16, or 32 could be selected depending on the activity of the material. Such a counter and associated circuit has proven to be extremely stable, with negligible sensitivity variations of long or short period, over many months. The support for the brass tube holding the active material was constructed so as to insure accurate reproducibility of the position of the active material

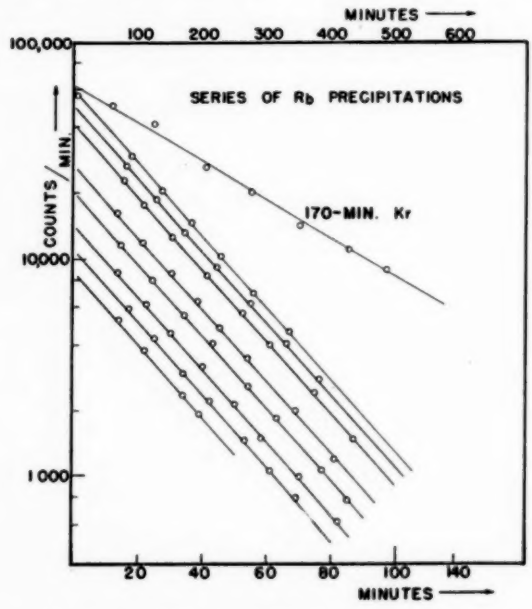

FIG. 2. A series of Rb separations made from a sample of active Kr produced in uranium fission. The period of the gas is indicated by the decay of the initial activities of the Rb samples.

[3] E. Rutherford, Phil. Mag. **49**, 161 (1900).

[4] The counter tube was made by Eck and Krebs, New York, New York. After pumping and baking the tube was filled with 8.5 cm of argon and 1 cm of alcohol.

relative to the counter tube. This precaution was particularly necessary in making absorption measurements.

Rb—17.8-Minute Half-Life

This isotope was one of the first products identified by Hahn and Strassmann,[2] and observed by Heyn, Aten and Bakker[2] to result from the decay of a gas produced in uranium fission. A Kr with a 3-hour period was observed by Langsdorf[5] and was assigned by Hahn and Strassmann as the parent of the Rb. The experiments described here were performed to determine this Kr period and to establish the genetic relationship between these two products. The procedure was to collect the active gas from the uranium solution a number of hours after the irradiation in order to eliminate the products arising from the shorter period gases. The waiting time was varied from about 3 hours to 12 hours with the result that the shorter time proved to be sufficient to obtain this active Rb without contamination, as determined by a comparison of the decay curves. The recoils from the disintegrating gas were collected for a definite length of time (15 minutes) on the platinum wire, and then washed off in a hot solution of saturated sodium bitartrate to which was added inactive RbCl. The rubidium bitartrate was precipitated by cooling the solution in ice. After filtering and drying the precipitate, the activity was followed for about four half-lives and extrapolated back to zero time (the time at which the wire was removed from the collection vessel). With the same sample of active gas the above procedure was repeated at 70-minute intervals, identical operations being performed in all respects. The series of decay curves obtained in this manner is shown in Fig. 2. The decay of the extrapolated initial activities in a number of such experiments indicates a half-life of 175 ± 10 minutes, which is interpreted as the period of the Kr giving rise to this Rb activity.

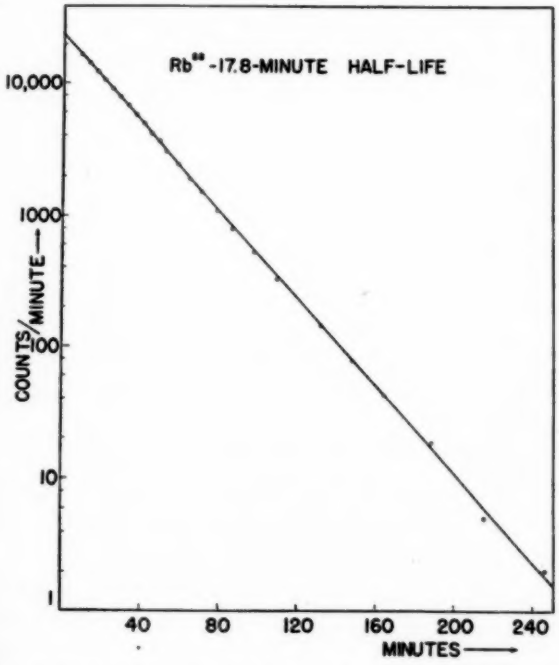

Fig. 3. Decay curve for the Rb product of the 175-minute Kr.

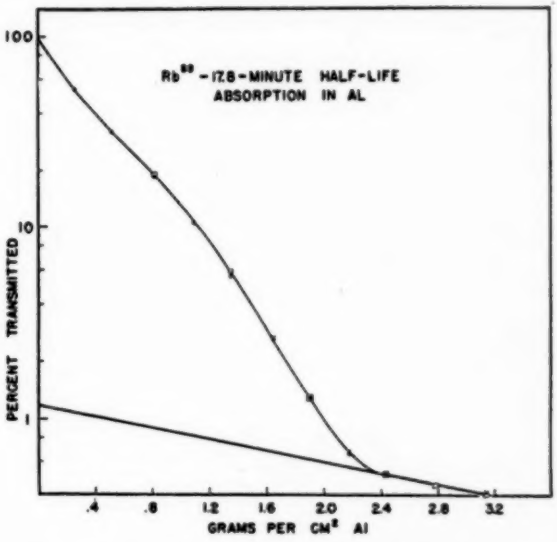

Fig. 4. Absorption in Al for the 17.8-minute Rb^{88}.

A number of experiments were performed to determine whether this Rb decays into an active Sr. A typical curve is shown, in Fig. 3, which is linear over 14 half-lives with the conclusion that the decay product is stable or that it has a period less than 5 minutes or greater than a year if the activity could be observed with the counter used. The half-life of this Rb isotope is found to be 17.8 ± 0.2 minutes. This activity has been assigned to the isotope Rb^{88} by Hahn and Strassmann on the basis of their conclusion that the Sr product is stable.

[5] A. Langsdorf, Jr., Phys. Rev. **56**, 205 (1939).

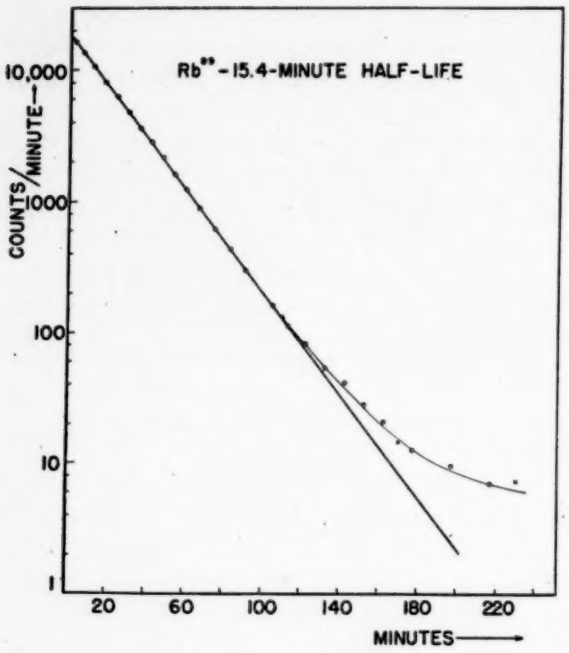

FIG. 5. Decay curve of Rb^{89} obtained from a short period Kr. The points marked with crosses were calculated for a 15.4-minute activity decaying into a 51-day product.

The absorption in aluminum of the β-particles from this activity was obtained by using cylindrical absorbers around the counter-tube with the active material mounted as indicated above under experimental procedure. An absorption curve is shown, in Fig. 4, in which the break is interpreted as giving the maximum range of the β-particles in Al. The range corrected for the absorption of the counter-tube wall is found to be 2.36 g/cm^2. According to Feather's[6] equation, $R=0.543E-0.160$, the maximum β-particle energy is 4.6 Mev. The fact that this energy appears somewhat high for such an activity might possibly suggest a very short period Sr as the decay product. The correction for the absorption of the wall of the counter was obtained by using a RaE source with the same absorbers and observing the shift of the absorption curve from that given by Feather.[6] This correction amounted to 0.06 g/cm^2.

Rb—15.4 Minute Half-Life

The high intensity of Rb activity resulting from a short irradiation (1 to 10 minutes) appeared inconsistent with that to be expected for the decay product of a long period gas. From absorption measurements it was apparent that there were two active Rb isotopes of approximately the same half-life. By applying the method of collecting the recoils during an irradiation, it was possible to obtain a Rb activity arising from a short period gas with inappreciable contamination due to the decay of the 3-hour Kr. This procedure, however, resulted in the complicating presence of intense activities due to Cs, Ba and Sr which had to be removed before the period of the Rb could be accurately determined. Because of the incompleteness of the separation of Cs from Rb by the known chemical methods (e.g. chloroantimonate, silicotungstate, etc.) it became necessary to adopt the following procedure; Rb was precipitated as the bitartrate in the presence of Cs, dissolved and reprecipitated five times, with additional inactive CsCl added each time. The fifth precipitate was dissolved in hot water to which was added inactive Ba and Sr chlorides. After two successive carbonate or sulphate precipitations to remove the Ba and Sr, the final filtrate was evaporated to dryness for the Rb activity. A typical decay curve for the material obtained in this manner is shown in Fig. 5 with the indicated half-life of 15.4±0.2 minutes: The active Sr into which this Rb decays was obtained under similar irradiation and collection conditions and was found to have a period of 51±2 days. It may

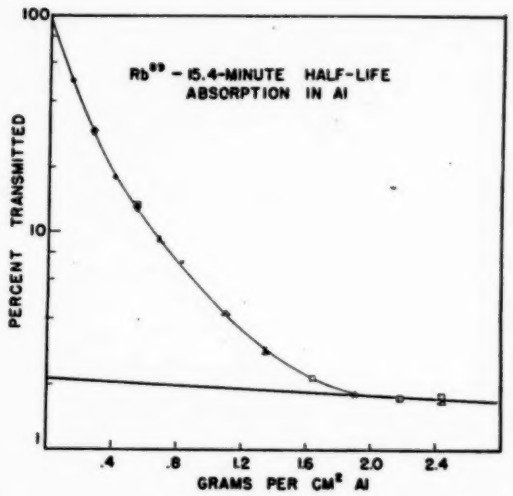

FIG. 6. Absorption in Al for the 15.4-minute Rb^{89} activity.

[6] N. Feather, Proc. Camb. Phil. Soc. **34**, 599 (1938).

be assumed that this is the same Sr isotope reported by Stewart[7] and by DuBridge and Marshall[8] as obtained from Sr(d, p) and assigned by them to Sr^{89}. The points marked with crosses in Fig. 5 were calculated on the basis of a 15.4-minute activity decaying into a 51-day product. From the manner in which this Rb activity is obtained it is estimated that the Kr parent must have a period of the order of one to five minutes.

An absorption curve for the β-particles from this Rb is shown in Fig. 6. The break in this curve indicates a corrected range in Al of 1.92 g/cm² corresponding to a maximum energy of 3.8 Mev. Due to the short period of this product and the loss of activity in the chemical procedure it was not possible to obtain a complete absorption curve on a single sample. The agreement obtained by using a number of samples of the Rb at different times is indicated by the multiple points in the case of several of the absorbers used. It might be remarked that in these absorption measurements several different sizes of the brass tube were employed to hold the active sample, with no marked effect being observed in the percent absorption due to the changed geometry between the counter and the sample. The counter tube was 2 cm in diameter and the brass tubes varied from 2.8 cm diameter to 4.8 cm diameter.

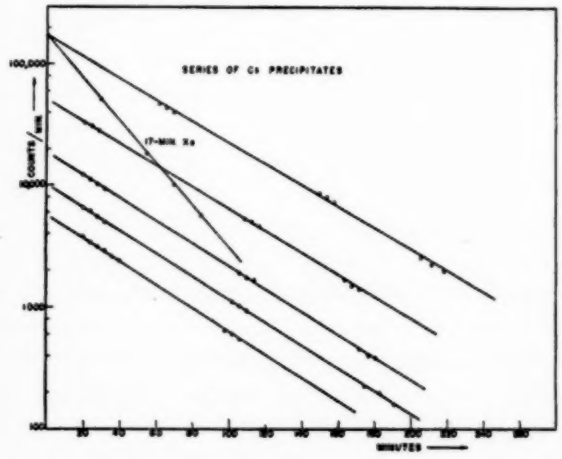

FIG. 7. A series of Cs separations made from a sample of active Xe produced in uranium fission. The period of the gas is indicated by the decay of the initial activities of the Cs samples.

[7] D. W. Stewart, Phys. Rev. **56**, 629 (1939).
[8] L. A. DuBridge and J. Marshall, Phys. Rev. **56**, 706 (1939); **57**, 348 (1939).

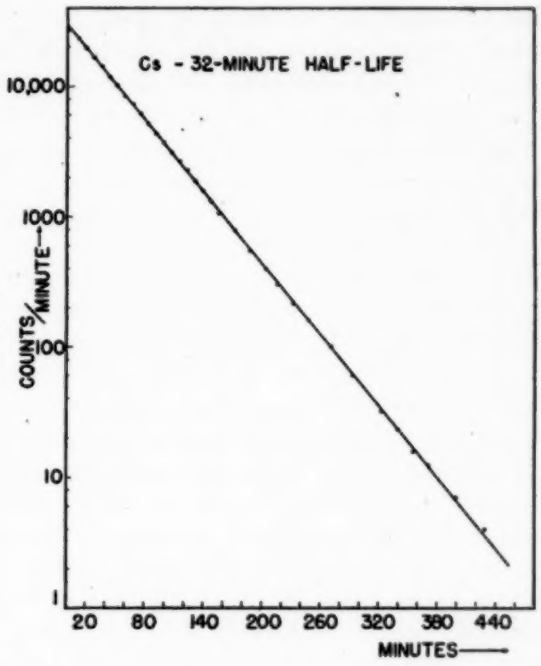

FIG. 8. Decay curve for the Cs product of the 17-minute Xe.

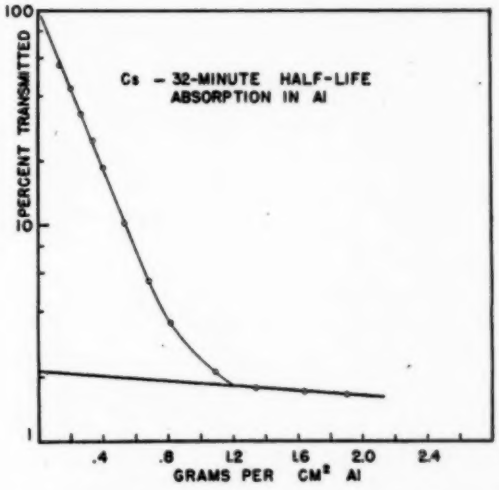

FIG. 9. Absorption in Al for the 32-minute Cs activity.

Cs—32-Minute Half-Life

A Cs activity with a period of 30 to 33 minutes has been reported by Hahn and Strassmann and by Heyn, Aten and Bakker[2] and was studied in these experiments to determine the period of the parent gas. The procedure followed was in general the same as that employed to determine the half-life of the parent gas for the 17.8-minute Rb. In this case, however, the active gas was collected five minutes after the irradiation, in

order to avoid contamination by products from the very short period gases. The result is shown in Fig. 7. The extrapolated initial activities were plotted to obtain the decay curve of the parent Xe, showing a half-life of 17 ± 1 minutes. Hahn and Strassmann estimated this period to be about 15 minutes from the rate of gas flow used in their experiments.

It was less difficult to obtain this Cs activity without contamination and of several chemical procedures tried the precipitation with silicotungstic acid from hot, 6*N* HCl solution was found the simplest and most rapid. A great many decay curves were taken for this activity with the result that there was no evidence for the formation of a 300 hour Ba as was reported by Hahn and Strassmann.[2,9] As shown in Fig. 8, the decay is linear over 14 half-lives and an activity ratio of 10,000. A long period Ba was observed, however, which decays into a La of about 40-hour half-life, by using the method of collecting recoils during an irradiation and with a very rapid air stream. This is probably the product reported by Hahn and Strassmann as arising from the 32-minute Cs. Measurements of the absorption in Al for this Ba activity indicated approximately the same absorption as observed for the Sr resulting from the decay of the 15.4-minute Rb. It is thus evident that this Ba activity should be observed by the departure of the Cs decay curve from linearity after about 9 half-lives. The conclusion to be drawn from these results is, therefore, that the 32-minute Cs decays into an inactive Ba or one whose period is less than 5 minutes or greater than a year.

An Al absorption curve for this Cs activity is shown in Fig. 9, with the range indicated to be 1.28 g/cm². This corresponds to a maximum energy for the β-particles of 2.6 Mev.

Conclusion

The results of these experiments may be summarized by the following genetic series for some of the radioactive products arising from gases produced in the slow neutron fission of uranium.

$$\mathrm{Kr}^{(88)} \xrightarrow{3\ \mathrm{hr.}} \mathrm{Rb}^{(88)} \xrightarrow[4.6\ \mathrm{Mev}]{17.8\ \mathrm{min.}} \mathrm{Sr}^{(88)}\ \text{probably stable,}$$

$$\mathrm{Kr}^{(89)} \xrightarrow{1\text{–}5\ \mathrm{min.}} \mathrm{Rb}^{(89)} \xrightarrow[3.8\ \mathrm{Mev}]{15.4\ \mathrm{min.}} \mathrm{Sr}^{(89)} \xrightarrow{51\ \mathrm{days}} \mathrm{Y}^{(89)}(?),$$

$$\mathrm{Xe} \xrightarrow{17\ \mathrm{min.}} \mathrm{Cs} \xrightarrow[2.6\ \mathrm{Mev}]{32\ \mathrm{min.}} \mathrm{Ba}\ \text{probably stable,}$$

$$\mathrm{Xe} \xrightarrow{\text{very short}} \mathrm{Cs} \xrightarrow{\text{very short}} \mathrm{Ba} \xrightarrow{300\ \mathrm{hr.}} \mathrm{La} \xrightarrow{40\ \mathrm{hr.}} \mathrm{Ce}(?).$$

Acknowledgments

The authors wish to express their appreciation to Dr. E. T. Booth, Professor J. R. Dunning and Dr. A. V. Grosse for many helpful suggestions. They also wish to thank Mr. H. Glassford and Mr. F. Simons for the able assistance rendered by them during the course of the experiments. Acknowledgment is made to the U. S. Work Projects Administration of New York City for assistance rendered under project number 24 and to the Research Corporation for financial aid.

[9] O. Hahn and F. Strassmann, Naturwiss. **28**, 61 (1940).

Radioactive Isotopes of Sr, Y and Zr

L. A. DuBridge and John Marshall
University of Rochester, Rochester, New York

(Received April 22, 1940)

Radioactive isotopes formed by bombardment of Rb, Sr and Y by protons, deuterons and neutrons are reported. The following are the periods and assignments: 2.75-hr. (Sr^{87*}, e^-, γ); 70-min. (Sr^{85}, e^-, γ); 66-day (Sr^{85}, K, γ); 80-hr. (Y^{87}, K); 14-hr. (Y^{87}, e^-, γ); 105-day (Y^{85}, K, γ); 4.5-min. (Zr^{89}, γ); 78-hr. (Zr^{89}, β^+). (In each case e^- means conversion electrons, not nuclear β-rays.) The electron spectrum of the 2.75-hr. Sr^{87*} shows a single line at 360 kev and this period is shown to grow from the 80-hr. Y^{87}, but not from the 14-hr. isomer.

THE bombardment of Rb, Sr and Y targets by 6.7-Mev protons, 4.5-Mev deuterons and slow and fast neutrons produces at least twelve radioactive periods. We have studied ten of these, many of which have also been studied by Stewart, Lawson and Cork[1] and by Stewart.[2] Our results show several periods not reported by them and an important change of assignment of one Sr period.[3] The stable isotopes of Sr, Y and Zr together with the probable assignments of the radioactive periods are shown in Fig. 1.[4]

The targets were usually in the form of chloride salts or in the case of Sr, the pure element. $SrCl_2$ could also be satisfactorily bombarded when fused onto a stainless steel plate contained in an evacuated cup attached to the exit window of the cyclotron. Beam currents to the cup were usually of the order of 1 or 2μa of protons or deuterons. In some cases targets were bombarded on an internal probe where the beam current is about 20μa. Activities were followed with a Freon-filled ionization chamber and d.c. amplifier.[5] A magnetic cloud chamber and a β-ray spectrograph were used to study β-ray and γ-ray spectra while a Geiger-Müller counter with a scale-of-eight was sometimes used for absorption measurements.

To separate Sr chemically from Rb the RbCl was dissolved in water and Na_2CO_3 was added in excess. There was no attempt made to recover the rubidium. Yttrium was separated from Sr either as the hydroxide by the addition of NH_4OH or, in the later experiments, with 8-hydroxyquinoline (oxine) by using a technique originally developed for the separation of Al from alkaline earths.[6] The method is as follows: 0.17 g of oxine is dissolved in 12.5 cm^3 of acetone and the solution is diluted to about 50 cm^3 with water. About 5 mg of YCl_3 is added as a carrier to the bombarded Sr which is dissolved in 15 cm^3 of water. 7.5 cm^3 of the oxine solution is added to this solution and NH_4OH is added by drops until the ammonia odor is noticeable. This solution is warmed on a water bath to coagulate the precipitate and is filtered out in a Gooch crucible containing filter paper. This method has the advantage that it gives more nearly complete separations than the hydroxide method and also gives a crystalline precipitate which is more rapidly filterable.

Zirconium was separated from bombarded Y as the iodate in nitric acid solution, with a trace of $Zr(NO_3)_4$ added as carrier.

In all cases the filtered precipitate was left on a disk of filter paper 2 cm in diameter and

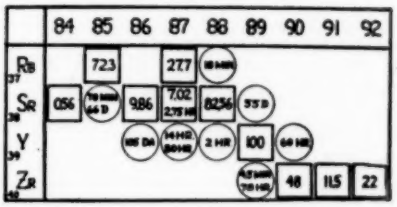

FIG. 1. Stable isotopes with relative abundance and probable assignment of radioactive periods.

[1] Stewart, Lawson and Cork, Phys. Rev. **52**, 901 (1937).
[2] D. W. Stewart, Phys. Rev. **56**, 629 (1939).
[3] L. A. DuBridge and J. Marshall, Phys. Rev. **56**, 706 (1939); **57**, 348A (1940).
[4] Our results, together with other unpublished data from this laboratory, were transmitted to Dr. G. T. Seaborg for inclusion in the table by J. J. Livingood and G. T. Seaborg, Rev. Mod. Phys. **12**, 30 (1940).
[5] S. W. Barnes, Rev. Sci. Inst. **10**, 1 (1939).
[6] F. L. Hahn and K. Vieweg, Zeits. f. anal. Chemie **71**, 122 (1927).

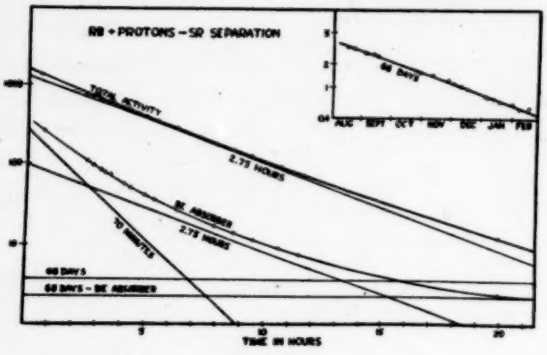

FIG. 2. Decay of Sr from Rb+H[1]. Upper curve, no absorbers, lower curve, 2 mm of Be.

held in place with Scotch tape, which provided a convenient form for the measurement of radioactivity.

1. RADIOACTIVE ISOTOPES OF Sr

Bombardment of Rb by protons produces a strong activity in the Sr fraction whose decay curve is shown in Fig. 2. The chief component is a period of 2.75±0.1 hr. If the bombarded Rb sample is covered with a Be plate 2 mm thick the 2.75-hr. period is greatly reduced in intensity while a period of 70 minutes and one of 66 days become evident (see lower curve). The 70-min. period is almost completely masked without the Be absorber. This Be plate has an absorbing power equal to about 90 mils of Al for β-rays but has negligible absorption for x-rays and γ-rays. Apparently therefore very few charged particles are associated with these 70-min. and 66-day periods, the radiation consisting largely of x-rays and γ-rays. The 2.75-hr. activity consists largely of negative electrons.

There are only two stable isotopes of Rb, of masses 85 and 87, the latter being naturally β-active with a period of 10^{10} years. Rb(p,n) reactions therefore would yield only Sr^{85} and Sr^{87}. Since Sr^{87} is stable it would appear necessary at first sight to assign all three periods to Sr^{85}. However it will be shown below that the 2.75-hr. period must be assigned to a metastable state of Sr^{87}. The 70-min. and 66-day periods are therefore assigned to Sr^{85}. Since Rb^{84} does not exist and Sr^{84} is very rare these Sr^{85} periods are not produced in observable amounts by deuteron or neutron bombardment of Rb or Sr.

Sr^{85} (70 min. and 66 day)

As shown in Fig. 2 the activity of these two periods is only slightly reduced by covering the sample with Be. Since no positrons can be observed and since Y^{85} is not stable it is concluded that this isotope decays by K capture to Rb^{85}. The γ-ray spectrum of the short period can not easily be obtained because of the presence of the strong 2.75-hr. period. However in β-ray spectrograph plates taken to get the electron spectrum of this latter period, a faint electron line is observed at 160 kev. (Fig. 3.) Since this line does not appear when the 2.75-hr. period is formed in other ways it can probably be associated with the 70-min. Sr^{85}. It seems probable then that the 70-min. isomer decays to the 66-day isomer with the emission of a partly converted γ-ray of about 170 kev (the K-ionization energy for Sr being about 10 kev).

The decay of the 66-day isomer by K capture to Rb^{85} is accompanied by a γ-ray whose absorption coefficient in lead indicates an energy of about 0.8 Mev.

Sr^{87*} (2.75 hr.)

As indicated in an earlier communication[3] this period is the same as the 3.0-hr. period reported by Stewart Lawson and Cork[1] and by Stewart.[2] It was formed in their experiments by Sr+d and Sr+n and assigned to Sr^{89}, isomeric with the 55-day period. The formation of this activity by protons on Rb eliminates this possible assignment. Its formation by Sr+d and Sr+n would allow its assignment to Sr isotopes 85 (weak), and 87 as well as 89. Since Sr^{87} is stable it would be natural to make the assignment to Sr^{85}. However it is found that the same period is also formed by Sr+p. The only way in which a Sr activity could be formed from Sr+p is either by a $p-p$ reaction leading to a metastable state of a stable isotope, or by decay of an yttrium activity formed during the bombardment. If the latter is formed by a $p-n$ process the decay product must also be an isomeric state of a stable nucleus thus eliminating assignment to Sr^{85}. As will be seen below the 2.75-hr. period does indeed grow from an 80-hr. Y activity formed both by Sr+p and Sr+d, an activity which can be independently assigned to Y^{87}.

This makes the assignment of the 2.75-hr. period to a metastable state of Sr^{87} quite certain.

In the $Sr+n$ bombardments an activity assigned to Sr^{87*} could be formed either by the $n-\gamma$ or the $n-n$ excitation process. We have mounted a pure Sr sample in a Cd box immediately behind a Be probe within the cyclotron chamber. Since it was there exposed to a high intensity of medium fast neutrons and but few slow neutrons the $n-\gamma$ process would probably be unimportant. On the other hand, the neutrons formed by $Be+p$ are not fast enough to cause an $n-2n$ process. The 2.75-hr. period was produced under these conditions with fair intensity, suggesting the $n-n$ process. By mounting an In sample of similar dimensions adjacent to the Sr sample an estimate of the relative yields of the two reactions $Sr^{87}(n,n)Sr^{87*}$ and $In^{115}(n,n)In^{115*}$ (4.1 hr.)[7] could be made. The yield for the latter process (calculated for infinite bombardment of the pure isotope) is about 2 to 4 times as great as for the former. The actual ratio may be greater than this since the $n-\gamma$ process may contribute in the first case (Sr^{86} being fairly abundant) but not in the second (since In^{114} is not stable). This difference in yields may be connected with the fact that the spin of the ground state of In^{115} is 9/2 and of Sr^{87} is $\frac{1}{2}$. Hence the spin of the isomeric In^{115} is probably $\frac{1}{2}$ and of Sr^{87*} probably 9/2.

The electron and γ-ray spectrum of this 2.75-hr. period is of particular interest. If it is assigned to either Sr^{85} or Sr^{87*} the decay must be either by positron emission or K capture since the corresponding Y isotopes are not stable. The cloud-chamber measurements of Stewart *et al.*[1,2] showed an apparently continuous

FIG. 3. (A) Electron spectrum of Sr from $Rb+H^1$. (70 min., 2.75 hr.) (B) Spectrum of Sr bombarded with protons. (80-hr. period).

[7] Goldhaber, Hill and Szilard, Phys. Rev. **55**, 47 (1939).

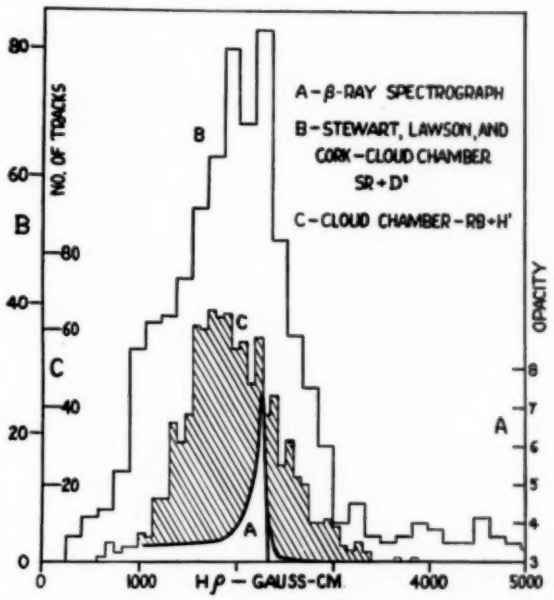

FIG. 4. Comparison of cloud chamber and β-ray spectrograph measurements of the electron spectrum of 2.75-hr. Sr.

spectrum of low energy negative electrons. This was indeed a strong reason for assigning the period to Sr^{89} where it could decay by electron emission to stable Y^{89}. Our cloud-chamber histogram (C) is compared to theirs (B) in Fig. 4. For clarity the two are drawn to different scales. The high energy tracks above $H\rho$ 3300 in curve B are from the 55-day Sr^{89} also present in their specimen, but not in ours. Stewart, Lawson and Cork found this histogram to fit a K−U plot.

However, when a thin specimen showing this activity is placed in the β-ray spectrograph a spectrum consisting only of a single line at $H\rho$ 2360 is obtained. Two such plates are shown in Fig. 3, one taken with a $Rb+p$ specimen and the other from $Sr+p$. Exactly similar plates were obtained from a $Sr+d$ bombardment. The microphotometer curve for one of these plates is plotted as A in Fig. 4, showing a much narrower peak than the cloud-chamber data. It is evident that for electrons of this low energy (360 kev) the scattering of the particles in the cloud-chamber gas (plus self-absorption in the specimen if thick) broadens out the histogram to such an extent as to conceal the homogeneity of the electron spectrum.

The results with the β-ray spectrograph make it certain that the observed electrons are con-

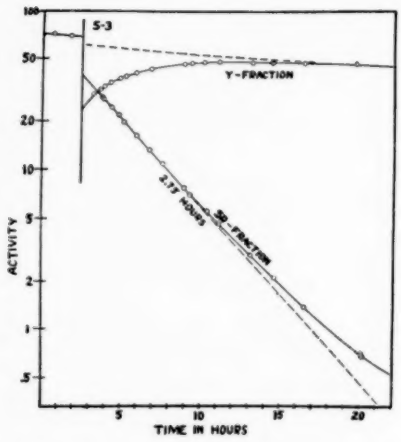

FIG. 5. Typical curves of the growth and decay of activity in Y and Sr fractions from previous Y separation from Sr+H[1].

version electrons accompanying a transition gamma-ray and are not nuclear β-rays. The final necessity of assignment of this period to Sr^{89} is removed and the assignment to Sr^{87*} becomes unambiguous.

That Sr^{87*} decays by isomeric transition to the stable state Sr^{87} rather than by K capture to Rb^{87} is almost certain since Rb^{87} is itself naturally β-active decaying to Sr^{87}. This latter decay must always be to the ground state of Sr^{87} since the maximum β-ray energy is[8] only 130 kev and there is no evidence in the Rb^{87} spectrum of the Sr^{87*} electrons. Also we have been unsuccessful in separating active Sr from natural Rb.[3]

That the x-rays accompanying the Sr^{87*} transition are Sr rather than Rb K x-rays was shown roughly by absorption experiments in Se and Br. Thin evaporated layers of Se on Al foil and distilled layers of CBr_4 on Al were used as absorbers. The absorption coefficient in Br was of the same order of magnitude as in Se, whereas for Rb K x-rays it should have been several times smaller. The measurements are only rough because the only samples of the 2.7-hr. period strong enough for these tests were those formed by Rb(p,n) in which the Sr^{85} periods were also strong.

2. Radioactive Isotopes of Y

Bombardment of Sr with protons yields four periods in Y. A 2-hr. positron emitting period has been observed by Stewart, Lawson and Cork.[1] They assign it to Y^{88} formed by $Sr^{87}(d,n)$ and $Y^{89}(n,2n)$. We have evidence that it is also formed by $Sr^{88}(p,n)$, but have no good determination of the period because of the masking effect of Sr^{87*}.

In addition to the 2-hr. period we have observed three other periods produced by protons: 14 ± 2 hours, 80 ± 3 hours, and 105 ± 5 days. Since the 14-hr. and the 80-hr. period are also produced by the bombardment of Sr with deuterons (also observed by Stewart) they can be assigned only to Y^{87} or Y^{88}. Stewart, Lawson and Cork, however, found only the 2-hr. period as a result of the reaction $Y^{89}(n,2n)$. Therefore, we must assume that the 14-hr. and 80-hr. period are isomers of Y^{87}.

Beta-ray spectrograph measurements showed that the electrons which accompany the 80-hr. period have a line spectrum identical with that of the 2.7-hr. Sr, which period was then not yet definitely assigned. When an aged Y fraction from a Sr+p or Sr+d target is dissolved and Sr and Y separations again made, the Sr fraction decays with the 2.7-hr. period and the Y fraction activity grows with this period. A typical pair of curves is shown in Fig. 5. This shows that the 2.7-hr. period grows from the decay of the 80-hr. period confirming the assignment to Sr^{87*} and Y^{87}, respectively.

The decay curves for five such successive separations are shown in Fig. 6, correction being made for the loss (of about 10 percent) in each separation. The initial activities of the successive Sr fractions fall off with the 80-hr. period,

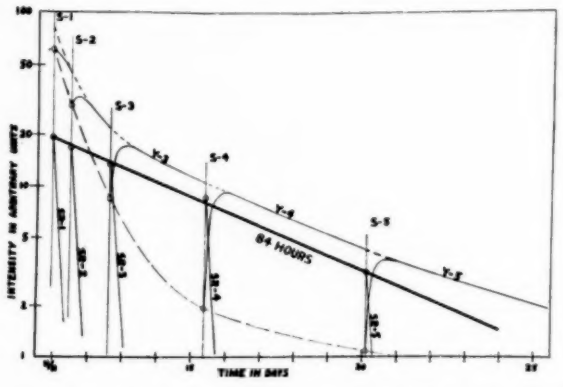

FIG. 6. Multiple separations from Sr+H[1]. Normalized at each separation to compensate for loss in chemical separation.

[8] W. F. Libby and D. D. Lee, Phys. Rev. **55**, 245 (1939).

showing that the isomeric 14-hr. period of Y^{87} does not decay to Sr^{87*}. Presumably this 14-hr. state decays to the 80-hr. state with gamma-ray emission.

Also the initial activities of the Y fractions decay along a curve which does not show any 80-hr. component, indicating that practically the entire activity of this period is assignable to the Sr^{87*} conversion electrons. When these electrons are filtered out with a Be plate there is, however, evidence for the Sr$-K$ x-rays which accompany the K-capture decay of Y^{87} to Sr^{87*}. We have detected no 80-hr. gamma-ray, however.

The 14-hr. isomeric transition in Y^{87} appears from absorption measurements (made immediately after separation) to be accompanied by a gamma-ray of about 500 kev and a few corresponding conversion electrons. Measurements of these are made difficult, however, by the rapid rise of the 2.7-hr. activity.

The 100-day period appears to decay by K-electron capture and the emission of a fairly high energy unconverted γ-ray. Absorption measurements of the γ-ray in Pb, Al, and Cu indicate a γ-ray of about 2 Mev, but absorption measurements at these energies are quite uncertain and the γ-ray may even be as low as 1 Mev in energy, or may be a mixture of two or more. The fact that the 100-day period is formed by protons on Sr, but not by deuterons makes the most probable assignment Y^{86}.

In one of the earlier multiple separations after deuteron bombardment of Sr we found a 15±2-day period in the Y fraction. We assigned it tentatively to Y^{85} since it was not observed as a product of proton bombardment. This separation was done by the hydroxide method. A later attempt to find this period was unsuccessful with the oxine method of separation, and hence was undoubtedly due to an impurity (P^{32}?).

TABLE I. *Characteristics of radioactive isotopes of* Sr, Y *and* Zr. *I.T.=isomeric transition, e^-=conversion electrons, β^+=positrons, K=K capture.*

PERIOD	EMITTED PARTICLE	ASSIGNMENT	FORMED BY	ENERGY (MEV)
2.75 ±0.1 hr.	e^-, γ I.T.	Sr^{87*}	Rb-p-n, Sr-d-p Sr-n-γ, Sr-n-n Sr-p-p(?), $Y^{87}+e_K$	e^-, 0.360
70 min.	I.T., e^-, γ	Sr^{85}	Rb-p-n	e^-, 0.160(?)
66 day	K, γ	Sr^{85}	Rb-p-n	γ, 0.8
80 hr.	K (to Sr^{87*})	Y^{87}	Sr-p-n, Sr-d-n	no γ(?)
14 hr.	I.T., e^-, γ	Y^{87}	Sr-p-n, Sr-d-n	e^-, γ, ~0.5
105 day	K, γ	Y^{88}	Sr-p-n	γ~2.0(?)
4.5 min.	I.T., γ	Zr^{89}	Y-p-n	
78 hr.	β^+	Zr^{89}	Y-p-n	β^+~1.0 no γ

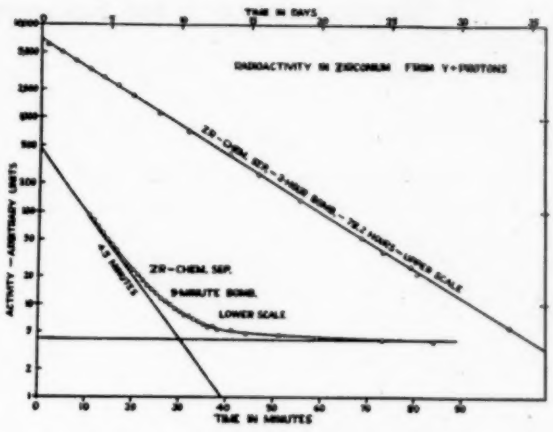

FIG. 7. Decay of Zr from Y+H[1].

3. Zr PERIODS

The bombardment of Y with protons produced two strong periods of 4.5 min. and 78±1 hour (see Fig. 7), which are chemically identified as Zr. The 4.5-min. period appears to be associated with an isomeric transition in Zr^{89}. This is shown by the cloud-chamber observation that many γ-rays are present while the 4.5-min. period is strong, but after this period has died out only positrons are observable. Range measurements in Al show these to have a maximum energy of about 1 Mev. There are no γ-rays associated with the 78-hr. period.

These two activities must be isomers of Zr^{89} because no other Zr isotope can be produced from Y by a $p-n$ reaction.

The results reported herein are summarized in Table I. The 55-day Sr^{89} and the 2-hr. Y^{88} are omitted since though we observed them we have nothing to add to the data of Stewart.[2]

The authors are indebted to many members of the laboratory for help with this work. Especially we wish to thank Mr. R. L. McCreary and Dr. G. E. Valley for assistance with the cloud chamber and the β-ray spectrograph, and Mr. Gerhard Dessauer for assistance with the chemical separations.

Transmutation of the Separated Isotopes of Neon by Deuterons

ERNEST POLLARD AND WILLIAM W. WATSON
Sloane Physics Laboratory, Yale University, New Haven, Connecticut

(Received May 15, 1940)

Under bombardment by 2.6-Mev deuterons, neon is observed to emit a large yield of protons which fall into at least four groups of energy change values 1.02, 2.15, 3.13, and 4.88 Mev. To assign these to the appropriate isotope, samples of neon enriched in Ne^{22} and Ne^{20} prepared by the thermal diffusion method were bombarded with the result that all groups are found to correspond to excited states of Ne^{21}. The reaction involved is $Ne^{20}(dp)Ne^{21}$. The maximum energy of the protons leads to the value 21.00017 for the mass of Ne^{21}. The bombarded gas was found to be radioactive and the presence of Ne^{23} due to $Ne^{22}(dp)Ne^{23}$ and Na^{21} due to $Ne^{20}(dn)Na^{21}$ was established. By absorption the beta-rays from Ne^{23} were found to consist of a single group of maximum energy 4.1 Mev which leads to a probable value of 23.0010 for the mass of Ne^{23}.

INTRODUCTION

APART from the discovery, by Snell,[1] of the formation of F^{18} from neon and of Na^{22} by Laslett,[2] the deuteron bombardment of neon has not been closely studied. In particular, no observations of proton groups have been made. Such observation is complicated by the fact that neon consists of three isotopes with percentage composition Ne^{20} 90 percent, Ne^{21} 0.27 percent, and Ne^{22} 9.73 percent. While the yield from Ne^{21} can be neglected in comparison with that from the two more abundant isotopes, there is no justification for assuming that Ne^{22} will not contribute appreciably to the protons observed, and therefore unless observations are made with some separation of the isotopes the groups observed cannot be assigned to the appropriate nucleus. Fortunately, the thermal diffusion coefficient of neon is relatively large so that separation by the thermal diffusion method is easy and gives large samples. Such samples have been made and bombarded in this work.

The Oppenheimer-Phillips reaction should give rise to Ne^{21}, Ne^{22}, and Ne^{23}, of which the last is unstable, decaying into Na^{23} with a half-life of 43 seconds.[3] The (d, n) type reaction yields Na^{21}, Na^{22}, both positron radioactive nuclei, and stable Na^{23}. The (d, α) reaction yields F^{18}, F^{19}, F^{20}, well-known nuclei. The work described here has been of two types: the first a direct study of the protons emitted in the Oppenheimer-Phillips reactions, and the second an observation of the induced radioactivity in the gas. The first part showed the existence of a considerable yield of protons, divided into several groups, all of which could be assigned to the formation of Ne^{21} in excited states. The protons due to the reaction $Ne^{22}(dp)Ne^{23}$ were masked by the more prolific yields from $Ne^{20}(dp)Ne^{21}$. The second part showed the formation of Ne^{23} and Na^{21}. The former emits an electron whose maximum energy was determined while the latter, already studied by Creutz, Fox, and Sutton[4] who produced it from Ne^{21} by the reaction $Ne^{21}(pn)Na^{21}$, was found to emit gamma-rays, a result to be expected since Ne^{21}, the resulting nucleus, is found to be rich in excitation levels.

EXPERIMENTAL PROCEDURE

Two features of the experimental work are of interest: the first the production of separated isotopes of neon, the second the bombardment and detection arrangement.

The production of rather large samples of neon gas with good separation of the isotopes by the method of thermal diffusion has already been briefly described by one of us.[5] Since, for one thing, neon atoms are about as close to elastic spheres as any available molecules, the thermal separation of their isotopes would be expected to proceed well. The gas circulated in a single thermal diffusion column two meters long made

[1] A. H. Snell, Phys. Rev. **51**, 143 (1937).
[2] L. J. Laslett, Phys. Rev. **52**, 529 (1937).
[3] E. Amaldi, O. D'Agostino, E. Fermi, B. Pontecorvo, F. Rasetti, and E. Segrè, Proc. Roy. Soc. **149**, 522 (1935); T. Bjerge, Nature **139**, 757 (1937); M. E. Nahmias and R. J. Walen, Comptes rendus **203**, 71 (1936).
[4] E. C. Creutz, J. G. Fox, and R. Sutton, Phys. Rev. **57**, 567 (1940).
[5] W. W. Watson, Phys. Rev. **57**, 899 (1940).

entirely of copper. As the inner hot surface a G.E. Calrod heater $\frac{1}{2}''$ in diameter was used. This heater was mounted concentrically in a vertical, water-cooled copper pipe of 1" I.D. Between the two surfaces a temperature difference of 400°C was maintained, the differential expansion being taken up by a sylphon bellows at the lower end.

At the lower end of the column a glass volume of about 300 cc was connected by means of two glass tubes, one of which was heated electrically. During the run the gas thus circulated convectively between this volume and the "heavy" end of the column. A metal leak at the upper end led to a glass manifold to which three break-seal bulbs each of about 125 cc capacity were attached. Two liters of pure neon gas were pumped into the column with a Toepler pump to a pressure of 1.5 atmospheres. Since the speed of separation should vary[6] as the square root of the pressure, with this fairly high gas pressure approximate equilibrium in the column should have been attained in somewhat less than a day. However, the gas was circulated for two days, after which it was bled off at the top at the rate of about 20 cc an hour into the three break-seal bulbs until the pressure in the column had dropped nearly to atmospheric. The lower end-volume was next isolated from the column by means of two stopcocks in each convector tube, and was then cut off. Finally the contents of the column were pumped back into the original flask for use in some of the bombardment experiments.

Mass-spectrographic analyses showed that the percentages of Ne^{20}, Ne^{21}, and Ne^{22} in this "heavy" gas were 84, 0.43, and 15.7, respectively, while in one of the "light" samples the corresponding percentages were 97.6, 0.163, and 2.28. The ratio of Ne^{22} in the heavy gas to that in the light was thus 6.88, a sufficiently large ratio to produce very appreciable difference in the activities in the two samples when subjected to deuteron bombardment. The Ne^{20} ratio in the two was still so nearly one, however, that in our experiments no differences in the intensity of the resulting proton groups could be detected. And in all samples the Ne^{21} content was so low that no reactions from the bombardment of this isotope could be assigned with any certainty. A subsequent separation of a like amount of gas was carried out in exactly the same manner. Although these second samples of separated neon were not analyzed with a mass spectrometer, we feel certain from our measurement of the relative amounts of Ne^{23} β-activity in the heavy and light samples that the difference in the Ne^{22} content of the two was at least as great as that of the first separation. To test the separation factor in this way a standard volume of neon was bombarded for two minutes with a known beam and the amounts of 43-second activities compared. A factor of between four and eight was estimated in this way, the inaccuracy resulting from difficulties in keeping the beam constant, a certain amount of O^{15} contamination due to residual air in the bombardment chamber and some short-lived effects due to Na^{21}. We estimate the most probable ratio of the Ne^{22} in the two samples to be six.

The arrangement for bombardment and proton detection is shown in Fig. 1. The beam is deflected from the dees of a cyclotron by the usual deflector arrangement and passes through an aluminum foil of 2.7 cm air equivalent[7] into a bombardment chamber as indicated. The foil, which is liable to have to stand pressure in both directions was held in place between rubber gaskets and gave no trouble at all. A system of baffles as indicated confined the effective part of the gas to a volume situated, on the average, 2.5 cm from the entrance foil and 8.5 cm from the exit foil (air equivalent 4.4 cm). The beam continued past the effective bombardment volume into a plate insulated by hard rubber which was used for measurement of the beam current. It is not perfectly clear from the diagram, but care was taken that no proton produced by bombardment of metal surfaces could "see" the exit hole so that no corrections need be made for surface contaminations. On pumping the gas out the yield dropped to the background value. The yield from the neon exceeds that from the same amount of air so that small amounts of air contamination do not affect the results. Such air contamination is liable to be present since the Hyvac pump used to evacuate the bombardment chamber was not run long enough to reduce the

[6] W. H. Furry, R. C. Jones and L. Onsager, Phys. Rev. **55**, 1083 (1939).

[7] 1 cm air equivalent = 1.52 mg/cm².

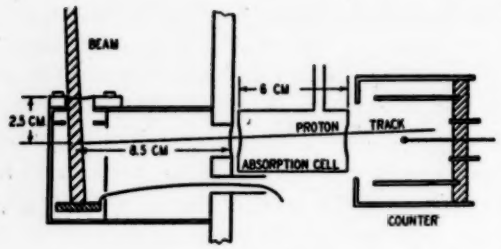

FIG. 1. Arrangement of bombardment chamber and detection apparatus. The beam enters through an aluminum foil and bombards neon gas in the enclosure. Protons emerging at 90° to the beam are detected after passing through various thicknesses of absorption.

air pressure below $\frac{1}{10}$ mm mercury. The protons from the bombarded gas pass into an absorption cell and through a foil changer (not shown) into a proportional counter attached to a conventional amplifier and either a direct or a scale-often recorder. We used pressures varying between five and twenty centimeters of mercury in the chamber and in each case made correction for the absorption introduced both in the incident beam and the emerging protons by the gas itself.

The question of the energy of the incident beam requires some attention. This can be measured in a variety of direct ways but the results are not wholly satisfactory. We found, by varying the pressure of air in the chamber that the maximum energy of the beam *emerging from the deflection plate* was 3.5 Mev, the calculated value. However, there is considerable spread (0.5 Mev) in the energy as measured in this way and it is not easy to decide on the appropriate value to use. We nevertheless find we can determine proton ranges accurately to 1 cm air or less in some cases, and so we used the proton groups from a layer of boron as a means of standardizing the beam energy, with the result that the value 3.2 Mev was decided on. Using this value we have measured the Q values for $H^2(dp)H^3$ and $O^{16}(dp)O^{17}$ with this apparatus and found agreement to within 0.1 Mev, the experimental error. The same figure has been used in many solid target experiments (e.g., $C^{12}(dp)C^{13}$ and $Na^{23}(dp)Na^{24}$) with accurate agreement between our work and that of previous workers. The effective energy in our gas bombardment cell varies between 2.45 and 2.75 Mev according to the pressure of gas used.

Absorbing foils were of aluminum, used in conjunction with the variable air pressure in the air absorption cell. The effective depth of the counter was measured with ThC′ alpha-particles, making allowance for the counting levels and the difference in ionization between protons and alpha-particles.

An account of the use of the cyclotron in observing proton groups is given in a previous paper from this laboratory.[8]

EXPERIMENTAL RESULTS

Proton groups

The first results of bombarding heavy and light samples are shown in Fig. 2. The counting level was set so as to include small "kicks"as well as large, and the two absorption curves are shown together. They have been adjusted as regards yield figures to lie together: the fact that the heavy curve lies at shorter ranges than the light is due to the greater gas pressure in the absorption cell which diminishes the energy of the beam. It can be seen at once that the two curves lie together indicating that the majority of the protons in both cases are due to the overwhelming excess of Ne^{20} in both samples. Two well marked groups appear at 24 cm and 58 cm range while a third is indicated at 35 cm range. To examine the structure of these protons in more detail we changed the counting level to include only large kicks and obtained the results of Fig. 3 where the 35-cm group now shows clearly and in addition a fourth group of still shorter range at 15 cm. The different samples again show no appreciable difference with the possible exception that a group at 40 cm is enhanced in the heavy sample. It should be emphasized that the shape of an absorption curve is strongly dependent on the counting level chosen and that erroneous conclusions can easily be drawn from a limited sample of data. We have taken many runs with the conditions maintained the same throughout as near as we can and in no case have the ratios of the yields of the four groups changed by as much as a factor of two, if we except the doubtful group at 40-cm range. Since our separation factor cannot be less than four we can say definitely that all four clearly marked

[8] E. Pollard, W. L. Davidson, Jr., and H. L. Schultz, Phys. Rev. **57**, 1117 (1940).

groups are due to one neon isotope. That the Ne^{20} isotope is responsible can be deduced in three ways. First, no great change in absolute yield is observed, which means that an isotope whose amount hardly changes is responsible. This is Ne^{20} which is never present to less than 80 percent of the total. Second, the maximum proton range fits well with the expected value from the accurately known masses of Ne^{20} and Ne^{21}. Third, the yield of radioactive Ne^{23} is much less than would result from the observed proton yield. Hence we conclude that the reaction $Ne^{20}(dp)Ne^{21}$ is responsible for the four groups. On this basis we can calculate the Q values for the various groups and determine the excited states of Ne^{21}. In Table I we give various values, obtained from different runs, for the various energy change values. The data are reduced by the procedure given in Livingston and Bethe's article. The values are not of equal weight but are included to give an idea of the amount of scatter possible. We consider our best values to be correct to 0.1 Mev in each case. The largest Q value leads to the value 21.00017 ± 0.00020 for the mass of Ne^{21}, which is to be compared with 20.99968 ± 0.00023 obtained by Bainbridge. The two limits of error nearly overlap. It seems likely that there is a small but significant difference. Such differences between transmutation and mass spectrograph values have recently been reported by Allison.

The group of greatest energy change is rather wider than the others. It may, perhaps, be multiple. We have examined this group in some

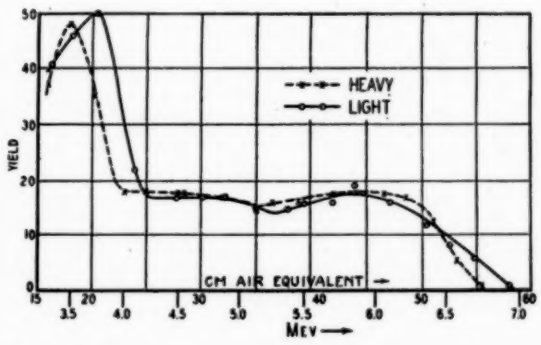

FIG. 2. Absorption curve for protons from heavy and light samples of neon without attempting great resolution. The two curves are almost the same, the difference being due to a slight increase in the bombarding energy for the light sample. All three of the groups are thus due to excited states of Ne^{21}.

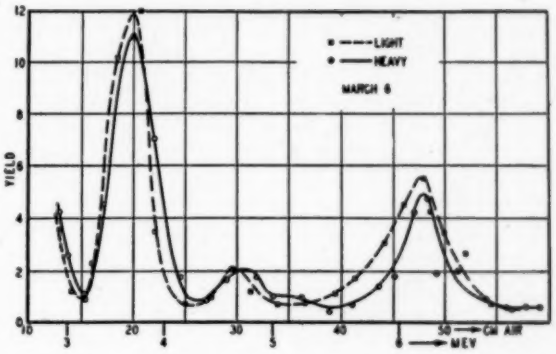

FIG. 3. Differential absorption curve for protons in which only particles near the end of their range are recorded. Four groups are present with an uncertain fifth. The similarity between the curves for heavy and light neon means that all four clearly marked groups are due to excited states of Ne^{21}. The slight hump ending between 5 and 6 Mev could possibly be due to protons from Ne^{22}.

detail in several runs but can find no consistent evidence for structure although we cannot deny the possibility. The difficulty encountered when the counting level is increased still more to increase resolution is the very high background due to neutron recoils, which produce large kicks also. If these were reduced by coincidence counting the resolution might be attempted.

Induced radioactivity

On withdrawing the gas after bombardment and testing it with a Geiger counter it was found to be radioactive decaying with a half-life of 43 ± 3 seconds. This agrees with the period found for Ne^{23} by Amaldi, *et al.*, and by Nahmias and Walen,[3] and so we ascribe it to the new reaction $Ne^{22}(dp)Ne^{23}$, a fact which is proved by the enhancement of the activity in the heavy sample. Our first experiments aimed at plotting an absorption curve for the beta-rays from Ne^{23}. About fifteen samples of ordinary neon were bombarded and quickly transferred to a perforated brass cell with a thin aluminum foil over the top. The brass was thick enough to stop any possible beta-ray. These fifteen samples were placed under a Geiger counter whose wall thickness was calibrated with radiophosphorus, and aluminum absorption foils placed over the cell. The decay of the sample was followed by taking several counts at zero absorption and in this way an absorption curve was gradually built up. This curve is shown in Fig. 4 where two sets of data are shown separately,

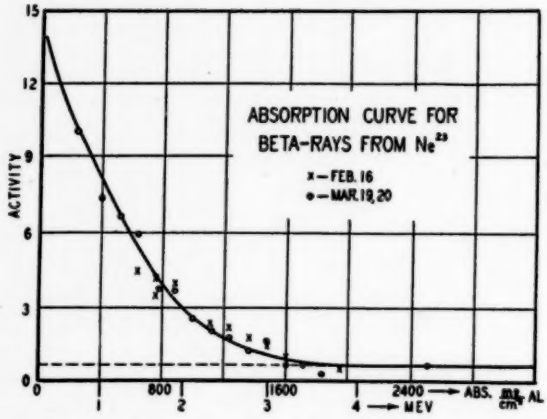

FIG. 4. Reduction of the number of counts in a Geiger-Müller counter as foils of aluminum are placed over a cell containing gas which had been in the bombardment chamber. An end point at 4 Mev is indicated.

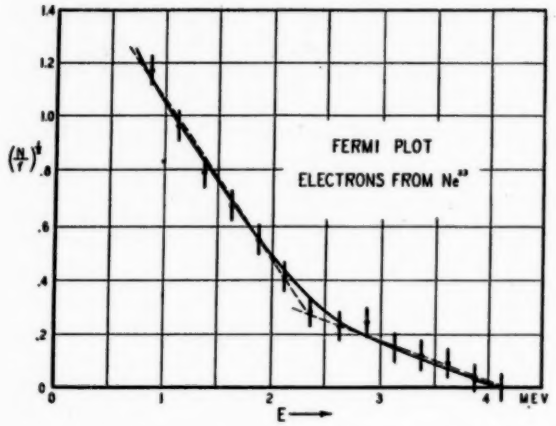

FIG. 5. The data for Fig. 4 reduced to give a Fermi plot. The curvature is probably due to back scattering and variable absorption in the counter. The possibility of two groups as indicated by the dotted lines is discounted by the absence of gamma-rays from this reaction. The end point is 4.1 Mev.

those marked with circles being taken with more counts. The curve appears to reach a maximum value around 4 Mev as determined by Feather's empirical relation

$$\text{Max g/cm}^2 = 0.543E - 0.16.$$

The maximum so obtained uses only the rather poor data where the counts are lowest. We therefore constructed a rough Fermi plot, by marking off the absorption into Mev intervals using the above rule (which checks quite well with magnetic bending work) and reducing the resulting distribution curve in the manner of Kurie, Richardson and Paxton[9] to give a Fermi plot.

TABLE I. *Various energy change values for the reaction* Ne^{20} (dp) Ne^{21}.

EXCITATION	ENERGY CHANGE VALUES (MEV)	BEST VALUE
Ground	4.74, 5.08, 4.80, 4.52, 4.92, 4.92	4.88
First	3.19, 3.17, 3.17, 3.00	3.13
Second	2.20, 1.99, 2.01, 2.23, 1.97, 1.91, 2.01	2.15
Third	1.01, 1.05, 0.98, 0.98	1.02

This is shown in Fig. 5. It will be seen to be either two straight lines or a curve. A calibration Fermi plot using V^{52} prepared by Mr. W. L. Davidson showed the same type of curvature which is to be expected in view of back scattering by the brass and also the variable basic absorption of the cylindrical counter. The Fermi plot however shows a definite intercept with the energy axis at 4.1 Mev which is therefore the appropriate upper limit.

Since the possibility that Na^{23} has an excited state to which Ne^{23} could decay is partly suggested by the shape of the Fermi plot, we looked for the resulting gamma-radiation. A rather weak gamma-ray was found but this did not decay with the 43-second half-life expected. In Fig. 6 the decay curve is shown. It has a half-life of 26 ± 3 seconds and is almost certainly to be identified with Na^{21} discovered by Creutz, Fox, and Sutton[4] and here produced by the reaction

$$Ne^{20}+H^2 \rightarrow Na^{21}+n.$$

As Na^{21} emits positrons this gamma-radiation might easily be due to annihilation radiation, but in view of the large number of excited states of Ne^{21} found we think it more likely that decay to an excited state takes place. An attempt was made to determine the absorption coefficient and values ranging between 2 and 3×10^{-25} for the absorption coefficient per electron in aluminum and brass absorbers were obtained. These indicate that gamma-rays of higher energy than annihilation radiation are present but the low yield and the short half-life made the measurements very difficult. It is probable that our technique of pumping off the bombarded gas operated selectively against sodium which would be deposited on the walls. We feel sure this also accounts for the absence of effects due to fluorine.

[9] F. N. D. Kurie, J. R. Richardson and H. C. Paxton, Phys. Rev. **49**, 368 (1936).

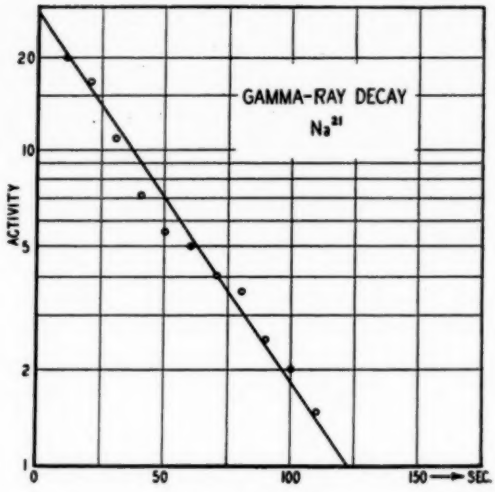

FIG. 6. Decay curve for the gamma-rays found. These are due to Na^{21} and probably consist of a mixture of annihilation radiation and 1.75-Mev gamma-rays from a transition in Ne^{21}.

It would be better to collect the active deposit on a quickly removable solid collector and study the radiations from the deposit.

DISCUSSION

In Fig. 7 we show energy level diagrams for Ne^{21} from our work and comparison values for Ne^{20} taken from Bonner's work on the $F^{19}(dn)Ne^{20}$ reaction.[10] The two are not particularly similar. The possible gamma-ray transitions are indicated. The first excited state for Ne^{21} has recently been observed by Murrell and Smith[11] who studied the $Na^{23}(d\alpha)Ne^{21}$ reaction. They obtain a short range group of alpha-particles corresponding to an excitation energy of 1.6 Mev to be compared with our value of 1.75 Mev. It is very interesting that in our reaction the yield in the first excited state is about one-fourth of that in the ground state, whereas in the mode of formation from $Na^{23}(d\alpha)Ne^{21}$ Murrell and Smith observe roughly equal yields in these two groups. This may be connected with the fact that in our experiments the Oppenheimer-Phillips process is taking place so that there is no compound nucleus in the usual sense.

The Na^{21} gamma-rays we observe are probably a composite of annihilation radiation and gamma-rays from an Ne^{21} nucleus formed in the first excited state.

The mass of Ne^{23} could be found from our measurement of the maximum energy of the beta-particles from Ne^{23} and the mass of Na^{23}. This latter is not definitely known. The work of Murrell and Smith above, together with Bainbridge's mass for Ne^{21} gives a value 22.9961 $\pm$0.0003. Experiments by Pollard and Brasefield[12] on the reaction $Ne^{20}(\alpha p)Na^{23}$ led to a published value of 22.9972$\pm$0.0002, which disagrees with them. Murrell and Smith suggest that a group of greater energy protons was missed. This is unlikely, as careful tests were made by Pollard and Brasefield, and also because no excited state of Na^{23} is apparent in the beta-ray spectrum of Ne^{23}. If the data on the reaction $Ne^{20}(\alpha p)Na^{23}$ are recalculated according to the procedure of Livingston and Bethe a lower value 22.9970 for Na^{23} is found. If now we take our figure for the mass of Ne^{21}, also derived from Ne^{20}, we can deduce from the data of Murrell and Smith the value 22.9966 which gives agreement within the limits of error. Using this we get for Ne^{23} 23.0010 $\pm$0.0005. A check on this is obtained by assuming that the extremely weak group at 41-cm

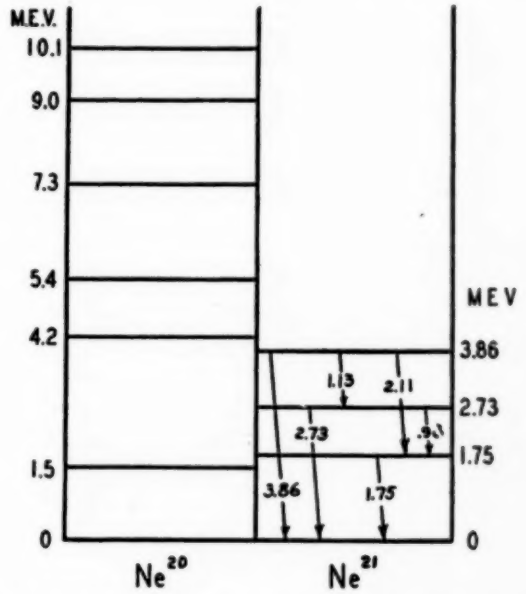

FIG. 7. Energy levels of Ne^{21} compared with those of Ne^{20}. The possible gamma-rays are indicated. The level at 1.75 Mev is to be compared with the figure 1.6 Mev given by Murrell and Smith.

[10] T. W. Bonner, Proc. Roy. Soc. **174**, 339 (1940).
[11] E. B. M. Murrell and C. L. Smith, Proc. Roy. Soc. **173**, 410 (1939).
[12] E. Pollard and C. J. Brasefield, Phys. Rev. **51**, 8 (1937).

range is due to protons from $Ne^{22}(dp)Ne^{23}$ and corresponds to the transition to the ground state. The Q value calculated is 3.6 Mev which gives a mass of 23.0012 for the mass of Ne^{23}. The agreement is reasonable but such data should not be pushed too far.

The proton yield for the $Ne^{22}(dp)Ne^{23}$ reaction can be calculated from the radioactivity observed. With our solid angle for counting we should obtain between ten and thirty per minute. Since when set for great resolution the counter only records about one-twentieth of the total protons passing through it, the size of group to be expected is about that of the indicated group at 41 cm so that it is not surprising that the heavy yields due to Ne^{20} mask the Ne^{22} group. It might be pointed out that without separated isotopes the temptation to ascribe the 33-cm group to Ne^{22} would have been irresistible and an incorrect level scheme for Ne^{21} thus deduced.

In conclusion we wish to thank Mr. W. L. Davidson, Jr., for help in general operations, Messrs. Harry Schultz and A. R. Tobey for keeping the beam in tune during many long hours, and Professor E. O. Lawrence for the gift of the vacuum chamber. The cyclotron construction has been greatly helped by a grant from the George Sheffield Fund.

JULY 1, 1940 PHYSICAL REVIEW VOLUME 58

On the Resonance Levels of Rhodium and Indium

J. HORNBOSTEL, *New York University, Washington Square College, New York, New York*
H. H. GOLDSMITH, *Columbia University, New York, New York*

AND

J. H. MANLEY, *University of Illinois, Urbana, Illinois*

(Received April 15, 1940)

Self-absorption curves as well as mutual absorption curves of the In and the Rh neutron capture levels have been measured. From the experiments, the following values were obtained for the absorption coefficients for self-indication K_s, the resonance cross sections σ_0, the natural widths Γ, the neutron width Γ_N and the spacing $|E_{0\text{In}}-E_{0\text{Rh}}|$ of the two levels: $K_s=11.5$ cm²/g, $\sigma_0=4100\times10^{-24}$ cm², $\Gamma=0.13$ ev, $\Gamma_N=3.5\times10^{-4}$ ev for Rh; $K_s=52$ cm²/g, $\sigma_0=23{,}000\times10^{-24}$ cm², $\Gamma=0.07$ ev, $\Gamma_N=1\times10^{-3}$ ev for In; $|E_{0\text{In}}-E_{0\text{Rh}}|=0.15$ ev.

THE total and the neutron width of a resonance level for slow neutron capture are quantities important in nuclear theory, since from them the probabilities of γ-ray emission and neutron re-emission of compound nuclei can be calculated. On the assumption that only one resonance level is responsible for the neutron capture, the total width Γ of the level may be computed from

$$\Gamma=2E_0^{\frac{3}{2}}E_{th}^{\frac{1}{2}}(K_{th}/K_0)^{\frac{1}{2}}. \qquad (1)$$

Here, E_{th} is the thermal and E_0 the resonance energy, K_{th} the thermal absorption coefficient and K_0 the absorption coefficient at exact resonance, and it is assumed that $E_0\gg E_{th}$ and $E_0\gg\Gamma$. The neutron width Γ_N may be found from the relation[1]

$$\sigma_0=\frac{1.30\times10^6}{E_0}\left(1\pm\frac{1}{2j+1}\right)\frac{\Gamma_N}{\Gamma}, \qquad (2)$$

if the cross section at exact resonance σ_0 is measured in units of 10^{-24} cm² and E_0 in ev. The factor $(1\pm1/(2j+1))$, with j designating the spin of the capturing nucleus, is unknown and shall, therefore, be included in Γ_N.

In an earlier work,[2] self-absorption measurements to determine σ_0 for the one-volt level of rhodium were performed with thick detectors.

[1] H. A. Bethe, Rev. Mod. Phys. **9**, 69 (1937) (Henceforth referred to as B.), Eq. (548).
[2] Manley, Goldsmith and Schwinger, Phys. Rev. **55**, 39 (1939).

The mathematical evaluation was complicated by the well-known phenomenon of self-reversal of the absorption line which causes a strong dependence of the observed absorption on the thickness of the detector. This effect is so large that for great absorber and detector thicknesses the absorption becomes independent of σ_0. As a consequence, the evaluation of the Rh data was somewhat unreliable and in the case of In only a lower limit for the resonance cross section was obtained.[3]

In view of these difficulties it was found desirable to measure the self-absorption coefficients of In and Rh with thin detectors.

Supplementary information was gained from the mutual absorption method which can be applied because of the proximity of the Rh and In levels. From data on the mutual absorption, the ratio of the widths of the two levels Γ_1/Γ_2 and their spacing $|E_{01}-E_{02}|$ can be computed from[4]

$$\Gamma_1/\Gamma_2=K_{12}K_{02}/K_{21}K_{01} \tag{3}$$

and

$$|E_{01}-E_{02}|=\tfrac{1}{2}(\Gamma_1+\Gamma_2)\times\left(\frac{K_{01}K_{02}}{K_{12}K_{02}+K_{21}K_{01}}-1\right)^{\frac{1}{2}}. \tag{4}$$

Here, K_{01} and K_{02} are the resonance cross sections of the two substances, K_{12} and K_{21} the absorption coefficient of substance 1 or 2 for the activity of substance 2 or 1, respectively. The equations are valid only if both detectors and absorbers are thin and if Doppler broadening can be neglected.

Experimental Procedure

The neutron source was a mixture of 200 mC of Ra with Be, embedded 3 cm below the surface of a paraffin cylinder 15 cm high and 20 cm in diameter. The Rh detectors were made from foil weighing 16.5 mg/cm² cemented to a nickel backing. As In detectors nickel slabs were used on which 7.3 mg/cm² of In was electrolytically deposited. (In the earlier work, the "thin" Rh detector weighed 110 mg/cm² and the In detector 80 mg/cm².) The thinnest absorbers consisted of sets of slabs identical with the detectors; the thicker ones were made either from Rh (123 mg/cm²) and In (10, 26, 89 and 185 mg/cm²) foil, or from powdered Rh metal (60 and 100 mg/cm²). In each case, sets of four Cd shielded detector slabs, each measuring 2.2 by 4 cm, were irradiated at a standard elevation of 35 mm above the paraffin surface in an arrangement in which they covered an area of 4.5×8 cm. For counting, the four detectors were placed on a frame which fitted around a thin-walled Geiger-Mueller counter. The counter was connected to a scale-of-eight circuit. The 44″ period of Rh and the 54′ period of In were used. The routine of counting and irradiation was, of course, strictly standardized, both with regard to geometrical arrangement and to timing. The statistical error in the determination of each point was less than 2 percent. The results are represented in Figs. 1 and 2, where the transmissions are plotted against the absorber thickness in mg/cm².

Geometrical Considerations

In the earliest papers on neutron absorption[5] it was already pointed out that the absorption shown by a given absorber will strongly depend on the angular distribution of the emerging neutrons. For the thermal region, Fermi[6] has shown that the number of neutrons emerging between the angles ϑ and $\vartheta+d\vartheta$ is proportional to $(\cos\vartheta+\sqrt{3}\cos^2\vartheta)$. Frisch[7] has computed expressions for the absorption of a monokinetic beam of neutrons which obeys Fermi's formula for the angular distribution up to a maximum angle θ, but which contains no neutrons emerging at angles larger than θ. His results showed that for θ near 90° accurate knowledge of θ is essential for correct evaluation of absorption experiments. For $\theta\leqslant 65°$, the absorption varies more slowly with θ and is, both for thin and thick detectors, very nearly exponential, down to transmissions of the order of 10 percent. The slope of the exponential (plotted semi-logarithmically) is larger than in the case of a parallel beam by a

[3] Manley, Goldsmith and Schwinger, Phys. Rev. **55**, 107 (1939).
[4] B., Eqs. (540), (541).
[5] E. Amaldi and E. Fermi, Phys. Rev. **50**, 899 (1936).
[6] E. Fermi, Ricerca Scient. **72**, 13 (1936).
[7] O. R. Frisch, Kgl. Danske Vidensk. Selskab. Math. Fys. Medd. **14**, No. 12 (1937).

factor f which is function of θ. In other words, experiments carried out with a partly collimated beam ($\theta \leqslant 65°$) of neutrons show the same absorption in a layer of the thickness η as a parallel beam in a layer of the thickness $f\eta$.

Frisch's formulae cannot, however, be applied directly to our experimental conditions, since the value of θ is unknown. θ cannot be computed from the size of the neutron source (paraffin cylinder) and the distance between the paraffin and the detector, because the paraffin surface does not act as a homogeneous source of neutrons. On the contrary, the neutron intensity as measured by cadmium-shielded Rh detectors, drops almost linearly from a maximum at the center of the cylinder to practically zero at the edges. The proper reduction factor f was, therefore, determined semi-empirically instead by comparing with Cd shielded *thick* Rh and In detectors the boron absorption curve obtained in the above-described standard arrangement with a curve obtained with a practically parallel beam.[8] These investigations confirmed Frisch's calculations in that the absorption was exponential within the experimental error and yield $f=1.32$, corresponding to $\theta=65°$. For $\theta=65°$, the f factor for *thin* detectors is found from Frisch's results to change from 1.41 to 1.37 for transmissions varying from near 100 percent down to 30 percent. We have here assumed that the ratio of the f factors for thin and thick detectors is not materially affected by the deviation of the actual angular distribution of resonance neutrons from Fermi's expression for thermal neutrons. Calculations for a cosine distribution show, for instance, that in this case the ratio differs by less than 2 percent from the former value.

The preceding discussion is not generally applicable to self-absorption experiments where the neutron beam is not monokinetic. However, as long as the factor f is the same for all parts of the neutron spectrum, that is as long as θ is not larger than 65° and the transmission at exact resonance is not smaller than 10 percent, the only effect of the angular distribution is to increase the apparent thickness of the absorber and the above considerations still apply. Inspection of a theoretical absorption spectrum shows that even for still thicker absorbers quite accurate results may be expected from this representation. If, therefore, the transmission is plotted against $fK_s\eta$, K_s being the self-absorption coefficient and η the thickness of the absorber, the resulting curve should follow closely the self-absorption curve[9] for a parallel beam.

[8] These experiments were performed and will be described by Dr. W. J. Horvath to whom we are obliged for his kind permission to quote his results before publication.

Detector Thickness

Our detectors are so thin that the electron absorption in the detector material may be neglected. They may not, however, be considered ideally thin neutron absorbers. If the Doppler width $\Delta \ll \Gamma \ll E_0$, correct evaluation of the experimental results, taking into account the finite detector thickness, is obtained in the following way: Let $G(y)=e^{-y}J_0(iy)$ be the self-absorption function for ideally thin detectors (J_0 is the zero-order Bessel function). $y=fK_s\eta$ and will be called the absorptive power. If the absorptive power of the detector, having a thickness ζ, is z, the transmission T_y of the absorber is given by

$$T_y=\int_y^{y+z} G(\xi)d\xi \Big/ \int_0^z G(\xi)d\xi. \qquad (5)$$

Since the ratio $z/y=\zeta/\eta$ is known, y can be obtained from this equation. By numerically carrying out the integration in the special case $y=z$ for various values of z, the z corresponding to the observed T_z was found. It was then used to evaluate the transmissions of the other absorbers.

If the detectors can be considered to be ideally thin in first approximation, the calculation is greatly simplified by first obtaining an approximate absorptive power z_1 from the equation

$$T_z=G(z_1), \qquad (6)$$

Table I. *Indium self-absorption.*

η MG/CM²	T_y%	z_1	T_y'%	$y+\frac{1}{2}z$	f	K_s CM²/G
7.3	66.6±0.7	0.45	54.0	0.76	1.41	52±1.8
17.3	45.5±0.7	—	36.8	1.49	1.40	52±1.5
26.0	37.4±0.6	—	30.3	2.02	1.38	50±1
33.3	34.0±0.6	—	27.6	2.42	1.37	48±1

[9] B., Fig. 16, curve z.

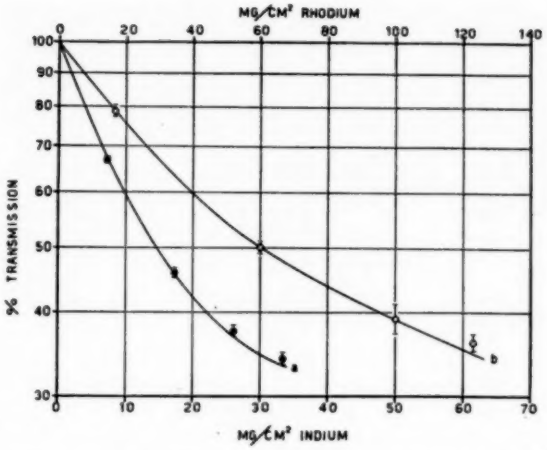

FIG. 1. Self-absorption, percent transmission *vs.* absorber thickness. *a*, In-In (lower abscissa scale); *b*, Rh-Rh (upper abscissa scale).

by then substituting $z_1G(\frac{1}{2}z_1)$ and $z_1G(y+\frac{1}{2}z_1)$ for the integrals

$$\int_0^z G(\xi)d\xi \quad \text{and} \quad \int_y^{y+z} G(\xi)d\xi,$$

respectively, and solving for y. In the special case $y=z$, z was larger than z_1 by 11 percent for the Rh detectors, and by 20 percent for the In detectors. Both the direct and the approximate evaluation gave the same result, showing that the approximations are adequate.

It follows from the computations that a detector may, in first approximation, be considered thin, if its activity is reduced by an absorber of the same thickness by less than 40 percent. For this limiting value, the approximate method of evaluation yields an absorption coefficient too low by only 3 percent.

Table I shows the procedure of evaluation for the case of indium. Column 1 gives the thickness of the absorbers in mg/cm²; column 2 the experimental transmissions; column 3 the preliminary absorptive power z_1 of the thinnest absorber, as found from Eq. (6); column 4 the quantities $T_y'=G(\frac{1}{2}z_1)T_y$ and column 5 the absorptive powers $y+\frac{1}{2}z_1$ determined from the relation $T_y'=G(y+\frac{1}{2}z_1)$; column 6 the f factors. From columns 1, 5, and 6, the absorption coefficients K_s in column 7 are computed. The first two values are deemed to be most reliable and $K_s=52\pm2$ cm²/g was, therefore, adopted as a basis for the subsequent calculations. In Fig. 1, curve (*a*) represents the absorption curve as computed from Eq. (6) for $K_s=52$ cm²/g. Similarly, for Rh $K_s=11.5\pm0.5$ cm²/g and curve (*b*), Fig. 1, were obtained.

The limits of error include the experimental fluctuations as well as the uncertainties in the f factors. The corrections for Doppler broadening which must be made before the cross section at exact resonance can be derived from the absorption coefficient for self-indication will be discussed below.

MUTUAL ABSORPTION

The evaluation of experiments on the mutual absorption of the levels of two different substances is complicated by the fact that the shape of the absorption curve depends on the ratio of the width Γ_1/Γ_2 of the two levels and their spacing $|E_{01}-E_{02}|$. Rough values for these quantities can be derived from the initial slope of the absorption curves by means of Eqs. (3) and (4). However, for accurate values these equations must be replaced by an expression which gives the transmission as a function of the parameters Γ_1/Γ_2 and $|E_{01}-E_{02}|$ not only for thin but also for thick absorbers. The finite thickness of the detector (substance 2, absorptive power z) may approximately be taken into account by replacing in the computation the actual fairly thin detector by a very thin detector in combination with a filter of the absorptive power $\frac{1}{2}z=\frac{1}{2}fK_{s2}\zeta$. Neglecting the effects of Doppler broadening,[10] assuming Γ_1, Γ_2 and $|E_{01}-E_{02}|$ all $\ll E_{01}$, and using the abbreviations

$$x=\frac{E-E_{02}}{\frac{1}{2}\Gamma_2}, \quad a=(\Gamma_2/\Gamma_1)^2, \quad b=\frac{E_{01}-E_{02}}{\frac{1}{2}\Gamma_2},$$

we derive from the Breit-Wigner formula[11] for the transmission T of an absorber of the absorptive power $y=fK_{s1}\eta$:

$$T=\frac{\int_{-\infty}^{+\infty}\frac{dx}{1+x^2}\exp\left(\frac{-2y}{1+a(x-b)^2}-\frac{z}{1+x^2}\right)}{\int_{-\infty}^{+\infty}\frac{dx}{1+x^2}\exp\left(\frac{-z}{1+x^2}\right)}. \quad (7)$$

[10] Note that in this case $K_0=2K_s$.
[11] B., Eq. (530).

By substituting $x=tn\frac{1}{2}\psi$ and performing the integration in the denominator, we may bring this in a form convenient for numerical evaluation:

$$T=\frac{1}{2\pi G(\frac{1}{2}z)}\int_{-\pi}^{+\pi}\exp\left[(1+\cos\psi)\times\left(\frac{-2y/c}{1-\{1-(4a/c^2)\}^{\frac{1}{2}}\sin(\psi-\varphi)}-\frac{z}{2}\right)\right]d\psi, \quad (8)$$

with $c=1+a+ab^2$ and $tn\varphi=(1-a+ab^2)/2ab$.

Width and Doppler Broadening

It is, of course, impracticable to compute T from Eq. (8) for all possible values of the parameters y, a, and b in order to obtain, by comparison with the experiments, the widths and spacing. Eq. (8) was, therefore, evaluated only for a few slightly differing tentative sets of the parameters. These were obtained by inserting into Eqs. (3) and (4) approximate values for K_{InRh} and K_{RhIn}, determined from the initial slope of the mutual absorption curves. The other parameters in these equations, $K_{0\text{In}}$ and $K_{0\text{Rh}}$, were derived from the experimental $K_{s\text{In}}$ and $K_{s\text{Rh}}$ by applying Doppler correction in the following way: First, an estimate for the width of the Rh level was deduced from Eq. (1) by inserting $K_s=11.5$ cm²/g, $K_{th}=0.74$ cm²/g,[12] $E_{th}=0.024$ ev, and $E_0=0.85$ ev.[8] Here, E_{th} is a function of the transmission of the absorber used in determining K_{th} and was taken from a plot given by Bethe.[13] The implicit assumption that only one level contributes to the thermal neutron absorption in Rh is well justified, since it has been shown[14] that the 44″ and 4.2′ periods are due to the same level and since no other periods induced by slow neutrons are known. (The hypothetical levels of higher energy considered below should not greatly affect the thermal absorption.)

It is not safe to apply the same procedure to the In level because of the unknown contribution of the 40^d period to the thermal absorption. An approximate Γ_{In} was found, therefore, from Eq. (3) by inserting the approximate K_{InRh} and K_{RhIn}, and $K_{s\text{In}}$ and $K_{s\text{Rh}}$ instead of $K_{0\text{In}}$ and $K_{0\text{Rh}}$. For the Doppler correction, K_s/K_0 as a function of Δ/Γ, with Δ the Doppler width, was taken from a graph given by Bethe and Placzek.[15] The equation

$$\Delta=(2/A)(E_0E_{th})^{\frac{1}{2}} \quad (9)$$

(A is the atomic weight) yields $\Delta=0.031$ ev both for In and Rh. Because of the effects of lattice binding,[16] the effective thermal energy $E_{th}\backsimeq 1.2kT$ of the crystal is used in (9). Combining Δ with the tentative values for Γ, $K_{0\text{Rh}}=24\pm1$ cm²/g and $K_{0\text{In}}=116\pm6$ cm²/g are obtained as final Doppler-corrected absorption coefficients at exact resonance. The corresponding cross sections are $\sigma_0=4100\times10^{-24}$ cm² for Rh and $\sigma_0=23{,}000\times10^{-24}$ cm² for In[115].

The In cross section is larger than the lower limit of $20{,}000\times10^{-24}$ cm² deduced from the thick detector work (l.c.). The Rh cross section agrees with Jaeckel's[14] result, but is lower by 30 percent than the value given by Manley, Goldsmith and Schwinger.[2,17]

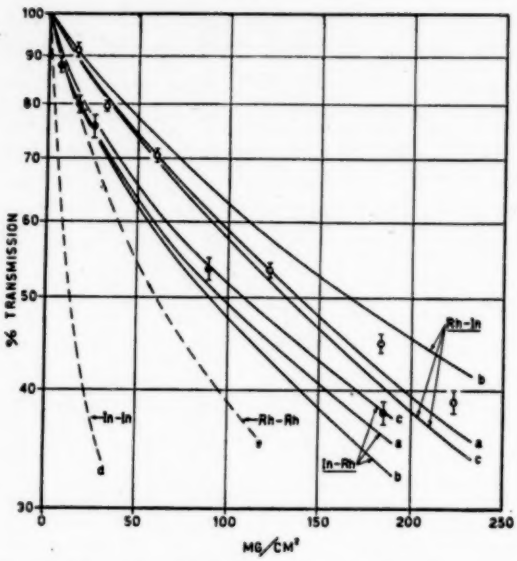

FIG. 2. Mutual and self-absorption of Rh and In, percent transmission *vs.* absorber thickness. Full curves calculated for (*a*), $K_{\text{InRh}}=12.5$ cm²/g, $K_{\text{RhIn}}=4.8$ cm²/g; (*b*), $K_{\text{InRh}}=12.5$ cm²/g, $K_{\text{RhIn}}=4.2$ cm²/g; (*c*) $K_{\text{InRh}}=11.5$ cm²/g, $K_{\text{RhIn}}=4.8$ cm²/g.

[12] Powers, Fink and Pegram, Phys. Rev. **49**, 650 (1936).
[13] B. Fig. 15.
[14] R. Jaeckel, Zeits. f. Physik **107**, 669 (1937).
[15] H. A. Bethe and G. Placzek, Phys. Rev. **51**, 450 (1937).
[16] W. E. Lamb, Phys. Rev. **55**, 190 (1939).
[17] In the case of the data these authors got with their "thin" detector (see their Fig. 2, lower curve), better agreement could be obtained by fitting a calculated curve more closely to the three experimental points at more than

The calculated mutual absorption curves are shown in Fig. 2. The best simultaneous fit (curves *a*) with the experimental points both of the Rh-In and the In-Rh absorption experiments was obtained with $K_{\mathrm{InRh}}=12.5$ cm²/g, $K_{\mathrm{RhIn}}=4.8$ cm²/g, $\Gamma_{\mathrm{In}}/\Gamma_{\mathrm{Rh}}=0.5_3$, $|E_{0\mathrm{In}}-E_{0\mathrm{Rh}}|/\Gamma_{\mathrm{Rh}}=1.1_4$.

To show the sensitivity of the shape of the curves to changes in the parameters, the curves (*b*) Fig. 2, were computed with $K_{\mathrm{InRh}}=12.5$ cm²/g, $K_{\mathrm{RhIn}}=4.2$ cm²/g, ($\Gamma_{\mathrm{In}}/\Gamma_{\mathrm{Rh}}=0.60$, $|E_{0\mathrm{In}}-E_{0\mathrm{Rh}}|/\Gamma_{\mathrm{Rh}}=1.26$) and the curves (*c*) with $K_{\mathrm{InRh}}=11.5$ cm²/g and $K_{\mathrm{RhIn}}=4.8$ cm²/g, ($\Gamma_{\mathrm{In}}/\Gamma_{\mathrm{Rh}}=0.49$, $|E_{0\mathrm{In}}-E_{0\mathrm{Rh}}|/\Gamma_{\mathrm{Rh}}=1.12$). Curves (*b*) and (*c*) show that the ratios of widths and spacing have an error of less than 10 percent. For comparison, the self-absorption curves of Fig. 1 are also reproduced in Fig. 2.

The final absolute values of the natural width and the spacings are $\Gamma_{\mathrm{Rh}}=0.13$ ev, $\Gamma_{\mathrm{In}}=0.07$ ev and $|E_{0\mathrm{In}}-E_{0\mathrm{Rh}}|=0.15$ ev. They are less accurate than the ratios because of their dependence on K_{th} which is not too accurately known. The spacing is in agreement with the difference in resonance energy as determined by the cadmium[18] and the less sensitive boron[19] absorption method.

From Eq. (1), we obtain $\Gamma_{\mathrm{In}}=0.063$ ev by inserting $K_{th}=0.74$ cm²/g [5] and $E_0=1.0$ ev (the In resonance energy is known to be higher than the Rh resonance energy[19]). Since the above value of K_{th} is rather uncertain, the agreement can be considered as satisfactory and shows that the major portion of the thermal absorption of In is contributed by the one-volt level.

By inserting the data given in the preceding paragraphs into Eq. (2), we obtain for the neutron width $[1\pm1/(2j+1)]\Gamma_{N\mathrm{Rh}}=3.5\times10^{-4}$ ev and $[1\pm1/(2j+1)]\Gamma_{N\mathrm{In}}=1\times10^{-3}$ ev.

The deviation of the experimental points from the tail of the calculated curves which is also apparent in the self-absorption curves of Fig. 1 shows that some of our assumptions become invalid at smaller transmissions. Neglect of Doppler broadening in the derivation of Eqs. (5) and (8) should introduce only a very small error and would cause the observed transmissions to be *smaller* than the calculated ones at larger absorber thicknesses. Inadequacy of the *f* factors to account for the angular distribution gives a deviation from the computed data by less than 0.3 percent. The assumption, however, that only one level is responsible for the activity is open to doubt. In view of the fact that the average spacing between levels is theoretically expected to be of the order of 10 ev, and that experiments in the case of silver[19] and iodine[20] have confirmed that expectation, it is reasonable to assume that a small portion of the activity is contributed by levels of higher energies which should have a smaller K_s and would not contribute to the mutual absorption. A contribution of only 3 percent by these higher levels to the In activity would be sufficient to explain the discrepancy at the end of curve *a*, Fig. 1, and curve *a*, Rh-In, Fig. 2.

We wish to thank Mr. S. Hedelman for his help with the experiments. One of us (J. H.) gratefully acknowledges a grant from the Diamond Jubilee Fund.

40 percent transmission. However, the discrepancy with the absorption coefficient derived from the initial portion, particularly the first point, of their "thick" detector curve (their Fig. 2) is difficult to explain. The tail of this curve is already insensitive to changes in the absorption coefficient.

[18] H. H. Goldsmith and J. H. Manley, Phys. Rev. **51**, 382 (1937).

[19] H. H. Goldsmith and F. Rasetti, Phys. Rev. **50**, 328 (1936).

[20] J. Hornbostel and F. A. Valente, Phys. Rev. **55**, 108 (1939).

Radiative K Capture

P. MORRISON AND L. I. SCHIFF
Department of Physics, University of California, Berkeley, California
(Received May 7, 1940)

Accompanying K capture, as in β-activity, there is a weak continuous high energy gamma-ray spectrum. The major contribution to the effect is from magnetic radiative capture of a K electron. For an allowed transition using Fermi or Gamow-Teller coupling, the number of gamma-quanta per K electron captured is $(\alpha/12\pi)(W/mc^2)^2$, where W is the available energy. For other couplings and forbidden transitions, the effect is of the same order of magnitude.

ACCOMPANYING the emission of electrons and positrons from a radioactive nucleus, there is a low intensity continuous spectrum of gamma-radiation. This radiation has been measured by several observers,[1] and the effect has been discussed theoretically by Bloch[2] and by Knipp and Uhlenbeck.[3] The origin of the radiation is the sudden change in the atomic electric moment when the charge of the heavy particle, confined to the nucleus, is released as a free electron or positron. An entirely analogous effect will take place when a nucleus falls to a stable state by the capture of an atomic electron. Here the available energy will most frequently go off with the neutrino, but may be shared between a neutrino and a gamma-quantum. If the energy difference between the isobaric nuclei is $E_Z-E_{Z-1}=\Delta E$, the available energy for the capture process includes the rest energy of the atomic electron and is $W=\Delta E+mc^2$. When $0<W<2mc^2$ only electron capture will be energetically allowed. Then only the unobservable neutrino and the low energy x-ray quanta from the final nucleus will be emitted in the ordinary capture process, and the radiative capture gamma-rays will be observable without a background of other ionizing radiation; we shall see that most of the gamma-quanta have a good fraction of the energy W. The most favorable cases for observation will be those where: (1) there is only electron capture, with no positrons; (2) Z is not too large, so that the x-rays are of low energy; and (3) the available energy W is of the order of hundreds of kilovolts. Under these conditions the capture radiation will be observable without the necessity for the elaborate corrections for ordinary bremsstrahlung made in the case of the radiation accompanying electron or positron activity. The elements V^{47} and Y^{86} satisfy conditions (1) and (2), and may be suitable substances for a study of this effect.[4]

We have calculated the ratio of the number of gamma-quanta emitted with a given energy to the number of electrons captured. The radiationless capture is a first-order process, and its probability per unit time is:

$$w_C=(2\pi/\hbar)\rho_\nu(W)\,|(f|H|0)|^2,$$

where ρ_ν is the density of final neutrino states per unit energy range, and H is the coupling energy between heavy and light particles. For all interesting cases the available energy will be greater than the K-shell binding energy, and the K electrons, which spend the most time in the region of the nucleus, will give the great bulk of the capture processes whether they are allowed or forbidden. The radiative capture is a second order process, and its probability per unit time when the gamma-quantum has an energy between k and $k+dk$ is:

$$w_k dk=\frac{2\pi}{\hbar}\rho_\nu(W-k)\rho_\gamma(k)dk \times\left|\sum_i\frac{(f|H|i)(i|e\alpha\mathbf{A}_k|0)}{E_0-E_i}\right|^2,$$

where ρ_γ is the density of final gamma-ray states per unit energy range. For allowed transitions,

[1] S. Bramson, Zeits. f. Physik **66**, 721 (1930). E. Stahel and J. Guillissen, J. de phys. et rad. [8] **1**, 12 (1940). C. S. Wu, private communication; we are indebted to Miss Wu for informing us of her results on the radiative beta-emission of P^{32} prior to publication.

[2] F. Bloch, Phys. Rev. **50**, 472 (1936).

[3] J. K. Knipp and G. E. Uhlenbeck, Physica **3**, 425 (1936).

[4] J. J. Livingood and G. T. Seaborg, Rev. Mod. Phys. **12**, 30 (1940).

the intermediate state of the electron must be an s state. From an initial K-state magnetic dipole radiation will be produced, while from an initial L_{II}-state electric dipole radiation can occur. The electric radiation depends on the transverse component of the current which is proportional to the momentum of the initial state; that is, to αZ, where α is the fine structure constant. As is well known from the theory of the photoelectric effect, the electric radiation cannot be calculated correctly without taking into account the effect of the Coulomb field on the intermediate state wave functions. However, an estimate shows that the electric radiation probability is of order $(\alpha Z)^2/10$ compared to the magnetic radiation probability for $W \sim mc^2$, and only becomes comparable with it for the uninteresting case of available energies of the order of the K-shell binding energy. For forbidden transitions, the intermediate electron state need not be an s state, since either the electron (and thence the gamma-quantum) or the neutrino can take up the angular momentum of the nucleus. There are then many more possible transitions; however, those transitions which start from a K state will be most likely, since their probability contains the fewest powers of αZ.

Since we are dealing with an initial K state whose binding energy is small compared to the gamma-ray recoil energy, we can neglect Z consistently throughout and use plane waves for the electrons, taking the initial state to have zero momentum. For allowed transitions, the calculation can then be performed in the usual way, assuming a point nucleus, and summing over spins of the initial and final states and over spins and both signs of the energy of the intermediate state by the usual method of projection operators. With either Fermi or Gamow-Teller couplings, we obtain:

$$\frac{w_k dk}{w_C} = \frac{\alpha}{\pi}\left(\frac{W}{mc^2}\right)^2 (1-\epsilon)^2 \epsilon d\epsilon, \quad \epsilon \equiv \frac{k}{W},$$

giving for the ratio of the total number of gamma-rays to the total number of K captures:

$$\int_0^W \frac{w_k dk}{w_C} \equiv \frac{w_R}{w_C} = \frac{\alpha}{12\pi}\left(\frac{W}{mc^2}\right)^2.$$

The Konopinski-Uhlenbeck coupling gives a slightly different result:

$$\frac{w_k dk}{w_C} = \frac{\alpha}{\pi}\left(\frac{W}{mc^2}\right)^2 (1-\epsilon)^4 \epsilon d\epsilon, \quad \frac{w_R}{w_C} = \frac{\alpha}{30\pi}\left(\frac{W}{mc^2}\right)^2.$$

Because of the magnetic character of the radiation, most of the quanta have a considerable fraction of the available energy.

As is usually the case with forbidden transitions, the calculations here are essentially more complicated, since they are more dependent on the type of coupling and on the nuclear matrix element. With the Fermi coupling, for example, the contributions of the nuclear charge and current terms become comparable, and it is no longer possible to cancel out the nuclear matrix elements between w_k and w_C. However, it is easy to see that w_R/w_C will not be changed in order of magnitude, although the spectrum of the emitted gamma-rays will be altered considerably in shape. An estimate indicates that w_R/w_C is about half as large for a singly forbidden as for an allowed transition.

Knipp and Uhlenbeck[3] have suggested an alternative method of calculation for such problems as radiative emission and capture. It consists in treating the effect not as a second-order process involving the form of both the beta-coupling and the electromagnetic coupling, but as a process of the first order. They calculate the probability of a radiative transition from an electron state which represents a source of electrons at the nucleus to a plane wave. (For the capture effect, a state representing a sink at the nucleus would be used.) They indicate then that it is sufficient to use the observed momentum distribution of outgoing electrons to predict the total effect. But it is easy to see that the "first-order" and the "second-order" calculations will give the same result only for a restricted form of beta-coupling. For if we take the beta-coupling energy to be a function of the electron and neutrino momenta $f(\mathbf{k}_e, \mathbf{k}_\nu)$, we find that the "first-order" probability is proportional to $|f(\boldsymbol{L}, \mathbf{k}_\nu)|^2$ where $\boldsymbol{L}$ is the momentum of the outgoing electron before it has radiated, while the "second-order" probability is proportional to $|f(\mathbf{K}, \mathbf{k}_\nu)|^2$, where $\mathbf{K}$ is the difference of the momenta of the gamma-quantum and the final electron. In general, $\boldsymbol{L}$ and

K are not the same, so that the two calculations will give the same result only if f is independent of $\mathbf{k}_r$. This condition is satisfied for allowed transitions with the three couplings commonly employed, although not for forbidden transitions. A detailed study of the radiative beta-activity and radiative capture might thus give further information on the actual form of the beta-coupling.

The authors are very grateful to Professor J. R. Oppenheimer for suggesting this calculation and for much helpful discussion.

JULY 1, 1940 PHYSICAL REVIEW VOLUME 58

The Scattering of Thermal Neutrons by Deuterons*

LLOYD MOTZ, *Columbia University, New York, New York*

AND

JULIAN SCHWINGER,† *The University of California, Berkeley, California*

(Received April 13, 1940)

The cross section for the scattering of very slow neutrons by deuterons is calculated by numerical methods. Polarization is completely neglected and the wave equation for the process is set up in such a form as to take correctly into account exchange effects between the incident neutron and the neutron initially in the deuteron. This wave equation is then replaced by an integral equation the solution of which is correctly symmetrized and has the right asymptotic value to describe the scattering process. The numerical integration is performed by replacing the integral equation by a finite set of simultaneous linear algebraic equations. The work is greatly simplified by the use of a sum of two Gauss functions to approximate the ground state deuteron wave function. It is assumed throughout this paper that the interactions between like and unlike particles are equal and are of the general form

$$V_{ij}=-[(1-g-g_1-g_2)P_{ij}+gP_{ij}Q_{ij}+g_1+g_2Q_{ij}]J(r_{ij}),$$

where the symbols have their usual meanings and where $J(r_{ij})$ is a Gauss function. The calculation is carried out for two sets of g's. For the first set, $g_1=g_2=0$, $g=0.2$, the cross section is found to be equal to 4.57×10^{-24} cm², and for the second set of g's, $g_2=2$, $g=0.22-g_2$, $g_1=0.25-0.8g_2$, the value of the cross section is found to be equal to 6.91×10^{-24} cm². The experimental value is at least 20 percent smaller than the first of these values.

INTRODUCTION

SINCE the scattering of neutrons by deuterons involves a fundamental process in which only three particles take part, the solution of this problem can be expected to throw a great deal more light on the nature of the forces between elementary particles than is now available. This, coupled with the fact that an exact theoretical treatment is impossible because of the complexity of the equations, must justify a step-by-step attack on the problem in which various simplified models are considered in some detail. A complete treatment must take into account polarization as well as exchange effects. If polarization is entirely neglected, as has been done in the present calculation, it is possible to set the problem up in such a form that one can obtain a numerical solution without an undue amount of work. Calculations in which polarization has been neglected have already been carried out by Schiff[1] and by Yukawa and Sakata[2] who proceeded somewhat indirectly by introducing auxiliary potentials which enabled them to simplify their equations considerably. The present paper differs from the aforementioned ones in two respects: the calculations are carried through using the most general type of interaction between the particles (we assume only that the forces between like and unlike particles are equal); exchange effects are accurately taken account of to the order of approximation employed.

* Publication assisted by the Ernest Kempton Adams Fund for Physical Research of Columbia University.

† National Research Fellow.

[1] L. I. Schiff, Phys. Rev. **52**, 149 (1937).

[2] H. Yukawa and S. Sakata, Proc. Phys.-Math. Soc. Japan **19**, 542 (1937).

The Integral Equation of the Collision Process

The general form of the wave equation for a system consisting of three particles of equal mass and having a total spin S is

$$[-(\hbar^2/2M)(\Delta_1+\Delta_2+\Delta_3)+V_{12}+V_{13}+V_{23}-E] \times\Psi_S(\mathbf{r}_1, \mathbf{r}_2, \mathbf{r}_3)=0, \quad (1)$$

where $\mathbf{r}_1$, $\mathbf{r}_2$, and $\mathbf{r}_3$ are the vector coordinates of the three particles, M is the common mass and V_{ij} are the interaction energies. In the present calculation we have taken the most general form for the potential[3]

$$V_{ij}=-[(1-g-g_1-g_2)P_{ij}+gP_{ij}Q_{ij} +g_1+g_2Q_{ij}]J(r_{ij}). \quad (2)$$

P_{ij} is the operator which exchanges the positions of particles i and j, and Q_{ij} is the spin exchange operator, which we write in the form $\frac{1}{2}(1+\boldsymbol{\sigma}_i\cdot\boldsymbol{\sigma}_j)$, where the $\boldsymbol{\sigma}_i$, $\boldsymbol{\sigma}_j$ are Pauli spin matrices of unit amplitude.

We now transform the wave equation to the center of mass coordinate system, which is defined by the equations (see Fig. 1)

$$\mathbf{r}=\mathbf{r}_1-\tfrac{1}{2}(\mathbf{r}_2+\mathbf{r}_3), \quad \boldsymbol{\rho}=\mathbf{r}_2-\mathbf{r}_3, \quad \mathbf{R}=\tfrac{1}{3}(\mathbf{r}_1+\mathbf{r}_2+\mathbf{r}_3). \quad (3)$$

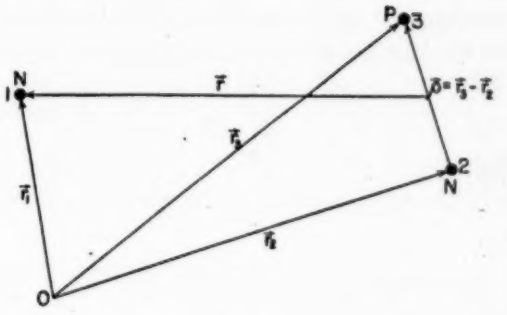

FIG. 1.

The subscript 1 refers to the incoming neutron and 2 to the neutron initially in the deuteron, so that $\boldsymbol{\rho}$ is the coordinate of the deuteron system. On factoring out the motion of the center of mass, we obtain the wave equation in the coordinates $\boldsymbol{\rho}$ and $\mathbf{r}$

$$[-(\hbar^2/2M)(2\Delta_\rho+\tfrac{3}{2}\Delta_r)+V_{12}+V_{13}+V_{23}-E] \times\Psi_S(\boldsymbol{\rho}, \mathbf{r})=0, \quad (4)$$

where the V_{ij}'s are now functions of ρ and r only.

If $\psi_0(\boldsymbol{\rho})$ and $\psi(\boldsymbol{\rho}, \epsilon)$ are the deuteron ground state and continuum wave functions, respectively, then $\Psi_S(\boldsymbol{\rho}, \mathbf{r})$ can be written as the following expansion:

$$\Psi_S(\boldsymbol{\rho}, \mathbf{r})=F_0(\mathbf{r})\psi_0(\boldsymbol{\rho})\chi_S(123)+\chi_S(123)\int_0^\infty F(\mathbf{r}, \epsilon)\psi(\boldsymbol{\rho}, \epsilon)d\epsilon, \quad (5)$$

where $\chi_S(123)$ is the spin wave function for a definite value S of the total spin of the system. In order to take exchange effects into account, we set down a similar expansion for $P_{12}Q_{12}\Psi_S(\boldsymbol{\rho}, \mathbf{r})$

$$P_{12}Q_{12}\Psi_S(\boldsymbol{\rho}, \mathbf{r})=G_0(\mathbf{r})\psi_0(\boldsymbol{\rho})\chi_S(123)+\chi_S(123)\int_0^\infty G(\mathbf{r}, \epsilon)\psi(\boldsymbol{\rho}, \epsilon)d\epsilon. \quad (6)$$

Substituting (5) and (6), both of which are solutions, into the wave equation, we obtain the two equations

$$\begin{aligned}
&-(\hbar^2/2M)(2\Delta_\rho+\tfrac{3}{2}\Delta_r)[F_0(\mathbf{r})\psi_0(\boldsymbol{\rho})\chi_S(123)+F_S(\mathbf{r}\ \boldsymbol{\rho})]+[\sum_{i=2,3}V_{1i}+V_{23}][F_0(\mathbf{r})\psi_0(\boldsymbol{\rho})\chi_S(123)\\
&\qquad +F_S(\mathbf{r}, \boldsymbol{\rho})]=E[F_0(\mathbf{r})\psi_0(\boldsymbol{\rho})\chi_S(123)+F_S(\mathbf{r}, \boldsymbol{\rho})]\\
&-(\hbar^2/2M)(2\Delta_\rho+\tfrac{3}{2}\Delta_r)[G_0(\mathbf{r})\psi_0(\boldsymbol{\rho})\chi_S(123)+G_S(\mathbf{r}, \boldsymbol{\rho})]+[\sum_{i=2,3}V_{1i}+V_{23}]\\
&\qquad \times[G_0(\mathbf{r})\psi_0(\boldsymbol{\rho})\chi_S(123)+G_S(\mathbf{r}, \boldsymbol{\rho})]=E[G_0(\mathbf{r})\psi_0(\boldsymbol{\rho})\chi_S(123)+G_S(\mathbf{r}, \boldsymbol{\rho})],
\end{aligned} \quad (7)$$

where

$$F_S(\mathbf{r}, \boldsymbol{\rho})\equiv\chi_S(123)\int_0^\infty F(\mathbf{r}, \epsilon)\psi(\boldsymbol{\rho}, \epsilon)d\epsilon, \quad G_S(\mathbf{r}, \boldsymbol{\rho})\equiv\chi_S(123)\int_0^\infty G(\mathbf{r}, \epsilon)\psi(\boldsymbol{\rho}, \epsilon)d\epsilon.$$

[3] G. Breit and E. Feenberg, Phys. Rev. **50**, 850 (1936).

These equations can now be reduced to simpler form by making use of the deuteron wave equation. If the binding energy of the deuteron is E_0, then $\psi_0(\rho)$ satisfies the following equation:

$$-(\hbar^2/M)\Delta_\rho\psi_0(\rho)+V_{23}\psi_0(\rho)=E_0\psi_0(\rho).$$

Multiplying (7) by $\psi_0^*(\rho)\chi_S^*(123)$, integrating over the configuration space of ρ, and summing over spins, we obtain with the aid of the deuteron equation

$$\begin{aligned}&-\frac{3}{4}\frac{\hbar^2}{M}\Delta_r F_0(\mathbf{r})+\sum_{\text{spins}}\sum_{i=2,3}\chi_S^*(123)V_{1i}F_0(\mathbf{r})\chi_S(123)\\&\qquad+\sum_{\text{spins}}\sum_{i=2,3}\int d\tau_\rho\chi_S^*(123)\psi_0^*(\rho)V_{1i}F_S(\mathbf{r},\rho)=(E-E_0)F_0(\mathbf{r}),\\&-\frac{3}{4}\frac{\hbar^2}{M}\Delta_r G_0(\mathbf{r})+\sum_{\text{spins}}\sum_{i=2,3}\chi_S^*(123)V_{1i}G_0(\mathbf{r})\chi_S(123)\\&\qquad+\sum_{\text{spins}}\sum_{i=2,3}\int d\tau_\rho\chi_S^*(123)\psi_0^*(\rho)V_{1i}G_S(\mathbf{r},\rho)=(E-E_0)G_0(\mathbf{r}).\end{aligned}\tag{8}$$

If in these equations we replace $F_S(\mathbf{r},\rho)$ and $G_S(\mathbf{r},\rho)$ by the equivalent expressions obtained from (5) and (6), and then take the difference of the resulting equations, we have left the equation

$$\begin{aligned}&-\frac{3}{4}\frac{\hbar^2}{M}\Delta_r[F_0(\mathbf{r})-G_0(\mathbf{r})]+\sum_{\text{spins}}\sum_{i=2,3}\int d\tau_\rho\chi_S^*\psi_0^*(\rho)V_{1i}[\Psi_S(\mathbf{r},\rho)-P_{12}Q_{12}\Psi_S(\mathbf{r},\rho)]\\&\qquad=(E-E_0)[F_0(\mathbf{r})-G_0(\mathbf{r})].\end{aligned}\tag{9}$$

This equation is exact, but before we can proceed further, we must introduce an approximation which is equivalent to neglecting polarization effects. We place

$$\Psi_S(\mathbf{r},\rho)-P_{12}Q_{12}\Psi_S(\mathbf{r},\rho)=\left\{F_0(\mathbf{r})-G_0(\mathbf{r})-P_{12}Q_{12}[F_0(\mathbf{r})-G_0(\mathbf{r})]\right\}\psi_0(\rho)\chi_S(123)\equiv[\phi(\mathbf{r})-P_{12}Q_{12}\phi(\mathbf{r})]\psi_0(\rho)\chi_S(123).\tag{10}$$

With the aid of (10) we can now obtain an equation for $\phi(\mathbf{r})$,

$$-\frac{3}{4}\frac{\hbar^2}{M}\Delta\phi(\mathbf{r})+\sum_{\text{spins}}\sum_{i=2,3}\int d\tau_\rho\chi_S^*\psi_0^*(\rho)V_{1i}[\phi(\mathbf{r})\psi_0(\rho)\chi_S(123)-P_{12}Q_{12}\phi(\mathbf{r})\psi_0(\rho)\chi_S(123)]=E'\phi(\mathbf{r}),\tag{11}$$

where we have placed $E-E_0=E'$. If polarization is neglected, then $\phi(\mathbf{r})$ is the correctly symmetrized wave function of the system.

We can simplify (11) by carrying out the summation over the spins. To do this we first introduce the expression (2) for the potential functions, and thus obtain the equation

$$\begin{aligned}&-\frac{3}{4}\frac{\hbar^2}{M}\Delta\phi(\mathbf{r})-\sum_{\text{spins}}\int d\tau_\rho\chi_S^*\psi_0^*(\rho)\{(g_1+\mathfrak{M}P_{12}+g_2Q_{12}+gP_{12}Q_{12})J(r_{12})[\phi(\mathbf{r})\psi_0(\rho)\chi_S\\&\qquad-P_{12}Q_{12}(\phi(\mathbf{r})\psi_0(\rho)\chi_S)]+(g_1+\mathfrak{M}P_{13}+g_2Q_{13}+gP_{13}Q_{13})\\&\qquad\times J(r_{13})[\phi(\mathbf{r})\psi_0(\rho)\chi_S-P_{12}Q_{12}(\phi(\mathbf{r})\psi_0(\rho)\chi_S)]\}=E'\phi(\mathbf{r}),\end{aligned}\tag{12}$$

where we have placed $\mathfrak{M}=1-g-g_1-g_2$.

On performing the multiplications indicated in the integrand, we see that the following terms are present.

(a) Three terms involving no exchange operators

$$g_1\phi(\mathbf{r})\int d\tau_\rho\psi_0^*(\boldsymbol{\rho})J(r_{12})\psi_0(\boldsymbol{\rho}),$$

$$-g\phi(\mathbf{r})\int d\tau_\rho\psi_0^*(\boldsymbol{\rho})J(r_{12})\psi_0(\boldsymbol{\rho}), \tag{13}$$

$$g_1\phi(\mathbf{r})\int d\tau_\rho\psi_0^*(\boldsymbol{\rho})J(r_{13})\psi_0(\boldsymbol{\rho}).$$

(b) Three terms involving only spin exchange operators

$$g_2\phi(\mathbf{r})\sum_{\text{spins}}\chi_s^*Q_{12}\chi_s\int d\tau_\rho\psi_0^*(\boldsymbol{\rho})J(r_{12})\psi_0(\boldsymbol{\rho}),$$

$$-\mathfrak{M}\phi(\mathbf{r})\sum_{\text{spins}}\chi_s^*Q_{12}\chi_s\int d\tau_\rho\psi_0^*(\boldsymbol{\rho})J(r_{12})\psi_0(\boldsymbol{\rho}), \tag{14}$$

$$g_2\phi(\mathbf{r})\sum_{\text{spins}}\chi_s^*Q_{13}\chi_s\int d\tau_\rho\psi_0^*(\boldsymbol{\rho})J(r_{13})\psi_0(\boldsymbol{\rho}).$$

(c) Three terms involving only space exchange operators

$$\mathfrak{M}\int d\tau_\rho J(r_{12})\psi_0^*(\boldsymbol{\rho})P_{12}\phi(\mathbf{r})\psi_0(\boldsymbol{\rho}),$$

$$-g_2\int d\tau_\rho J(r_{12})\psi_0^*(\boldsymbol{\rho})P_{12}\phi(\mathbf{r})\psi_0(\boldsymbol{\rho}), \tag{15}$$

$$\mathfrak{M}\int d\tau_\rho J(r_{13})\psi_0^*(\boldsymbol{\rho})P_{13}\phi(\mathbf{r})\psi_0(\boldsymbol{\rho}).$$

(d) Seven terms involving both spin and space exchange operators

$$-g_1\sum_{\text{spins}}\chi_s^*Q_{12}\chi_s\int d\tau_\rho\psi_0^*(\boldsymbol{\rho})J(r_{12})P_{12}\phi(\mathbf{r})\psi_0(\boldsymbol{\rho}),$$

$$g\sum_{\text{spins}}\chi_s^*Q_{12}\chi_s\int d\tau_\rho\psi_0^*(\boldsymbol{\rho})J(r_{12})P_{12}\phi(\mathbf{r})\psi_0(\boldsymbol{\rho}),$$

$$-g_1\sum_{\text{spins}}\chi_s^*Q_{12}\chi_s\int d\tau_\rho\psi_0^*(\boldsymbol{\rho})J(r_{13})P_{12}\phi(\mathbf{r})\psi_0(\boldsymbol{\rho}),$$

$$\mathfrak{M}\sum_{\text{spins}}\chi_s^*Q_{12}\chi_s\int d\tau_\rho\psi_0^*(\boldsymbol{\rho})J(r_{13})P_{13}P_{12}\phi(\mathbf{r})\psi_0(\boldsymbol{\rho}), \tag{16}$$

$$-g_2\sum_{\text{spins}}\chi_s^*Q_{13}Q_{12}\chi_s\int d\tau_\rho\psi_0^*(\boldsymbol{\rho})J(r_{13})P_{12}\phi(\mathbf{r})\psi_0(\boldsymbol{\rho}),$$

$$g\sum_{\text{spins}}\chi_s^*Q_{13}\chi_s\int d\tau_\rho\psi_0^*(\boldsymbol{\rho})J(r_{13})P_{13}\phi(\mathbf{r})\psi_0(\boldsymbol{\rho}),$$

$$-g\sum_{\text{spins}}\chi_s^*Q_{13}Q_{12}\chi_s\int d\tau_\rho\psi_0^*(\boldsymbol{\rho})J(r_{13})P_{13}P_{12}\phi(\mathbf{r})\psi_0(\boldsymbol{\rho}).$$

To evaluate the sums over the spins, we need only consider the term $\sum\chi_S^*Q_{12}\chi_S$, since $Q_{13}=Q_{13}Q_{12}=Q_{12}$. This is immediately evident from the fact that the spins of the neutron and proton in the deuteron are parallel. We have in fact

$$\begin{aligned} Q_{12}&=\tfrac{1}{2}(1+\mathfrak{d}_1\cdot\mathfrak{d}_2)\\ &=\tfrac{1}{2}[1+\mathfrak{d}_1\cdot(\mathfrak{d}_2+\mathfrak{d}_3)/2]\\ &=\tfrac{1}{2}(1+\mathfrak{d}_1\cdot\mathfrak{d}_D)=Q_{13}, \end{aligned} \tag{17}$$

where $\mathfrak{d}_D$ is the spin matrix for the deuteron. Also

$$\begin{aligned} Q_{13}Q_{12}\chi_S(1\overline{23})=Q_{13}\chi_S(2\overline{13})&=\chi_S(2\overline{31})\\ &=\chi_S(\overline{213})\\ &=Q_{12}\chi_S(1\overline{23}), \end{aligned} \tag{18}$$

where the bar has been used to indicate the deuteron unit. We can now calculate the matrix element $\sum\chi_S^*Q_{12}\chi_S$ by making use of (17). We have

$$\begin{aligned} \sum_{\text{spins}}\chi_S^*Q_{12}\chi_S&=\tfrac{1}{2}(\sum\chi_S^*\chi_S+\tfrac{1}{2}\sum\chi_S^*\mathfrak{d}_1\cdot\mathfrak{d}_D\chi_S)\\ &=\tfrac{1}{2}(1+\tfrac{1}{2}\sum\chi_S^*\mathfrak{d}_1\cdot\mathfrak{d}_D\chi_S). \end{aligned} \tag{19}$$

We can evaluate the sum in (19) by noting that

$$\begin{aligned} \tfrac{1}{2}\mathfrak{d}_1\cdot\mathfrak{d}_D&=\tfrac{1}{4}(\mathfrak{d}_1+\mathfrak{d}_D)^2-\tfrac{1}{4}\mathfrak{d}_1^2-\tfrac{1}{4}\mathfrak{d}_D^2\\ &=(\tfrac{1}{2}\mathfrak{d}_1+\tfrac{1}{2}\mathfrak{d}_D)^2-(\tfrac{1}{2}\mathfrak{d}_1)^2-(\tfrac{1}{2}\mathfrak{d}_D)^2. \end{aligned} \tag{20}$$

If we remember that the spin of the deuteron is one and denote by S the total spin of our system, then we obtain from (20)

$$\begin{aligned} \tfrac{1}{2}\mathfrak{d}_1\cdot\mathfrak{d}_D&=S(S+1)-(3/4)-2\\ &=S(S+1)-(11/4). \end{aligned}$$

Hence

$$\begin{aligned} \sum\chi_S^*Q_{12}\chi_S=\sum\chi_S^*Q_{13}\chi_S&=\sum\chi_S^*Q_{12}Q_{13}\chi_S\\ &=\tfrac{1}{2}[S(S+1)-(7/4)]. \end{aligned} \tag{21}$$

We must now consider the space exchange operators. From Fig. 1 and Eqs. (3) it can be seen that

$$\begin{aligned} P_{12}\mathbf{r}=P_{12}[\mathbf{r}_1-\tfrac{1}{2}(\mathbf{r}_3+\mathbf{r}_2)]&=\mathbf{r}_2-\tfrac{1}{2}(\mathbf{r}_1+\mathbf{r}_3)\\ &=\mathbf{r}-(3/2)[\mathbf{r}+\tfrac{1}{2}(\mathbf{r}_3-\mathbf{r}_2)]\\ &=-\tfrac{1}{2}(\mathbf{r}+(3/2)\boldsymbol{\varrho}),\\ P_{12}\boldsymbol{\varrho}=P_{12}(\mathbf{r}_3-\mathbf{r}_2)&=\mathbf{r}_3-\mathbf{r}_1=\tfrac{1}{2}\boldsymbol{\varrho}-\mathbf{r}\equiv-\mathbf{r}_{13},\\ P_{13}\mathbf{r}=\mathbf{r}_3-\tfrac{1}{2}(\mathbf{r}_1+\mathbf{r}_2)&=\tfrac{1}{2}(3\boldsymbol{\varrho}/2-\mathbf{r}),\\ P_{13}\boldsymbol{\varrho}=\mathbf{r}_1-\mathbf{r}_2&=-(\mathbf{r}+\tfrac{1}{2}\boldsymbol{\varrho})\equiv\mathbf{r}_{12},\\ P_{13}P_{12}\mathbf{r}=P_{12}\mathbf{r}&=-\tfrac{1}{2}(\mathbf{r}+3\boldsymbol{\varrho}/2),\\ P_{13}P_{12}\boldsymbol{\varrho}=P_{13}(\mathbf{r}_3-\mathbf{r}_1)&=-(\mathbf{r}_1-\mathbf{r}_3)=-P_{12}\boldsymbol{\varrho}=\mathbf{r}-\tfrac{1}{2}\boldsymbol{\varrho}. \end{aligned} \tag{22}$$

If we now introduce (21) and (22) into (14), (15), and (16) and collect terms, we obtain the follow-

ing integrals:

$$[g_1-g+\tfrac{1}{2}(g_2-\mathfrak{M})\{S(S+1)-(7/4)\}]\phi(\mathbf{r})\int d\tau_\rho\psi_0^*(\boldsymbol{\rho})J(|\mathbf{r}+\tfrac{1}{2}\boldsymbol{\rho}|)\psi_0(\boldsymbol{\rho}),$$

$$[g_1+\tfrac{1}{2}g_2\{S(S+1)-(7/4)\}]\phi(\mathbf{r})\int d\tau_\rho\psi_0^*(\boldsymbol{\rho})J(|\tfrac{1}{2}\boldsymbol{\rho}-\mathbf{r}|)\psi_0(\boldsymbol{\rho}),$$

$$[\mathfrak{M}-g_2+\tfrac{1}{2}(g-g_1)\{S(S+1)-(7/4)\}]\int d\tau_\rho\psi_0^*(\boldsymbol{\rho})J(|\mathbf{r}+\tfrac{1}{2}\boldsymbol{\rho}|)\phi(\tfrac{1}{2}\mathbf{r}+\tfrac{3}{4}\boldsymbol{\rho})\psi_0(\tfrac{1}{2}\boldsymbol{\rho}-\mathbf{r}), \quad (23)$$

$$[\mathfrak{M}+\tfrac{1}{2}g\{S(S+1)-(7/4)\}]\int d\tau_\rho\psi_0^*(\boldsymbol{\rho})J(|\tfrac{1}{2}\boldsymbol{\rho}-\mathbf{r}|)\phi(\tfrac{3}{4}\boldsymbol{\rho}-\tfrac{1}{2}\mathbf{r})\psi_0(\tfrac{1}{2}\boldsymbol{\rho}+\mathbf{r}),$$

$$-[\mathfrak{M}+g_1+g_2+g]\tfrac{1}{2}[S(S+1)-(7/4)]\int d\tau_\rho\psi_0^*(\boldsymbol{\rho})J(|\tfrac{1}{2}\boldsymbol{\rho}-\mathbf{r}|)\phi(\tfrac{1}{2}\mathbf{r}+\tfrac{3}{4}\boldsymbol{\rho})\psi_0(\tfrac{1}{2}\boldsymbol{\rho}-\mathbf{r}).$$

Since all the functions appearing under the integral signs depend only on the magnitudes of their vector arguments, we can combine the first and second and the third and fourth of the expressions (23). We are then left with three terms

$$[2g_1-g+(2g_2-\mathfrak{M})\varkappa]\phi(\mathbf{r})\int d\tau_\rho\psi_0^*(\boldsymbol{\rho})J(|\tfrac{1}{2}\boldsymbol{\rho}+\mathbf{r}|)\psi_0(\boldsymbol{\rho}),$$

$$[2\mathfrak{M}-g_2+(2g-g_1)\varkappa]\int d\tau_\rho\psi_0^*(\boldsymbol{\rho})J(|\tfrac{1}{2}\boldsymbol{\rho}+\mathbf{r}|)\phi(\tfrac{1}{2}\mathbf{r}+\tfrac{3}{4}\boldsymbol{\rho})\psi_0(\tfrac{1}{2}\boldsymbol{\rho}-\mathbf{r}), \quad (24)$$

$$-\varkappa\int d\tau_\rho\psi_0^*(\boldsymbol{\rho})J(|\tfrac{1}{2}\boldsymbol{\rho}-\mathbf{r}|)\phi(\tfrac{3}{4}\boldsymbol{\rho}+\tfrac{1}{2}\mathbf{r})\psi_0(\tfrac{1}{2}\boldsymbol{\rho}-\mathbf{r}).$$

In these expressions we have introduced the abbreviation $\varkappa=[\frac{1}{2}S(S+1)-(7/4)]$, and we have also made use of the definition of $\mathfrak{M}$.

On substituting (24) into the wave equation, we obtain

$$\Delta\phi(\mathbf{r})+k^2\phi(\mathbf{r})=(2\mu/\hbar^2)\Big\{\varkappa\int d\tau_\rho\psi_0^*(\boldsymbol{\rho})J(|\tfrac{1}{2}\boldsymbol{\rho}-\mathbf{r}|)\phi(\tfrac{3}{4}\boldsymbol{\rho}+\tfrac{1}{2}\mathbf{r})\psi_0(\tfrac{1}{2}\boldsymbol{\rho}-\mathbf{r})$$

$$-[2\mathfrak{M}-g_2+(2g-g_1)\varkappa]\int d\tau_\rho\psi_0^*(\boldsymbol{\rho})J(|\tfrac{1}{2}\boldsymbol{\rho}+\mathbf{r}|)\phi(\tfrac{1}{2}\mathbf{r}+\tfrac{3}{4}\boldsymbol{\rho})\psi_0(\tfrac{1}{2}\boldsymbol{\rho}-\mathbf{r})$$

$$-[2g_1-g+(2g_2-\mathfrak{M})\varkappa]\phi(\mathbf{r})\int d\tau_\rho\psi_0^*(\boldsymbol{\rho})J(|\tfrac{1}{2}\boldsymbol{\rho}+\mathbf{r}|)\psi_0(\boldsymbol{\rho})\Big\} \quad (25)$$

where we have placed $\mu=\frac{3}{4}M$ and $k^2=(2\mu/\hbar^2)E'$. Since we are seeking the solution of this equation which has the asymptotic form

$$\phi(\mathbf{r})\rightarrow\exp[i\mathbf{k}\cdot\mathbf{r}]+(1/r)e^{ikr}f(\theta),$$

we may replace (25) by the integral equation[4]

$$\phi(\mathbf{r})=\exp[i\mathbf{k}\cdot\mathbf{r}]+\frac{\mu}{2\pi\hbar^2}\Big\{[2\mathfrak{M}-g_2+(2g-g_1)\varkappa]\int\int\frac{d\tau_\xi d\tau_\rho}{|\mathbf{r}-\boldsymbol{\xi}|}\exp[ik|\mathbf{r}-\boldsymbol{\xi}|]\psi_0^*(\boldsymbol{\rho})J(|\tfrac{1}{2}\boldsymbol{\rho}+\boldsymbol{\xi}|)\psi(\tfrac{3}{4}\boldsymbol{\rho}+\tfrac{1}{2}\boldsymbol{\xi})$$

$$\times\psi_0(\tfrac{1}{2}\boldsymbol{\rho}-\boldsymbol{\xi})+[2g_1-g+(2g_2-\mathfrak{M})\varkappa]\int\int d\tau_\xi d\tau_\rho\frac{\exp[ik|\mathbf{r}-\boldsymbol{\xi}|]}{|\mathbf{r}-\boldsymbol{\xi}|}\psi_0^*(\boldsymbol{\rho})J(|\tfrac{1}{2}\boldsymbol{\rho}+\boldsymbol{\xi}|)\psi_0(\boldsymbol{\rho})\phi(\boldsymbol{\xi})$$

$$-\varkappa\int\int d\tau_\xi d\tau_\rho\frac{\exp[ik|\mathbf{r}-\boldsymbol{\xi}|]}{|\mathbf{r}-\boldsymbol{\xi}|}\psi_0^*(\boldsymbol{\rho})J(|\tfrac{1}{2}\boldsymbol{\rho}-\boldsymbol{\xi}|)\phi(\tfrac{3}{4}\boldsymbol{\rho}+\tfrac{1}{2}\boldsymbol{\xi})\psi_0(\tfrac{1}{2}\boldsymbol{\rho}-\boldsymbol{\xi})\Big\}. \quad (26)$$

[4] N. E. Mott and H. S. Massey, *The Theory of Atomic Collisions* (Oxford Univ. Press, New York, 1933), Chapter IV.

We can simplify this equation slightly by introducing new variables. We first replace ϱ by $-\varrho$, which results in the following changes:

$$J(|\tfrac{1}{2}\varrho+\xi|)\rightarrow J(|\xi-\tfrac{1}{2}\varrho|),$$
$$\phi(\tfrac{3}{4}\varrho+\tfrac{1}{2}\xi)\rightarrow\phi(\tfrac{1}{2}\xi-\tfrac{3}{4}\varrho),$$
$$\psi_0(\tfrac{1}{2}\varrho-\xi)\rightarrow\psi_0(\tfrac{1}{2}\varrho+\xi).$$
$$J(|\tfrac{1}{2}\varrho-\xi|)\rightarrow J(|\tfrac{1}{2}\varrho+\xi|),$$

all the other quantities in the integrands remaining unchanged. We next introduce the new variables r' and r'' defined by

$$\mathbf{r}'=\tfrac{3}{4}\varrho-\tfrac{1}{2}\xi;\quad \mathbf{r}''=\xi$$

in the first and third integrals and by

$$\mathbf{r}'=\xi,\quad \mathbf{r}''=\varrho$$

in the second integral. (26) now becomes

$$\phi(\mathbf{r})=\exp[i\mathbf{k}\cdot\mathbf{r}]+\frac{32\mu}{27\pi\hbar^2}[2\mathfrak{M}-g_2+(2g-g_1)\varkappa]\int\int\frac{d\tau'd\tau''}{|\mathbf{r}-\mathbf{r}''|}\exp[ik|\mathbf{r}-\mathbf{r}''|]\psi_0^*((4/3)\mathbf{r}'+\tfrac{2}{3}\mathbf{r}'')$$
$$\times J(|\tfrac{2}{3}(\mathbf{r}''-\mathbf{r}')|)\psi_0(\tfrac{2}{3}\mathbf{r}'+(4/3)\mathbf{r}'')\phi(\mathbf{r}')+\frac{\mu}{2\pi\hbar^2}[2g_1-g+(2g_2-\mathfrak{M})\varkappa]\int\int\frac{d\tau'd\tau''}{|\mathbf{r}-\mathbf{r}'|}$$
$$\times\exp[ik|\mathbf{r}-\mathbf{r}'|]\psi_0^*(\mathbf{r}'')J(|\tfrac{1}{2}\mathbf{r}''+\mathbf{r}'|)\psi_0(\mathbf{r}'')\phi(\mathbf{r}')-\frac{32\mu}{27\pi\hbar^2}\varkappa\int\int\frac{d\tau'd\tau''}{|\mathbf{r}-\mathbf{r}''|}$$
$$\times\psi_0^*((4/3)\mathbf{r}'+\tfrac{2}{3}\mathbf{r}'')J(|\tfrac{2}{3}\mathbf{r}'+(4/3)\mathbf{r}''|)\psi_0(\tfrac{2}{3}\mathbf{r}'+(4/3)\mathbf{r}'')\phi(\mathbf{r}'). \quad (27)$$

In this paper we shall consider only the scattering of very slow neutrons, so that we may place $k=0$ in (27). On doing this we obtain the integral equation in its final form

$$\phi(\mathbf{r})=1+\frac{32\mu}{27\pi\hbar^2}[2\mathfrak{M}-g_2+(2g-g_1)\varkappa]\int\int\frac{d\tau'd\tau''}{|\mathbf{r}-\mathbf{r}''|}\psi_0^*((4/3)\mathbf{r}'+\tfrac{2}{3}\mathbf{r}'')J(|\tfrac{2}{3}\mathbf{r}''-\tfrac{2}{3}\mathbf{r}'|)\psi_0(\tfrac{2}{3}\mathbf{r}'+(4/3)\mathbf{r}'')$$
$$\times\phi(\mathbf{r}')+\frac{\mu}{2\pi\hbar^2}[2g_1-g+(2g_2-\mathfrak{M})\varkappa]\int\int\frac{d\tau'd\tau''}{|\mathbf{r}-\mathbf{r}'|}\psi_0^*(\mathbf{r}'')J(|\tfrac{1}{2}\mathbf{r}''+\mathbf{r}'|)\psi_0(\mathbf{r}'')\phi(\mathbf{r}')$$
$$-\frac{32\mu}{27\pi\hbar^2}\varkappa\int\int\frac{d\tau'd\tau''}{|\mathbf{r}-\mathbf{r}''|}\psi_0^*((4/3)\mathbf{r}'+\tfrac{2}{3}\mathbf{r}'')J(|\tfrac{2}{3}\mathbf{r}'+(4/3)\mathbf{r}''|)\psi_0(\tfrac{2}{3}\mathbf{r}'+(4/3)\mathbf{r}'')\phi(\mathbf{r}'). \quad (28)$$

Transforming the Integral Equation to a Form Suitable for Numerical Integration

Before we can proceed to the numerical integration of (28), we must specify the functional forms of J and $\psi_0(r)$. To facilitate the numerical work, we must choose these so as to make the integrands fall off very rapidly. For this reason we have chosen a Gauss function for J

$$J(|\mathbf{r}_{ij}|)=V_0\exp[-r_{ij}^2/a^2]$$

with the depth V_0 and the range a the same for the interactions between like and unlike particles.

For a Gauss potential the ground state wave function of the deuteron can be obtained only by quadratures, so that we have a graph but not an analytical expression for this function. To simplify the calculations we have replaced the numerical solution for ψ_0 by a sum of two Gauss functions.

For $V_0=72mc^2$ and for $a=0.25(\hbar/(Mm)^{\frac{1}{2}}c)$ cm [5]

[5] In a recent paper, Phys. Rev. **55**, 1018 (1939) Breit, Thaxton and Eisenbud have suggested a somewhat shorter range and deeper well than those here used. Since our calculations had already proceeded considerably at the time of the publication of this paper, we did not use these values. An examination of the integral equation (31) would seem to indicate that the use of the smaller range would reduce and thus somewhat improve the value of the cross section obtained.

the function

$$\psi_0(r)=(1.23\pi^{\frac{1}{2}}a^3)^{-\frac{1}{2}} \times(0.80e^{-0.60(r^2/a^2)}+0.12e^{-0.056(r^2/a^2)}) \quad (29)$$

approximates the exact wave function sufficiently well for our purpose. The graphical fit is extremely good for small values of r/a, and only for $r/a>4$ does the deviation from the exact curve begin to become important. As a check on the wave function (29), we calculated the amount of binding energy given by it and found that it gives all but about 6 percent.

With these expressions for J and ψ_0 we can now simplify (28) by integrating over the configuration space of r''. All the integrations which have to be performed are of the type

$$\int \frac{d\tau_{\mathbf{X}}}{X}\exp -\frac{1}{a^2}\{(m^2\beta+n^2\alpha+p^2)r'^2+(n^2\beta+m^2\alpha+q^2)r^2+(n^2\beta+m^2\alpha+q^2)X^2 +2mn(\beta+\alpha+pq/mn)\mathbf{r}\cdot\mathbf{r}'-2[mn(\alpha+\beta+pq/mn)\mathbf{r}'+(m^2\alpha+\beta^2+q^2)\mathbf{r}]\cdot\mathbf{X}\},$$

where we have placed $\mathbf{X}=\mathbf{r}-\mathbf{r}''$ and where the constants m, n, p, q are the coefficients of $\mathbf{r}'$ and $\mathbf{r}''$ in the arguments of ψ_0 and J. α and β are the constants which appear in the exponents of (29) which we rewrite in the form

$$\psi_0(r)=A\ \exp\ [-\alpha(r/a)^2]+B\ \exp\ [-\beta(r/a)^2].$$

The integration over $\mathbf{X}$ can be carried out by transforming to spherical coordinates and introducing

$$2\{mn[\alpha+\beta+(pq/mn)]\mathbf{r}'+(m^2\alpha+\beta^2+q^2)\mathbf{r}\}$$

as the polar axis. After the integration over $\mathbf{X}$ is performed, there remains an integral over the $\mathbf{r}'$ space.

Since $\phi(\mathbf{r}')$ is independent of angle, we can integrate over the angles and thus obtain the integral equation in a form which is suitable for numerical calculation. Since the details of the analytical integration are straightforward and uninteresting, we shall merely give the equation in its final form

$$\phi(r)=1+\frac{24\pi}{\hbar^2}\frac{\mu V_0a^4}{r}\Bigg\{[2\mathfrak{M}-g_2+(2g-g_1)\varkappa]\int_0^\infty dr'r'\phi(r')\sum_{i,j=1,2}A_{ij}\frac{\exp\left[-\frac{4(\alpha^{ij}+\beta^{ij}+\alpha^{ij}\beta^{ij})}{a^2(4\alpha^{ij}+\beta^{ij}+1)}r'^2\right]}{(2\alpha^{ij}+2\beta^{ij}-1)(4\alpha^{ij}+\beta^{ij}+1)}$$

$$\times\Omega\left[\frac{2(2\alpha^{ij}+2\beta^{ij}-1)r'+2(4\alpha^{ij}+\beta^{ij}+1)r}{3a(4\alpha^{ij}+\beta^{ij}+1)^{\frac{1}{2}}}\right]+\frac{2\pi^{\frac{1}{2}}}{3}[2g_1-g+(2g_2-\mathfrak{M})\varkappa]\int_0^\infty dr'r'^2\phi(r')$$

$$\times\sum_{i,j=1,2}A_{ij}\frac{\exp\left[-\frac{4}{a^2}\frac{(\alpha^{ij}+\beta^{ij})}{(4\alpha^{ij}+4\beta^{ij}+1)}r'^2\right]}{(1+4\alpha^{ij}+4\beta^{ij})^{\frac{1}{2}}}-\varkappa\int_0^\infty dr'r'\phi(r')$$

$$\sum_{i,j=1,2}A_{ij}\frac{\exp\left[-\frac{4}{a^2}\frac{\beta^{ij}(\alpha^{ij}+1)}{(4\alpha^{ij}+\beta^{ij}+4)}r'^2\right]}{(2\alpha^{ij}+2\beta^{ij}+2)(\beta^{ij}+4\alpha^{ij}+4)}\Omega\left[\frac{2(2\alpha^{ij}+2\beta^{ij}+2)r'+2(\beta^{ij}+4\alpha^{ij}+4)r}{3a(\beta^{ij}+4\alpha^{ij}+4)^{\frac{1}{2}}}\right]\Bigg\}, \quad (30)$$

where we have used the following notation:

$$A_{11}=A^2;\quad A_{12}=A_{21}=AB;\quad A_{22}=B^2;\quad \alpha^{11}=\beta^{11}=\alpha;\quad \alpha^{12}=\beta^{12}=\alpha;\quad \beta^{21}=\alpha^{21}=\beta;\quad \alpha^{22}=\beta^{22}=\beta.$$

The function $\Omega(br'+cr)$ which appears in the integrands of (30) is an abbreviation for the difference of the integrals of error functions

$$\Omega(br'+cr)=\Lambda(br'+cr)-\Lambda(br'-cr),$$

where

$$\Lambda(x)=\int_0^x E(y)dy,\quad E(y)=\int_0^y e^{-z^2}dz.$$

If we place $r/a=x$ and $r'/a=\xi$, and introduce the numerical values for A, B, α, β into (30), we obtain

$$\phi(ax)=1+\frac{24}{\hbar^2}\frac{\mu}{\pi^{1/2}}\frac{V_0a^2}{(1.23)x}\Big\{[2\mathfrak{M}-g_2+(2g-g_1)x]\int_0^\infty d\xi\xi\phi(a\xi)[0.115e^{-1.56\xi^2}\Omega(1.33x+0.467\xi)$$
$$+0.0890e^{-0.798\xi^2}\Omega(1.24x+0.112\xi)+0.169e^{-1.51\xi^2}\Omega(0.900x+0.154\xi)$$
$$+0.0145e^{-0.360}\Omega(0.900x+0.458\xi)]+\frac{2\pi^{1/2}}{3}[2g_1-g+(2g_2-\mathfrak{M})x]\int_0^\infty d\xi\xi^2\phi(a\xi)$$
$$\times[0.0113e^{-0.828\xi^2}+0.0294e^{-0.724\xi^2}+0.00826e^{-0.309\xi^2}]$$
$$-x\int_0^\infty d\xi\xi\phi(a\xi)[0.0208e^{-0.549\xi^2}\Omega(1.76x+1.11\xi)+0.00449e^{-0.0555\xi^2}\Omega(1.70x+0.869\xi)$$
$$+0.00601e^{-0.525\xi^2}\Omega(1.46x+1.01\xi)+0.00144e^{-0.0553\xi^2}\Omega(2.03x+0.487\xi)]\Big\}. \quad (31)$$

The Numerical Integration

We integrated (31) numerically for two different sets of constants $\mathfrak{M}$, g, g_1, g_2. This involved solving four sets of equations because both the doublet scattering ($S=\frac{1}{2}$) and the quartet scattering ($S=\frac{3}{2}$) had to be calculated separately for each set of constants. The method adopted for solving the equations was that of replacing the integrals in (31) by sums extended over a finite number of rapidly converging terms. A brief examination of the exponentials and the functions $\Omega(bx+c\xi)$ which appear in the integrands (tables of these functions were prepared with little labor) shows that for $\xi \gtrless 13$ the contributions to the integrals are zero to our order of accuracy.

By means of Simpson's one-third rule we replaced each integral by a sum of twenty terms extended over the interval from $\xi=0$ to $\xi=13$. In this way we obtained a set of twenty simultaneous equations for each of the four groups of constants. Because of the presence of the Ω functions and the rapid convergence of the other factors in the integrands, the coefficients of the $\phi(ax_i)$ ($i=0, 1, \cdots$) in the later equations approach constant values quite rapidly. This enabled us to reduce our equations to the following form with very little labor:

$$a_{00}\phi(0)+\sum_{i=1}^{19}a_{0i}\phi(x_ia) = C_0,$$
$$0 + a_{11}\phi(x_1a) + \sum_{i=2}^{19}a_{1i}(x_ia) = C_1,$$
$$0 + 0 + a_{22}\phi(x_2a) + \sum_{i=3}^{19}a_{2i}\phi(x_ia) = C_2,$$
$$\cdots\cdots\cdots\cdots\cdots$$
$$0 + 0 + 0 + \cdots + a_{19,19}\phi(13a) = C_{19}.$$

From the last of these equations the value of ϕ(13a) can be read off directly, and since this is the asymptotic value of the wave function, the total cross section can be expressed in terms of it as follows:

$$\sigma_t=\int\sigma(\theta)d\omega=2\pi\int|f(\theta)|^2\sin\theta d\theta$$
$$=2\pi\int(13a)^2|\phi(13a)-1|^2\sin\theta d\theta. \quad (32)$$

We shall now give the results of our calculations for two special choices of the potential.

Case I. $g_1=g_2=0$; $g=0.2$; $\mathfrak{M}=0.8$.

It has been shown by Breit and Feenberg[3] that the values of the g's which may be selected in an interaction of type (2) are restricted by certain inequalities which are obtained from the consideration of the stability of nuclei. The simplest set of values satisfying all the requirements is obtained by placing $g_1=g_2=0$. Combining this with the empirical value $g+g_2=0.2$, we obtain $g=0.2$.

If we substitute this set of values in (31), the numerical integration can be performed for each value of $\varkappa$ separately. Since the doublet and quartet states are orthogonal,[1] no doublet→quartet or quartet→doublet transitions take place during the process. For this reason we may calculate the doublet and quartet cross sections separately and then combine the two in the ratio 2 : 1 to give the total cross section.

For the doublet (d) scattering we have $S=\frac{1}{2}$, $\varkappa=-\frac{1}{2}$, and we find from our equations $\phi_d(13a)=1.055$. Hence we have

$$|f_d(\theta)|=|\phi_d(13a)-1|(13a)=1.59\times10^{-13}\text{ cm}. \quad (33)$$

For the quartet (q) scattering we have $S=\frac{3}{2}$, $\varkappa=1$, and we obtain $\phi_q(13a)=0.749$. This gives us

$$|f_q(\theta)|=|\phi_q(13a)-1|(13a)=7.30\times10^{-13}\text{ cm}. \quad (34)$$

From (33) and (34) we can now obtain the total cross section

$$\sigma_t=(4\pi/3)(2|f_q(\theta)|^2+|f_d(\theta)|^2)=4.57\times10^{-24}\text{ cm}^2. \quad (35)$$

Case II. $g=0.22-g_2$; $g_1=0.25-0.8g_2$; $g_2=2$.

Another possible choice of g values has been given by Inglis.[6] The restrictions which are to be placed on the g's can be summarized by means of the inequality

$$1.25\gtrless1+5g_1+4g_2.$$

If a low enough binding energy is to be obtained for Li^6, the choice of g's must be limited to a one-parameter family defined by the relations

$$g=0.22-g_2;\quad g_1=0.25-0.8g_2.$$

With these relations the demands of the experimental data are best met by choosing $g_2=2$. It should be noted that for this case the potential function is a mixture of all four types of interactions.

Proceeding just as we did for case I, we obtain the following results:

$$\phi_d(13a)=0.820;\quad f_d(\theta)=5.24\times10^{-13}\text{ cm}$$
$$\phi_q(13a)=0.715;\quad f_q(\theta)=8.29\times10^{-13}\text{ cm}. \quad (36)$$

From (36) we obtain the total cross section for this case

$$\sigma_t=(4\pi/3)(2|f_q(\theta)|^2+|f_d(\theta)|^2)=6.91\times10^{-24}\text{ cm}^2. \quad (37)$$

Comparison with Experiment

The best experimental data on the scattering of slow neutrons by deuterons are to be found in the recent work of Carroll and Dunning (unpublished),[7] who obtained a value of 5.7×10^{-24} cm^2 for the cross section. If one takes molecular binding into account, this value has to be reduced by a factor that lies between 1.5 and 2[1,2] before it can be compared with the theoretical values. The actual value of the reduction factor is determined by the strength of the molecular binding; it is equal to 2 for infinite binding but may be as small as 1.5 for weak binding.

We see that the experimental value agrees best with the theoretical value obtained for case I. This would seem to argue in favor of the first set of g's (Heisenberg and Majorana forces only) as against that given by Inglis (Wigner and Bartlett forces in addition to the other two).

Even if we take 1.5 as the reduction factor, we see that the experimental value is about 20 percent lower than the theoretical value found for case I. This discrepancy can certainly not be accounted for by the approximations introduced

[6] D. R. Inglis, Phys. Rev. **51**, 531 (1937).

[7] We should like to express our thanks to Mr. Carroll and Professor Dunning for informing us of their results before publication.

to enable us to carry out the numerical integration of Eq. (28). These were twofold: The ground state wave function of the deuteron was approximated by a sum of two Gauss functions, and the integrals were replaced by sums over finite intervals. The first of these approximations can at most account for a few percent of the discrepancy because the assumed wave function for the deuteron deviates measurably from the true wave function only for large values of r/a, and it is just for these values of r/a that the contributions to the integrals are negligible. As we have already seen, the second approximation is not serious because of the rapid convergence of the integrals.

Since we have neglected polarization in this paper, it may well be that taking it into account will get rid of most of the discrepancy, provided an interaction energy of type (2) is adequate for the process we are considering. Although a calculation taking polarization into account would be exceedingly difficult, its undertaking at the present time seems warranted.

We wish to thank Mr. Jerome Rothstein of Columbia University for aiding in the numerical work.

JULY 1, 1940 PHYSICAL REVIEW VOLUME 58

Multiple Scattering of Electrons. II

S. GOUDSMIT AND J. L. SAUNDERSON*
University of Michigan, Ann Arbor, Michigan
(Received April 22, 1940)

The series developed in a previous paper representing the distribution for the multiple scattering of electrons has been evaluated numerically for a large number of cases; the results are given in Table I. An approximate expression is found for the value of sin θ averaged over the distribution per unit solid angle, $f(\theta)$. This expression, which agrees within a few percent with the exact computation, is

$$w\langle\sin\theta\rangle_{Av}\sim 1.76A^{\frac{1}{2}}(5.60-\tfrac{1}{3}\log Z+\tfrac{1}{2}\log A)^{\frac{1}{2}}, \quad (18)$$

in which w is the energy in units mc^2 and $A=24.8\times10^{-26}Z^2Nt$. For the scattering intensity per unit solid angle at 0°, that is $f(0)$, an approximate relation is

$$4\pi f(0)/w^2\sim 0.43/A(5.60-\tfrac{1}{3}\log Z+\tfrac{1}{2}\log A). \quad (19)$$

The accurate calculations show also that $f(\theta)/w^2$ is almost independent of the energy. A series formula is derived for the projected scattering distribution as observed in a cloud chamber. The averages of $w\sin\alpha$, α being the projected angle, are given in Table VI. These averages are smaller than the values computed by Williams and show a variation with energy. It is believed that the largest inaccuracy remaining in the results given is due to uncertainties in the single scattering law.

1. INTRODUCTION

IN a previous paper[1] we have treated the statistical problem of multiple electron scattering by thin foils. The principal purpose of the present article is to bring the results of that paper into a form which can be more easily compared with experimental data.

We consider an electron of total energy w (in units mc^2) which has traveled a path length t through scattering material of atomic number Z containing N atoms per cc. The normalized probability that the electron will be deflected into the angle between θ and $\theta+d\theta$ is given by the following series in Legendre polynomials

$$2\pi f(\theta)\sin\theta d\theta = \tfrac{1}{2}\sum(2l+1)G_lP_l(\cos\theta)\sin\theta d\theta. \quad (1)$$

The coefficients G_l depend only upon two param-

* Now at the Dow Chemical Company.
[1] S. Goudsmit and J. L. Saunderson, Phys. Rev. **57**, 24 (1940).

eters, μ and ξ,

$$G_l=\exp\{-2\mu l(l+1)\times[\log\xi-(\tfrac{1}{2}+\tfrac{1}{3}+\cdots 1/l)]\}. \quad (2)$$

The parameter μ is proportional to the path length,

$$\mu=\pi\kappa^2Nt=\pi\{Ze^2w/mc^2(w^2-1)\}^2Nt$$
$$=24.8\times10^{-26}Z^2Ntw^2/(w^2-1)^2$$
$$=0.151(\sigma Z^2/M)w^2/(w^2-1)^2. \quad (3)$$

In the last expression which is the most convenient one to use, σ is the superficial density of the foil in grams per cm^2 and M the atomic mass. The path length should, however, not be taken equal to the thickness of the foil but as a first approximation, may be taken as the thickness divided by the average of cos θ, that is, G_1. If this correction amounts to more than a few percent, the present theory is no longer sufficiently accurate.

The other parameter ξ depends upon the deviation of the true single scattering probability from the Rutherford law as a result of screening by orbital electrons. For a Thomas-Fermi atom, using the Born approximation, we find[2]

$$\xi=150(w^2-1)^{\frac{1}{2}}/Z^{\frac{1}{3}}. \quad (4)$$

For heavy elements the Born approximation may not be sufficient and for light elements the Thomas-Fermi atom may give inaccurate results. This causes some uncertainty in the numerical factor. Fortunately this has little influence upon the final results, but may well explain eventual small discrepancies between theory and experimental data.

2. The Scattering per Unit Solid Angle

The scattering per unit solid angle in the direction θ is $f(\theta)$, for which we have

$$4\pi f(\theta)=\sum(2l+1)G_lP_l(\cos\theta). \quad (5)$$

Table I shows the results of computations of $4\pi f(\theta)$ for twenty-one cases, for some of which as many as forty-eight terms in the series were used. In order to have a series which converges sufficiently rapidly, μ must be large enough that G_l becomes negligibly small when $l\ll\xi$. When this condition is not fulfilled the scattering is very nearly single. In such a case the exponent of Eq. (2) is no longer sufficiently accurate for the high terms in the series.

The table also gives the Rutherford single scattering, $\mu/\sin^4(\theta/2)$ for $\theta=45°$. With the exception of possibly eight cases, single scattering has evidently not yet been approached at that angle. It must be remarked, however, that the frequent change of sign of the P_l for the larger angles makes the results of the series computation less accurate than for the smaller angles.

3. The Average Sin θ

A quantity which is most easily computed and observed is the value of sin θ averaged over the scattering distribution per unit solid angle. This is defined as

$$\langle\sin\theta\rangle_{Av}=\int_0^\pi f(\theta)\sin\theta d\theta\Big/\int_0^\pi f(\theta)d\theta. \quad (6)$$

Substituting for $f(\theta)$ the series of Eq. (5), we see at once that all terms in the numerator except

Table I.* *Values of $4\pi f(\theta)$.*

	Appr.† 0°	0°	6°	12°	18°	24°	30°	45°	Ruth. 45°
log ξ=4									
μ=0.0025	107	120.9	72.6	26.3	8.3	2.7	1.1	0.1	0.12
0.0050	44.1	45.7	38.6	24.3	12.5	5.8	2.7	0.5	0.23
0.010	18.7	19.1	17.9	14.8	11.0	7.4	4.7	1.3	0.46
0.015	11.5	11.8	11.4	10.2	8.5	6.6	4.9	1.9	0.70
log ξ=5									
μ=0.0015	122	122.4	81.2	27.9	7.1	1.9	0.6	0.1	0.07
0.0025	66.0	65.8	53.1	28.9	11.8	4.2	1.5	0.2	0.12
0.0050	29.2	29.2	26.6	20.3	13.1	7.5	3.9	0.7	0.23
0.010	13.1	13.3	12.7	11.3	9.4	7.1	5.1	1.8	0.46
log ξ=6									
μ=0.0005	307	303.2	118.8	13.6	1.5	0.6	0.3		0.02
0.0015	85.6	85.3	65.3	30.6	9.8	2.7	0.9		0.07
0.0025	47.6	47.5	41.1	26.8	13.7	5.8	2.2	0.3	0.12
0.0050	21.8	21.9	20.5	16.9	12.3	8.0	4.7	1.0	0.23
0.010	10.2	10.3	10.0	9.2	7.9	6.5	5.0	2.2	0.46
log ξ=7									
μ=0.0005	226	224.3	113.9	19.0	2.2	0.5	0.3		0.02
0.0015	66.0	66.1	54.2	30.4	12.3	4.0	1.2	0.1	0.07
0.0025	37.3	37.7	34.7	24.9	14.2	7.0	3.0	0.4	0.12
0.0050	17.4	17.8	17.0	14.5	11.3	8.3	5.2	1.3	0.23
log ξ=8									
μ=0.0005	179	179.2	104.8	24.1	2.8	0.5	0.2		0.02
0.0015	53.6	54.3	46.3	28.9	13.6	5.1	1.1	0.1	0.07
0.0025	30.7	31.3	28.6	21.8	14.0	9.6	3.7	0.5	0.12
0.0050	14.5	15.0	14.4	13.0	10.2	7.7	5.3	1.6	0.23

* The normalizing factor is given by Eq. (8).
† The values in this column were obtained from the approximate Eq. (15).

[2] For a Wentzel potential the numerical factor is 160. Compare Eqs. (I 36) and (I 35). We shall denote equations in the first paper (reference 1) by a Roman I.

TABLE II.* *Average values of sin θ.*

log ξ = 4		5	6	7	8
μ = 0.00050			0.0667 (0.0656)	0.0768 (0.0764)	0.0853 (0.0859)
0.00075		0.0702 (0.0679)	0.0835 (0.0832)	0.0960 (0.0960)	0.1063 (0.1073)
0.0010	0.059 (0.059)	0.0826 (0.0816)	0.0995 (0.0981)	0.113 (0.113)	0.124 (0.127)
0.0015	0.078 (0.079)	0.106 (0.104)	0.125 (0.124)	0.141 (0.142)	0.154 (0.157)
0.0025	0.111 (0.111)	0.143 (0.142)	0.166 (0.166)	0.184 (0.188)	0.202 (0.208)
0.0050	0.174 (0.173)	0.212 (0.213)	0.242 (0.246)	0.266 (0.276)	0.288 (0.303)
0.010	0.262 (0.266)	0.307 (0.319)	0.342 (0.364)	0.374 (0.404)	0.402 (0.440)
0.015	0.327 (0.340)				

* The values given in parenthesis were found using the approximate Eq. (14).

the first vanish and that the denominator can be obtained from the development of cosec θ in a series of Legendre polynomials. Thus

$$\langle \sin\theta\rangle_{Av} = 2/\pi \sum_{\text{even } l} (2l+1) G_l \left(\frac{1\cdot 3\cdot 5\cdots l-1}{2\cdot 4\cdot 6\cdots l}\right)^2$$

$$= 1/2(0.786 + 0.983G_2 + 0.995G_4 + G_6 + \cdots). \quad (7)$$

The coefficients in Eq. (7) approach a common value very rapidly. The values of $\langle \sin\theta\rangle_{Av}$ computed in this way are entered in Table II.

The scattering per unit solid angle, $f(\theta)$, is not normalized to unity. The normalizing factor for the entries of Table I is given by

$$4\pi \int_0^\pi f(\theta) d\theta = 4\pi/\langle \sin\theta\rangle_{Av}. \quad (8)$$

These values can be computed with the help of Table II.

4. Approximate Formulas

If it were permissible to replace the partial harmonic series in the exponent of G_l by some constant average value, s, it would not be difficult to obtain an approximate value for the sum[3] of Eq. (7), for instance, by replacing it by an integral. Abbreviating

$$\gamma^2 = 2\mu[\log \xi - s], \quad (9)$$

we find that, approximately,

$$\langle \sin\theta\rangle_{Av} \sim 1 \Big/ \int_0^\infty e^{-\gamma^2 l^2} dl = (4\gamma^2/\pi)^{\frac{1}{2}}. \quad (10)$$

Similarly, for $\theta = 0$ we find from Eq. (5)

$$4\pi f(0) \sim \sum (2l+1) e^{-\gamma^2 l(l+1)} \sim 1/\gamma^2. \quad (11)$$

It is also possible to show that with the same degree of approximation the distribution may be represented by a Gaussian expression in

$$y = \sin\theta/2,$$

namely,

$$4\pi f(\theta) \sim e^{-y^2/\gamma^2}/\gamma^2. \quad (12)$$

This can be verified, for example, by expanding Eq. (12) in a series of Legendre polynomials.

Although these expressions are only approximate, they help in finding more accurate expressions for $\langle \sin\theta\rangle_{Av}$ and $4\pi f(0)$ which is done by adjusting s and the numerical factor in front until the results agree best with the direct numerical calculations. In this manner we found that a good fit is obtained when

$$-s = \tfrac{1}{2}\log\mu + 0.60 \quad (13)$$

and

$$\langle \sin\theta\rangle_{Av} \sim \{3.08\mu[\log\xi + \tfrac{1}{2}\log\mu + 0.60]\}^{\frac{1}{2}}, \quad (14)$$

$$4\pi f(0) \sim 0.43/\mu[\log\xi + \tfrac{1}{2}\log\mu + 0.60]. \quad (15)$$

The results of these approximate expressions are also given in Tables I and II for comparison with the direct computations.

5. Energy Dependence

It has been pointed out by Williams[4] that by considering $f(\theta)$ as a function of $w\theta$, the distribution function is of the Gaussian type whose shape is independent of the energy and depends only upon the thickness and the material of the scatterer. This method greatly facilitates the interpretation of experimental data. We shall see that the present formulas allow the same simplification to a sufficient degree of approximation.

[3] Formulas for such sums are given by L. S. Kassel, J. Chem. Phys. **1**, 576 (1933).

[4] E. J. Williams, Proc. Roy. Soc. **A169**, 531 (1939).

We now characterize the scatterer by two new parameters A and η, defined as follows

$$A=\mu(w^2-1)^2/w^2=24.8\times10^{-26}Z^2Nt$$
$$=0.151\sigma Z^2/M \quad (16)$$

and[5]

$$\eta=\xi/(w^2-1)^{\frac{1}{4}}=150/Z^{\frac{1}{3}}. \quad (17)$$

Substituting these parameters in the approximate Eq. (14) for $\langle\sin\theta\rangle_{Av}$ taking $w^2\gg1$, we find that the right-hand side of the following approximate expression is indeed independent of the energy.[6] Thus

$$\langle w\sin\theta\rangle_{Av}\sim1.76A^{\frac{1}{4}}(\log\eta+\tfrac{1}{2}\log A+0.60)^{\frac{1}{2}}$$
$$=1.76A^{\frac{1}{4}}(5.60+\tfrac{1}{2}\log A-\tfrac{1}{3}\log Z)^{\frac{1}{2}}. \quad (18)$$

Equation (18) is an approximate expression. Table III shows the values of $\langle w\sin\theta\rangle_{Av}$ computed from interpolations between the exact values of $\langle\sin\theta\rangle_{Av}$ for a few examples. It shows indeed a negligible dependence upon energy over a wide range of values, and demonstrates the sufficient accuracy of the approximate formula. This table can also be used for interpolations; it will be noticed that the entries are approximately proportional to $A^{\frac{1}{4}}$.

[5] The numerical coefficient is again based on the Thomas-Fermi atom but can of course be adjusted if required.

[6] In most cases $\sin\theta$ can be replaced by θ, giving $w\langle\theta\rangle_{Av}$. If expressed in Mev degrees, the numerical coefficient must be replaced by 50. When $H\rho\theta$ is recorded in gauss cm degrees, as is usual in cloud-chamber work, the coefficient is 1.70×10^3.

We can treat the approximate formula for $f(0)$ in the same manner, obtaining

$$4\pi f(0)/w^2\sim0.43/A[5.60+\tfrac{1}{2}\log A-\tfrac{1}{3}\log Z]. \quad (19)$$

Table IV shows the same quantity as interpolated from the exact values of $4\pi f(0)$. The exact values show that the function $4\pi f(0)/w^2$ is still slightly dependent upon the energy, although the variation is only 7 percent, over the range of energies given, for the thinnest foil calculated. As the foil becomes thicker, the energy dependence is reduced. It can be verified that within the same degree of approximation the whole distribution function $f(\theta)/w^2$ taken as a function of $w\theta$ is independent of the energy. A Gaussian curve of the form

$$4\pi f(\theta)/w^2=Ce^{-\frac{1}{4}C(w\theta)^2} \quad (20)$$

with

$$C=4\pi f(0)/w^2 \quad (21)$$

gives a fair approximation.

The data given in Table IV show an interesting dependence of $4\pi f(0)$ upon Z for constant Z^2Nt. For the thinnest foil the value of $f(0)$ for $Z=90$ is about 25 percent greater than for $Z=6$. This variation is somewhat reduced for the thicker foils. For foils used to approximate single scattering conditions at moderate angles, the variation of the scattering distribution at $\theta=0$ would be even larger for a similar range of Z. This indi-

TABLE III. *Values of $w\langle\sin\theta\rangle_{Av}$. For $w\langle\theta\rangle_{Av}$ in Mev degrees multiply these numbers by 28.4, for $H\rho\langle\theta\rangle_{Av}$ in gauss cm degrees multiply by 0.97×10^3.*

		Appr. Eq. (18)	$w=5$	7	10	15	20	30	40	50	60
$A=0.20$, $Z^2Nt=0.81\times10^{24}$											
$\log\eta=3.5$	$Z\sim90$	1.43	1.44	1.44	1.44	1.44	1.44				
$=4.0$	~24	1.53	1.53	1.53	1.53	1.53	1.54				
$=4.4$	~6	1.62	1.60	1.60	1.60	1.60	1.60				
$A=0.40$, $Z^2Nt=1.61\times10^{24}$											
$\log\eta=3.5$	$Z\sim90$	2.09		2.09	2.11	2.12	2.12	2.12			
$=4.0$	~24	2.26		2.19	2.22	2.24	2.26	2.26			
$=4.4$	~6	2.37		2.27	2.32	2.33	2.34	2.34			
$A=0.80$, $Z^2Nt=3.22\times10^{24}$											
$\log\eta=3.5$	$Z\sim90$	3.16			3.05	3.08	3.10	3.14	3.16		
4.0	~24	3.34			3.18	3.25	3.28	3.30	3.32		
4.4	~6	3.49			3.28	3.36	3.40	3.42	3.44		
$A=1.60$, $Z^2Nt=6.45\times10^{24}$											
$\log\eta=3.5$	$Z\sim90$	4.63				4.43	4.52	4.55	4.60	4.58	4.58
4.0	~24	4.90				4.65	4.74	4.78	4.84	4.81	4.81
4.4	~6	5.10				4.78	4.90	4.96	5.00	4.89	4.88

TABLE IV. *Values of* $4\pi f(0)/w^2$.

	Appr. Eq. (19)	$w=5$	7	10	15	20	30	40	50	60
$A=0.20$										
$\log\eta=3.5$ $Z\sim90$	0.654	0.605	0.622	0.634	0.644	0.650				
4.0 ~24	0.566	0.527	0.541	0.554	0.560	0.560				
4.4 ~ 6	0.513	0.478	0.494	0.504	0.509	0.510				
$A=0.40$										
$\log\eta=3.5$ $Z\sim90$	0.295		0.287	0.290	0.294	0.295	0.295			
4.0 ~24	0.260		0.251	0.257	0.258	0.260	0.260			
4.4 ~ 6	0.237		0.230	0.234	0.236	0.237	0.238			
$A=0.80$										
$\log\eta=3.5$ $Z\sim90$	0.135			0.134	0.134	0.135	0.134	0.134		
4.0 ~24	0.120			0.120	0.120	0.121	0.120	0.119		
4.4 ~ 6	0.110			0.111	0.112	0.111	0.110	0.110		
$A=1.60$										
$\log\eta=3.5$ $Z\sim90$	0.062				0.063	0.063	0.062	0.062	0.062	0.061
4.0 ~24	0.057				0.057	0.056	0.056	0.056	0.056	0.056
4.4 ~ 6	0.051				0.053	0.053	0.052			

cates that, for foils of constant Z^2Nt, the scattering is actually more multiple for the foils of small Z.

6. Scattering in Mixtures or Compounds

From the derivation of the expressions for coefficients G_l as given in the first paper we find for a mixture of two elements a and b that

$$G_l=G_l(a)G_l(b). \tag{22}$$

Considering the exponent of G_l in Eq. (2) we write

$$\mu[\log\xi-s_l]=\mu_a[\log\xi_a-s_l]+\mu_b[\log\xi_b-s_l]. \tag{23}$$

Thus for a compound containing two elements we introduce

$$\mu=\mu_a+\mu_b, \tag{24}$$

so that

$$\log\xi=(\mu_a\log\xi_a+\mu_b\log\xi_b)/(\mu_a+\mu_b). \tag{25}$$

Similarly for A and η we obtain

$$A=A_a+A_b \tag{26}$$

and

$$\log\eta=(A_a\log\eta_a+A_b\log\eta_b)/(A_a+A_b). \tag{27}$$

7. Projected Single Scattering

Most cloud-chamber observations do not yield the scattering angle θ but its projection on the plane of the cloud chamber. It is possible to transform Eq. (1) so as to give directly the projected distribution. We shall, however, derive the projected scattering in a somewhat different way which is closely related to Williams' treatment of the problem and emphasizes the advantages of the present method.

We denote the projected angle for a single scattering by ϕ and after multiple scattering by α. In our previous paper[7] we indicated that after ν collisions we have

$$G_m=\langle\cos m\alpha\rangle_{Av}=\exp\left[-\nu(1-\langle\cos m\phi\rangle_{Av})\right]. \tag{28}$$

We must therefore first obtain the Fourier coefficients for the single scattering law in order to calculate the coefficients G_m for the multiple scattering distribution. The latter will be obtained in the form[8]

$$\pi f(\alpha)=\sum G_m\cos m\alpha. \tag{29}$$

Normalization to unity requires that

$$G_0=\tfrac{1}{2}. \tag{30}$$

We take the Wentzel law for single scattering[9] and denote the angle with the normal to the plane of the cloud chamber by ψ. The scattering

[7] Compare Eq. (I 13) and the footnote 4 on page 25.

[8] If only the quadratic term in ϕ is taken in the exponent of G_m and if the Fourier series is replaced by an integral the results for $f(\alpha)$ will be a Gaussian curve. This treatment is identical with the classical derivation of the Gaussian distribution by Laplace and Poisson. It is slightly simpler here because the number of collisions is not fixed but has a Poisson distribution with an average value ν.

[9] Compare Eqs. (I 16) and (I 22).

law becomes

$$I(\theta)\sin\theta d\theta d\varphi = k^2 y dy d\varphi/(y^2+y_0^2)^2$$
$$= k^2\sin\psi d\psi d\phi/(1+2y_0^2-\sin\psi\cos\phi)^2. \quad (31)$$

This transformation was obtained by using

$$\cos\theta = \sin\psi\cos\phi;$$
$$\sin\theta d\theta d\varphi = \sin\psi d\psi d\phi. \quad (32)$$

In the foil the vertical scattering is not limited and we must integrate Eq. (31) over ψ from 0 to π which gives

$$2k^2 d\phi\int_0^{\pi/2}\sin\psi d\psi/(1+2y_0^2-\sin\psi\cos\phi)^2$$
$$=\frac{2k^2 d\phi}{(1+y_0^2)^2}\left[\frac{1}{\sin^2\phi'}+\frac{(\pi-\phi')\cos\phi'}{\sin^3\phi'}\right] \quad (33)$$

with ϕ' defined by

$$\cos\phi' = \cos\phi/(1+2y_0^2). \quad (34)$$

A sufficient approximation, normalized to unity is given by

$$W(\phi)d\phi \sim 2y_0^2 d\phi/\phi'^3 \sim 2y_0^2 d\phi/(\phi^2+4y_0^2)^{\frac{3}{2}}. \quad (35)$$

8. The Average Value of Cos $m\phi$

We use the approximate scattering law and write

$$\langle 1-\cos m\phi\rangle_{Av}$$
$$= 4y_0^2\left[\int_0^{\phi_1}(1-\cos m\phi)d\phi/(\phi^2+4y_0^2)^{\frac{3}{2}}\right.$$
$$\left.+\int_{\phi_1}^{\infty}(1-\cos m\phi)d\phi/(\phi^2+4y_0^2)^{\frac{3}{2}}\right]. \quad (36)$$

The small angle ϕ_1 is so chosen that in the first integral we may use $\frac{1}{2}(m\phi)^2$ for $(1-\cos m\phi)$ and that in the second integral we may neglect $4y_0^2$ in the denominator. In this approximation the final result does not contain the arbitrary angle ϕ_1.[10] The second integral is extended to infinity, which does not influence the result.[11] The integrations give

$$\langle 1-\cos m\phi\rangle_{Av} = 2y_0^2m^2\{-1+\log 2\phi_1-2y_0^2\}$$
$$+2y_0^2m^2\{\tfrac{3}{2}-Ci(m\phi_1)\}$$
$$\sim 2y_0^2m^2[-\log y_0+\tfrac{1}{2}-C-\log m]. \quad (37)$$

Here C stands for Euler's constant, 0.58. For Ci, the cosine integral, we took the first terms in the expansion.[12] Using Eqs. (I 23) and (I 35) we can write

$$\log\xi = -\log y_0-\tfrac{1}{2}, \quad (38)$$

which finally gives

$$\langle 1-\cos m\phi\rangle_{Av}$$
$$= 2y_0^2m^2[\log\xi+1-C-\log m]. \quad (39)$$

It is obvious that the last terms in the brackets are equivalent to the partial harmonic series which was obtained for the case of Legendre polynomials.

9. Projected Multiple Scattering

For the Fourier coefficients for the projected multiple scattering distribution, using $\nu y_0^2 = \mu$, we find

$$G_m = \exp\{-2\mu m^2[\log\xi+1-C-\log m]\}. \quad (40)$$

It is easy to determine again the average value of sin α, now given by

$$\langle\sin\alpha\rangle_{Av} = \int_0^{\pi} f(\alpha)\sin\alpha d\alpha \Big/ \int_0^{\pi} f(\alpha)d\alpha$$
$$= (4/\pi)[\tfrac{1}{2}-\sum_1^{\infty} G_{2n}/(4n^2-1)]. \quad (41)$$

This result is obtained by substituting for $f(\alpha)$

Table V. *Values of* $\langle\sin\alpha\rangle_{Av}$.

log ξ = 4		5	6	7	8
μ = 0.00050			0.076	0.084	0.092
0.0015	0.101	0.121	0.136	0.150	0.163
0.0025	0.134	0.158	0.176	0.195	0.210
0.0050	0.199	0.228	0.254	0.274	0.294
0.010	0.283	0.320	0.350	0.377	0.399
0.015	0.344				

[10] Williams' method consists essentially in making a special choice for ϕ_1 and omitting the second integral. The first integral alone gives a Gaussian curve for the multiple scattering distribution. Williams finally makes a correction to this distribution for scattering beyond ϕ_1.

[11] For larger angles Eq. (35) is no longer a very good approximation, but replacing it by a better formula made no difference in the results for Eq. (36).

[12] See for instance Jahnke-Emde, *Funktionentafeln*.

TABLE VI. *Values of $w\langle\sin\alpha\rangle_{Av}$. For $w\langle\alpha\rangle_{Av}$ in Mev degrees multiply these numbers by 28.4, for $H\rho\langle\alpha\rangle_{Av}$ in gauss cm degrees multiply by 0.97×10^5.*

	WILLIAMS	$w=5$	7	10	15	20	30	40	50	60
$A=0.20$, $Z^2Nt=0.81\times10^{24}$										
$\log\eta=3.5$ $Z\sim90$	1.69	1.51	1.53	1.56	1.58	1.60				
$=4.0$ ~24	1.75	1.57	1.60	1.64	1.66	1.68				
$=4.4$ ~6	1.80	1.64	1.67	1.71	1.73	1.74				
$A=0.40$, $Z^2Nt=1.61\times10^{24}$										
$\log\eta=3.5$ $Z\sim90$	2.46		2.16	2.23	2.28	2.31	2.34			
$=4.0$ ~24	2.54		2.27	2.35	2.40	2.43	2.45			
$=4.4$ ~6	2.62		2.33	2.41	2.48	2.52	2.54			
$A=0.80$, $Z^2Nt=3.22\times10^{24}$										
$\log\eta=3.5$ $Z\sim90$	3.55			3.12	3.24	3.31	3.39	3.42		
$=4.0$ ~24	3.66			3.26	3.40	3.40	3.56	3.58		
$=4.4$ ~6	3.77			3.38	3.53	3.60	3.68	3.71		
$A=1.60$, $Z^2Nt=6.45\times10^{24}$										
$\log\eta=3.5$ $Z\sim90$	5.18				4.60	4.74	4.86	4.93	4.97	4.98
$=4.0$ ~24	5.34				4.78	4.93	5.07	5.14	5.18	5.20
$=4.4$ ~6	5.50				4.89	5.07	5.23	5.30	5.35	5.38

the Fourier series of Eq. (29). Many other averages can be obtained in the same way. Eq. (41) converges rapidly, and numerical results are given in Tables V and VI for $\langle\sin\alpha\rangle_{Av}$ and $w\langle\sin\alpha\rangle_{Av}$. The latter can be compared with Williams' formula which in our notation[13] is

$$\langle\alpha\rangle_{Av}=1.76A^{\frac{1}{3}}[2.51-0.052\log Z+0.078\log A]. \quad (42)$$

Williams' results are also given in Table VI. It is interesting to note that $w\langle\sin\alpha\rangle_{Av}$ has a larger variation with energy than $w\langle\sin\theta\rangle_{Av}$.

10. CONCLUSION

The results derived in the present paper can still be refined in various ways. A small correction may arise from replacing the Thomas-Fermi field by the Hartree field. Consecutive impacts are not quite independent[14] as was assumed in the present treatment, with the result that the scattering may be decreased somewhat. Preliminary computations show that the relativistic terms in the Mott formula increase the average angle for lead by several percent, but the slow convergence of the relativistic correction terms makes this result uncertain. In cloud-chamber observations the vertical angle is limited by the depth of the illuminated layer, so that only a part of the projected scattering distribution is measured. A reliable correction for this cut off is rather complicated but fortunately $w\langle\sin\alpha\rangle_{Av}$ does not differ much from $w\langle\sin\theta\rangle_{Av}$.

All such corrections are not very useful at present because the experimental data are not sufficiently accurate. Moreover, the statistical complications of the multiple scattering problem make it rather unsuitable for testing the single scattering law, which is after all the ultimate purpose of the experiments.

This investigation was made in connection with work supported by the Horace H. Rackham Fund.

[13] This is Eq. (37) of Williams' paper.
[14] J. A. Wheeler, Phys. Rev. **57**, 352 (1940).

Evidence Against the Existence of an Excited State of He^3

R. D. PARK AND J. C. MOUZON
Duke University, Durham, North Carolina

(Received April 27, 1940)

Cloud-chamber measurements have been made on the recoil protons produced by neutrons from the d–d reaction. The distribution of the neutron energies has been determined from 126 recoil proton tracks. No evidence for a low energy group of neutrons and consequently an excited state of He^3 was obtained.

THERE has been conflicting evidence in regard to the energies of the neutrons from the $d-d$ reaction. In particular there has been some question as to the existence of a low energy group of neutrons which would imply an excited state of He^3. Evidence for a low energy group of neutrons has been given by Bonner[1,2] and Hudspeth and Dunlap.[3] Baldinger, Huber and Staub[4] also found some evidence for a low energy group but attributed it to scattered neutrons. Kanner and Harris[5] looked for γ-radiation, delayed β's and positrons from this reaction and reported negative results. Ruhlig[6] concluded that there were no γ-rays from the reaction. The low energy group of protons which was expected from a corresponding excited state of H^3 has been investigated by Myers and Langer,[7] Hudspeth and Bonner,[8] and Myers, Huntoon, Shull and Crenshaw[9] and was not found. Schiff[10] and Share[11] independently concluded that a stable excited state of He^3 was inconsistent with the present theory.

In an attempt to clarify this situation, we have made a cloud-chamber study of the neutrons from the $d-d$ reaction.

APPARATUS

A 3-gap linear accelerating tube was used with a Crane type ion source. The high voltage was supplied by one 300-kv and two 115-kv x-ray transformers in a conventional cascade circuit. These transformers were rebuilt with new primary, and tertiary driver coils were added. A peak voltage of 630 kv above ground has been obtained with this arrangement, showing it to be a practical scheme for moderately high voltages. The addition of another transformer to this set caused a decrease in the output voltage. This decrease was doubtless due to the fact that one of the transformers became overloaded, thus causing the transformer cores to be saturated and the group to become seriously out of phase. Because of the large amount of corona at the higher voltages the tube was usually operated at about 300 to 400 kv.

For recoil proton measurements a movable piston type cloud chamber 15 cm in diameter and filled with methane was used.[12] The chamber was placed 25 cm from a heavy ice target. The chamber was placed so that a center line made an angle of 90° to the deuteron beam. Two guide wires making ±10° angles to the 90° line were placed on the chamber top plate to facilitate angular measurements. The chamber was illuminated over its depth of 3.5 cm by two 1000-watt projection bulbs. A weak α-particle source of polonium on a silver wire was mounted inside the chamber for constant calibration of the stopping power of the methane and alcohol mixture. A Sept camera making stereoscopic views on each frame by means of a mirror and direct image was used. Transformers, ion source,

[1] T. W. Bonner, Phys. Rev. **53**, 711 (1938).
[2] T. W. Bonner, Nature **143**, 681 (1939).
[3] E. Hudspeth and H. Dunlap, Phys. Rev. **55**, 587 (1939).
[4] Baldinger, Huber and Staub, Helv. Phys. Acta **11**, 245 (1938).
[5] M. H. Kanner and W. T. Harris, Bull. Am. Phys. Soc., Abs. No. 4 (June, 1939).
[6] A. J. Ruhlig, Phys. Rev. **54**, 308 (1938).
[7] F. E. Myers and L. M. Langer, Phys. Rev. **54**, 90 (1938).
[8] E. Hudspeth and T. W. Bonner, Phys. Rev. **54**, 309 (1938).
[9] Myers, Huntoon, Shull and Crenshaw, Phys. Rev. **56**, 1104 (1939).
[10] L. I. Schiff, Phys. Rev. **54**, 92 (1938).
[11] S. S. Share, Phys. Rev. **53**, 875 (1938).
[12] H. R. Crane and J. C. Mouzon, Rev. Sci. Inst. **8**, 351 (1937).

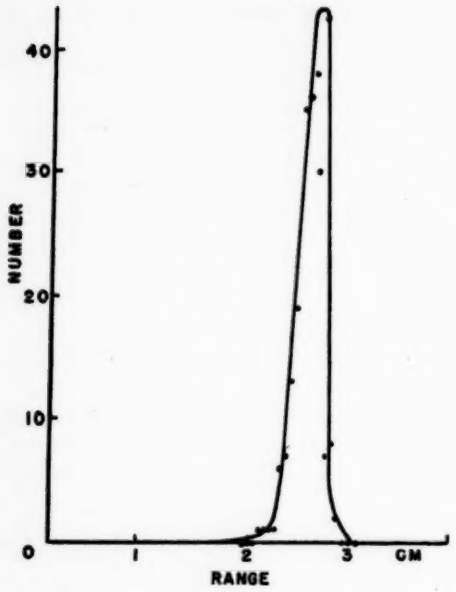

FIG. 1. Number-range curve for polonium alpha-particles from chamber calibrating source.

lights, cloud chamber expansion and camera were synchronized by a cam mechanism. This mechanism was adjusted so that good tracks could be photographed every 30 seconds. For reprojecting the pictures the camera assembly was mounted on a lathe bed equipped with a movable ground glass screen and inverted mirror. This arrangement allowed the tracks to be viewed stereoscopically.

An ionization chamber and linear amplifier were used to measure the intensity of neutrons scattered from the walls of the room. The ionization chamber consisted of a brass cylinder 5.5 cm in diameter and 12 cm long with a central collecting rod connected to the grid of the first stage of the amplifier. A paraffin disk 0.5 cm thick was placed in the end of the ionization chamber and recoil protons from the paraffin were measured. With the chamber filled with argon this arrangement was essentially directional because the pulses produced by recoil argon nuclei were very small and were indistinguishable from the background on the base line. Thus neutrons included in a solid angle of a little less than 2π could be detected. By pointing the ionization chamber directly away from the heavy ice target in the accelerating tube a measure of the neutrons scattered from the walls of the room could be obtained. A record of the pulses from the amplifier was made on 35-mm film in a magnetic oscillograph made from a permanent magnet dynamic speaker unit. The moving mirror was attached by a light rod to the voice coil of the speaker unit. This oscillograph was designed and built by Mr. William Hurst of the Duke University Instrument Shop.

MEASUREMENTS

About 1800 pairs of stereoscopic cloud-chamber pictures were examined. These pictures were taken with a deuteron beam at about 300 kv. Only tracks which started and stopped in the gas and which appeared to be due to neutrons coming from the target were accepted. This selection actually favors short tracks but no correction was made for this. The projected lengths of the tracks in the plane of the cloud chamber were noted and the angle θ (in the plane of the chamber) between the direction of the recoil proton and the incident neutron direction was measured. The majority of the accepted tracks had the angle $\theta < 35°$. The angle ϕ between the recoil proton track and the plane of the chamber was estimated visually in eleven of the 126 measured tracks. In the case of the remaining 115 tracks the angle ϕ was close to zero degrees. The actual length of a track is then $L/\cos\phi$ where L is the measured projected length. The reason for choosing such a small number of tracks which made appreciable angles with the plane of the chamber was that the criterion that the tracks had to start and stop in the chamber had to be satisfied. The cosine of the actual angle between a recoil proton and the incident neutron is easily seen to be $\cos\beta = \cos\theta\cos\phi$.

The lengths of α-particle tracks from the calibrating source were measured only when they were sensibly in the plane of the chamber. Whenever possible an α-track was measured in the frame where a measurable recoil proton was found. Fig. 1 is a plot of number as a function of the measured range of the polonium α-particles from the chamber calibrating source. The small spread in the range of the α-particles measured shows that the stopping power of the gas remained essentially constant throughout the experiment.

In order to calculate the energy of the neutrons the α-particle extrapolated range was taken from an integral curve to be 2.76 cm in our chamber. The stopping power of methane for 3.805 cm α-particles is 0.903 (relative to air) and hence the expected range in methane at 1 atmosphere is $3.805/0.903=4.21$ cm. Using mean ranges, one obtains the pressure of $4.21/2.73=1.55$ atmospheres. All proton tracks were reduced to actual lengths at one atmosphere of methane and then corrected to lengths at one atmosphere of air. Next the range-energy relation was applied and these energies were divided by $\cos^2\beta$ to give the energies of the neutrons, under the assumption that all recoil protons were due to neutrons whose direction was at 90° to the deuteron beam. In general the neutrons responsible for the recoil protons measured in the cloud chamber were not exactly perpendicular to the deuteron beam. The error thus introduced is unimportant for our purposes, as the presence of neutrons coming into the chamber at an appreciable angle would only tend to increase the number of short tracks measured in the specified direction. Consequently no corrections for it have been made.

The directional ionization chamber and linear amplifier were used to make a rough determination of the importance of neutrons scattered from the walls of the room. With the chamber pointed directly at the target and at a distance of 30 cm a counting rate of 60 counts/min. was observed. With the chamber directed away from the target and pointed at an 8-inch brick wall 70 cm from the target the counting rate was 3 counts/min. Since the beam current was fairly constant and the measurements were made under continuous operating conditions, it is estimated that the scattering measured was about 5 percent of the direct neutron beam. Because the wall 2.6 meters opposite this brick wall is a hollow tile wall from which the scattering is less it is estimated that the total scattering from all directions is something less than 10 percent of the number of neutrons coming from the target. The background count of 0.5 count/min. was taken with a deuteron beam and the whole apparatus running, the target being replaced by a clean aluminum plate. The background count of the ionization chamber when measured with the deuteron source off was also about 0.5 count/min., indicating that practically all neutrons originated at the target.

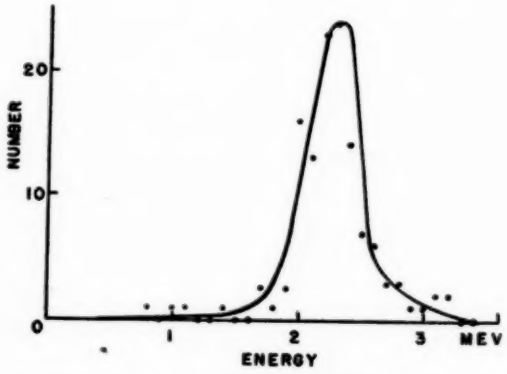

FIG. 2. Energy distribution of neutrons from the $d-d$ reaction. There is no evidence of a low energy group.

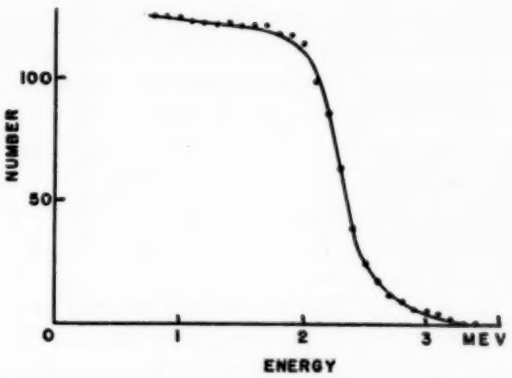

FIG. 3. Number of neutrons having energies greater than integral number-energy curve for the neutrons from the $d-d$ reaction.

RESULTS

A distribution curve of the neutron energies is plotted in Fig. 2. These energies were calculated as previously described. The most significant point about this curve is the lack of any indication of a low energy group of neutrons and consequently the absence of any evidence for the existence of an excited state of He^3. This conclusion is in agreement with the recent findings of Hudspeth and Dunlap.[13]

Because of the selection of tracks in the cloud chamber which satisfied certain conditions as to direction it is rather clear that less than 10 percent of those tracks measured were due to neutrons scattered from the walls of the room.

[13] E. Hudspeth and H. Dunlap, Phys. Rev. **57**, 1075(A) (1940).

From our ionization chamber measurements with the target replaced by a clean aluminum plate we conclude that the only source of neutrons in the accelerating tube was the target itself. It is conceivable, however, that with some experimental arrangements the scattering from the walls of the room might play an important role. It is also well known that in certain accelerating tubes an appreciable number of neutrons may be created at points other than the target. We feel that a low energy group of neutrons whose intensity amounts to as much as 10 percent of the main group should be evident in Fig. 2 if it exists.

We do not believe that the data presented here are sufficient to warrant a precise determination of the energy evolved in the $d-d$ reaction. We have, however, plotted an integral number-energy curve in Fig. 3. The extrapolation of this curve gives an energy of about 2.8 Mev for the neutron energy, corresponding to an extrapolated range of about 10.9 cm for the recoil protons. This agreement with Bonner's extrapolated range of 10.6 cm is satisfactory.

We wish to express our appreciation for the generous cooperation of various members of the staff in this work.

JULY 1, 1940 PHYSICAL REVIEW VOLUME 58

Note on a Field Theory of Nuclear Forces*

C. L. CRITCHFIELD, *Institute of Optics, University of Rochester, Rochester, New York*

AND

W. E. LAMB, JR., *Columbia University, New York, New York*

(Received May 3, 1940)

An interaction between nuclear particles and a field of light particles which obey Fermi-Dirac statistics is considered. It is shown that the energy of interaction between heavy and light particles can be calculated without resorting to perturbation theory in an approximation which neglects electric forces and the kinetic reaction of the heavy particles. Results which contain the effect of the rest mass of the field particles are presented for one heavy particle and for two heavy particles.

IT is the purpose of this note to extend the method which has been applied to the electron-positron-field theory of nuclear forces[1] to take account of effects dependent on the rest mass of the field particles. In the previous theory, the rest mass of the light particles was negligible. If the light particle field be that of mesons which obey Fermi-Dirac statistics, however, it is necessary to take the rest mass ($\sim$180 electron masses) into account, even in the approximation which neglects electric forces and the recoil of the heavy particles. The method which we present may then be used, for example, to derive the nuclear forces due to the meson-field introduced by Marshak,[2] without the use of perturbation theory.

The fundamental assumptions of the present method are (I) a heavy particle (neutron or proton) interacts strongly with a light particle (meson) if the light particle occupies a state of one particular space-dependence, $u(\mathbf{x})$, but does not influence the energy of mesons in any orthogonal state; (II) the state of the heavy particle is not changed by the interaction. Both assumptions require a nonrelativistic treatment of the heavy particle and permit the simplified device of fixing a heavy particle at the origin of the coordinate system and investigating its effect on the light particle states. Condition (II) must be changed to exclude spin direction if

* Publication assisted by the Ernest Kempton Adams Fund for Physical Research of Columbia University.

[1] Wigner, Critchfield and Teller, Phys. Rev. **56**, 530 (1939).

[2] R. E. Marshak, Phys. Rev. **57**, 1101 (1940).

spin-dependence of nuclear forces is to be explained but the modification is easily made[3] and will not be considered here. It is furthermore assumed for simplicity that the spatial dependence of $u(\mathbf{x})$ is spherically symmetrical about the position of the heavy particle.

Let $\psi(\mathbf{x})$ be the operator of the meson state as customarily defined in the formulism of quantized wave functions.[4] $\psi(\mathbf{x})$ has four spin-components which will be transformed by α and β in the way required by their use in the relativistic wave equation of Dirac. With a heavy particle remaining stationary at the origin explicit reference to its state need not be made and the operator of the proposed addition to the Hamiltonian of the mesons is

$$J=-\eta\int d\mathbf{x}\int d\mathbf{x}'\psi(\mathbf{x})^\dagger\beta\psi(\mathbf{x}')u(\mathbf{x})^*u(\mathbf{x}'), \quad (1)$$

where η is the constant giving the strength of the interaction. We shall take μc^2 as the unit of energy; μ is the mass of the meson. Making a Fourier transformation $u(\mathbf{x})$ may be replaced by $v(\mathbf{p})$ and $\psi(\mathbf{x})$ by $\phi(\mathbf{p})$

$$J=-\eta\int d\mathbf{p}\int d\mathbf{p}'\phi(\mathbf{p})^\dagger\beta\phi(\mathbf{p}')v(\mathbf{p})^*v(\mathbf{p}') \quad (2)$$

and $v(p)$ is normalized so that

$$\int_0^\infty v(\mathbf{p})^2 4\pi p^2 dp=1. \quad (3)$$

If $H^0\phi^\dagger\phi$ be the usual relativistic Hamiltonian (in quantized form) the Hamiltonian $H\phi^\dagger\phi=H^0\phi^\dagger\phi+J$ in which Coulomb interactions have been disregarded leads to a wave equation for the single light particles:

$$[E-(\boldsymbol{\alpha},\mathbf{p})-\beta]\phi(\mathbf{p})+\eta v(\mathbf{p})\beta\int v(\mathbf{p}')^*\phi(\mathbf{p}')d\mathbf{p}'=0. \quad (4)$$

$\mathbf{p}$ is also measured in units of μc^2. Although we follow the main lines of the method used for electron-positron pairs we shall, however, omit the transformation to eigenstates of kinetic energy. This step was useful in the former paper[1] to get a description of the interaction (1) in the language of pair-emission but it is not essential to the solution of (4).

$$\phi(\mathbf{p})=-\frac{E+(\boldsymbol{\alpha},\mathbf{p})+\beta}{E^2-1-p^2}\eta v(\mathbf{p})\beta\int v(\mathbf{p}')^*\phi(\mathbf{p}')d\mathbf{p}'. \quad (5)$$

Multiply (5) by $v(\mathbf{p})^*d\mathbf{p}$ and integrate over all angles and over all values of $|p|$.

$$\int v(p)^*\phi(\mathbf{p})d\mathbf{p}=-\int\frac{E+\beta}{E^2-1-p^2}\eta v(p)^2 4\pi p^2 dp\beta\int v(p')^*\phi(\mathbf{p}')dp'. \quad (6)$$

$v(p)$ is equivalent to $v(\mathbf{p})$ because of the assumed spherical symmetry. The integral equation (6) can be satisfied only if

$$4\pi\beta\eta\int\frac{E+\beta}{E^2-1-p^2}v(p)^2p^2dp=-1. \quad (7)$$

Let $q\equiv|(E^2-1)^{\frac{1}{2}}|$; the integral in (7) is then of the form which was evaluated in the former paper.[1] The method of evaluation is one by which the integral is replaced by a sum over momentum states quantized in a sphere of radius, L, so that $p_n=\pi\mu c^2\hbar n/L$. As a result of the interaction with the heavy particle the $(E^2-1)^{\frac{1}{2}}$ of an eigenstate with energy E, determined by Eq. (7), is changed by an amount $x\pi\mu c^2\hbar/L$, $|x|<1$. The x for a given E is determined by

$$(\beta E+1)\eta\{2\pi^2qv(q)^2\cot\pi x+f(q)\}=-1, \quad f(q)\equiv 4\pi\int_0^\infty[p^2v(p)^2-q^2v(q)^2](q^2-p^2)^{-1}dp. \quad (8)$$

[3] C. L. Critchfield, Phys. Rev. **56**, 540 (1939).
[4] P. Jordan and E. Wigner, Zeits. f. Physik **47**, 631 (1928).

The factor β can take either of two values, $+1$ or -1. Let x be the fractional shift of $(E^2-1)^{\frac{1}{2}}$ when $\beta=1$ and let x' be that for $\beta=-1$

$$\begin{aligned}\tan \pi x &= 2\pi^2 q(E+1)v(q)^2/[-\eta^{-1}-(E+1)f(q)],\\ \tan \pi x' &= 2\pi^2 q(E-1)v(q)^2/[\eta^{-1}-(E-1)f(q)].\end{aligned} \tag{9}$$

Let $dq=\pi\mu c^2\hbar/L$; then the combined displacement of the value of q for levels of essentially the same E is $(x+x')dq$ and the corresponding net change in energy for these levels is $(x+x')d|E|=(x+x')qdq/|E|$. The total change in the energy of all states of negative energy, ΔE, is then

$$\Delta E=-\frac{2}{\pi}\int_0^\infty \frac{qdq}{(q^2+1)^{\frac{1}{2}}}\,\mathrm{arctg}\,\frac{4\pi^2q^2v(q)^2[qf(q)-(\eta q)^{-1}]}{\eta^{-2}-q^2f(q)^2+4\pi^4q^4v(q)^4+2f(q)/\eta}. \tag{10}$$

The factor 2 represents the sum over spin directions of the mesons and ΔE is understood to be in units of μc^2.

Equation (10) gives the total interaction energy between one heavy particle and the field of all mesons in negative energy states. When two heavy particles are considered ΔE will depend upon their separation and forces will arise which might be identified with the forces in nuclei. The dependence of ΔE on the distance between heavy particles may be obtained by the same method which led to Eq. (10). The outlines of this application will now be sketched.

We modify the assumptions made above when considering one heavy particle only by considering two heavy particles of equal mass with their center of gravity at the origin of coordinates. Let the position vector of one be $c\hbar\mathbf{X}$ and of the other $-c\hbar\mathbf{X}$. An addition to the Hamiltonian of the type (2) must now be made for each heavy particle. This may be done by translating $v(p)$ from the origin to $c\hbar\mathbf{X}$ so that it becomes $e^{i(p,X)}v(p)$ in one case and from the origin to $-c\hbar\mathbf{X}$ in the other. The wave equation for mesons then becomes:

$$[E-(\boldsymbol{\alpha},\mathbf{p})-\beta]\phi(\mathbf{p})+\eta e^{i(p,X)}v(p)\beta\int v(p')^*e^{-i(p,X)}\phi(\mathbf{p}')d\mathbf{p}'$$

$$+\eta e^{-i(p,X)}v(p)\beta\int v(p')^*e^{i(p,X)}\phi(\mathbf{p}')d\mathbf{p}'=0. \tag{11}$$

We define the spinors:

$$\xi_1\equiv\int e^{-i(p,X)}v(p)^*\phi(p)dp,\quad \xi_2\equiv\int e^{i(p,X)}v(p)^*\phi(p)dp \tag{12}$$

and solve (11) for $\phi(\mathbf{p})$

$$\phi(\mathbf{p})=-\frac{E+(\boldsymbol{\alpha},\mathbf{p})+\beta}{E^2-p^2-1}\eta\beta\{e^{i(p,X)}v(p)\xi_1+e^{-i(p,X)}v(p)\xi_2\}. \tag{13}$$

$\mathbf{X}$ is simply a set of three numbers so that the exponentials and other functions of p commute. By multiplying (13) by $e^{-i(p,X)}v(p)^*d\mathbf{p}$ and integrating we get one equation in ξ_1 and ξ_2 and by multiplying (13) with $e^{i(p,X)}v(p)^*d\mathbf{p}$ and integrating we get another. These equations may be written formally:

$$\xi_1=-Q\xi_1-R\xi_2,\quad \xi_2=-R^*\xi_1-Q\xi_2. \tag{14}$$

The energy levels of (11) are then determined by the secular equation:

$$(1+Q)^2-R^*R=0 \tag{15}$$

and with the same notation as in Eq. (8)

$$Q=(\beta E+1)\eta\{2\pi^2 qv(q)^2\cot\pi x+f(q)\}, \tag{16}$$

$$R=-\int\frac{E+\beta}{q^2-p^2}\eta\beta 4\pi p^2 v(p)^2\frac{\sin pr}{pr}dp+i(\boldsymbol{\alpha},\mathbf{X})\int\frac{2\eta\beta}{r^2(q^2-p^2)}4\pi p^2 v(p)^2\left[\frac{\sin pr}{pr}-\cos pr\right]dp, \tag{17}$$

where $r\equiv 2|X|$, is $1/\hbar c$ times the separation of the heavy particles. It is evident that the integrals in (17) may be calculated by the same method by which Eqs. (8) and (16) were obtained if $v(p)^2$ be replaced by $v(p)^2\sin pr/pr$ for the first integral and by $v(p)^2[(\sin pr/pr)-\cos pr]$ for the second. In this way R may be represented by

$$R=-\eta(\beta E+1)\{2\pi^2 qv_1(q)^2\cot\pi x+f_1(q)\}+i(\boldsymbol{\alpha},\mathbf{X})\frac{2\beta}{r^2}\eta\{2\pi^2 qv_2(q)^2\cot\pi x+f_2(q)\} \tag{18}$$

with

$$v_1(q)^2=v(q)^2\sin qr/qr, \qquad f_1(q)=4\pi\int[p^2v_1(p)^2-q^2v_1(q)^2]/(q^2-p^2)dp,$$

$$v_2(q)^2=v(q)^2[\sin qr/qr-\cos qr], \quad f_2(q)=4\pi\int[p^2v_2(p)^2-q^2v_2(q)^2]/(q^2-p^2)dq.$$

The secular equation then becomes:

$$\eta^2[(\beta E+1)^2(v^4-v_1^4)-v_2^4/r^2](2\pi^2 q\cot\pi x)^2+2[\eta(\beta E+1)v^2+\eta^2(\beta E+1)^2(v^2f-v_1^2f_1)-\eta^2v_2^2f_2/r^2]$$
$$\times(2\pi^2 q\cot\pi x)+1+2\eta(\beta E+1)f+\eta^2(\beta E+1)^2(f^2-f_1^2)-\eta^2f_2^2/r^2=0. \tag{19}$$

This quadratic equation has the roots $\cot\pi x_1$ and $\cot\pi x_2$ corresponding to changes in q for two orthogonal eigenstates of energy E. Since we are interested only in the sum of all changes in energy we add x_1 and x_2

$$\tan\pi(x_1+x_2)=4\pi^2 q[\eta(\beta E+1)v^2+\eta^2(\beta E+1)^2(v^2f-v_1^2f_1)-\eta^2v_2^2f_2/r^2]$$
$$\times\{4\pi^4q^2\eta^2[(\beta E+1)^2(v^4-v_1^4)-v_2^4/r^2]-1+\eta^2f_2^2/r^2-2\eta(\beta E+1)f-\eta^2(\beta E+1)^2(f^2-f_1^2)\}^{-1}. \tag{20}$$

Let x_1 and x_2 represent the changes in q when $\beta=1$ and x_1', x_2' represent those when $\beta=-1$. Furthermore, we define K, L, M, and N in such a way that the tangent in Eq. (20) becomes $(K+\beta L)/(M+\beta N)$; then

$$\tan\pi(x_1+x_2)=(K+L)/(M+N), \quad \tan\pi(x_1'+x_2')=(K-L)/(M-N), \tag{21}$$

$$x_1+x_2+x_1'+x_2'=(1/\pi)\operatorname{arctg}2(KM-LN)/(M^2+L^2-N^2-K^2),$$
$$\Delta E=-\int_0^\infty 2(x_1+x_2+x_1'+x_2')qdq/(q^2+1)^{\frac{1}{2}}. \tag{22}$$

For a particular function $v(p)$, therefore, it is possible to express ΔE as an integral analogous to expression (10) but the explicit form of the one for two particles is necessarily complicated and is not presented.

The method presented above is an alternative to the usual perturbation method of calculating forces between heavy particles. In practice the integral (22) will be discouraging except perhaps for certain particular assumptions for $v(p)$.

The authors are indebted to Professor Wigner of Princeton University for many helpful discussions on this approach to a theory of nuclear forces. It is a pleasure to acknowledge Professor Wigner's interest and help.

Note on the Polarization of Light Emitted by Electrically Exploded Wires

WILLI M. COHN
El Cerrito-Berkeley, California

(Received May 6, 1940)

The polarization of light emitted by an electrically exploded wire was photographically investigated. No polarization was found, within the limits of accuracy. It is concluded that scattered and reflected light do not contribute to the emission from electrically exploded wires. This leaves temperature radiation and continuous electron radiation as the only factors causing the emission of the continuous spectrum.

THE discharge of one or several condensers through a thin wire will cause, for a very short period of time, the appearance of an intense light. Characteristics of "exploded wires" have been investigated by several authors.[1] During the initial part of the explosion a purely continuous spectrum is emitted which is followed by line plus continuous spectra. The intensity of the continuous spectrum depends upon pressure, surrounding gas, etc. Originally, it was thought that the continuous spectrum is due only to temperature radiation emitted by incandescent particles and vapors. The temperature during or immediately following the explosion was estimated to reach 20,000°K. However, later work showed that the intensity distribution in the continuous spectrum is different from the intensity distribution in the spectrum of a blackbody, particularly in the ultraviolet part.

Our present knowledge indicates that three distinct phenomena may contribute to the continuous emission observed. They are: (1) continuous blackbody radiation due to high temperature; (2) luminescent radiation due to continuous electron radiation; and (3) radiation scattered or reflected by gases, vapors, and fragments of the wire formed during or immediately after the explosion. It has not been possible, so far, to distinguish between the components of the continuous spectrum during the various parts of the explosion or to determine their relative amounts.

The polarization of the light emitted by an exploding wire was investigated in order to obtain a lead toward the identification of the components of the continuous spectrum. Scattered or reflected light will be completely or partially polarized depending on size and shape of particles, whereas both temperature radiation and continuous electron radiation will produce unpolarized light.[2] The relatively weak emission lines are unpolarized.

Experiments were carried out simultaneously with a study of the spectrum of wires exploded at atmospheric pressure (unpublished). The set-up was similar to that used in earlier work. It included a Campbell x-ray transformer with mechanical rectifier, a spark-gap, the wire to be exploded, and the condensers. Part of the work was carried out with five glass plate condensers, total capacity 0.28 microfarad, the remainder of the work being carried out with five General Electric condensers, type 9-CEIA-56, total capacity 1.8 microfarads. Voltages ranged from 20,000 to 31,000 volts. The wire was clamped to copper bars of $\frac{5}{8}\times\frac{5}{32}$ in. cross section which served as electrodes. The background was carefully screened by ivory-black "velours" paper in order to eliminate reflected light. The spectrum

[1] G. J. Singer and A. Crosse, Phil. Mag. **46**, 161–166 (1815). F. Braun, Ann. d. Physik **17**, 359–363 (1905). F. E. Nipher, Proc. Am. Phil. Soc. **52**, 283–286 (1913). J. A. Anderson, Astrophys. J. **51**, 37–48 (1920); Proc. Nat. Acad. Sci. **8**, 231–232 (1922); J. A. Anderson and S. Smith, Astrophys. J. **64**, 295–314 (1926). G. L. Wendt and C. E. Irion, J. Am. Chem. Soc. **44**, 1887–1894 (1922). R. A. Sawyer and A. L. Becker, Astrophys. J. **57**, 98–113 (1923). S. Smith, Proc. Nat. Acad. Sci. **10**, 4–5 (1924); Astrophys. J. **61**, 186–203 (1925). H. Nagaoka and T. Futugami, Proc. Imp. Acad. Tokyo **2**, 254–257; 387–389 (1926); H. Nagaoka, T. Futugami and T. Machida, *ibid.* **2**, 328–331 (1926); H. Nagaoka and T. Futugami, Sci. Papers Inst. Phys. Chem. Res. Tokyo **8**, 269–288 (1928). T. Hori, Sci. Papers Inst. Phys. Chem. Res. Tokyo **4**, 59–78 (1926). M. R. Déchène, J. de phys. et rad. **7**, 59–64 (1926). A. C. Menzies, Proc. Roy. Soc. **A117**, 88–110 (1927). L. Eckstein and I. M. Freeman, Zeits. f. Physik **64**, 547–555 (1930). W. Behrens, Diss. Hannover, 1935. M. Vaudet, Ann. de physique **9**, 645–722 (1938).

[2] W. M. Cohn, Zeits. f. Physik **70**, 662–694 (1931); **72**, 392–422 (1931); **73**, 662–676 (1932); **75**, 544–554 (1932). W. Finkelnburg, Phys. Rev. **45**, 341–342 (1934); *Kontinuierliche Spektren* (Springer, Berlin, 1938).

shows a strong continuous background, together with numerous emission lines.

The polarigraph consisted of a Voigtlaender camera, focal length, $35\frac{1}{4}$ in., equipped with a quartz Wollaston double-image prism. An auxiliary lens was inserted between the wire and the polarigraph. Two enlarged images of the explosion were obtained on the same photographic plate, the images being polarized in perpendicular planes. Since the dispersion of the Wollaston prism amounts to 1.1° the images overlap to some extent in the central part of the plate. Exposures were obtained with the shutter remaining open during the entire period of an explosion. Part of the plates received, after exposure, standard marks by means of a neutral wedge. Details of the polarigraph and the wedge may be found in an earlier publication.[3] Eastman Kodak plates of types Universal and 40, and Wratten hypersensitive panchromatic plates were used.

The images on the plates were measured with microphotometers of types Hartmann and/or Zeiss. Fig. 1 presents a microphotometer record through images A and C; part "B" of the curve due to the overlapping of the images was not used in the reduction. The reduction was carried out as previously,[3] the polarization p being computed from $p=100\cdot(l-r)/(l+r)$, in which l and r are the relative intensities of the two pictures. The probable error amounts to ± 0.2 percent polarization.

Wires of copper and constantan, 0.0013 in. and 0.0027 in. in diameter were exploded, the free length of the wires varying from 5 to 22.5 mm. A single explosion produced a record on the plate of sufficient density for microphotometer work.

The results of this work are summarized as follows:

(1) The emission of copper and constantan wires exploded at atmospheric pressure is, within the limits of accuracy, not polarized in integrated ("white") light, wave-lengths 389–565 mμ.

(2) The emissions from copper and constantan wires appear identical (spectrographically confirmed for the continuous spectrum, whereas the lines are partly different).

(3) While these tests integrate over the various parts of an explosion, the conclusion seems justified that, within the limits of accuracy, scattered or reflected light do not contribute to the emission during any part of the explosion.

The absence of polarized light in the emission of exploded wires leaves temperature radiation and continuous electron radiation the only factors causing the continuous emission from exploded wires. Therefore, the continuous emission of the exploded wire belongs to the group of phenomena which includes the radiation emitted if the front of a shock wave accompanying the detonation of a solid or gaseous explosive meets an obstacle, e.g., a solid wall or another shock wave; the radiation from the condensed and underwater sparks; the radiation from the high current arc and the high current vacuum tube. All these continuous spectra seem due to the superposition of temperature radiation and continuous electron radiation in the field of positive ions formed during the discharge.

FIG. 1. Microphotometer record MZ 10167a of the images of an exploded constantan wire.

ACKNOWLEDGMENTS

Thanks are due to Dr. G. R. Harrison of Massachusetts Institute of Technology for the loan of condensers; to Drs. R. G. Aitken and W. H. Wright of the Lick Observatory for permission to use the Hartmann microphotometer; to Dr. R. T. Birge of the Physics Department, University of California, for permission to use the Zeiss microphotometer, and to Mr. A. W. Anthony, Jr., of Cambridge, Massachusetts, for help in some experiments.

[3] W. M. Cohn, Astrophys. J. **87**, 284–334 (1938); Astron. Nachr. **267**, 205–216 (1938).

Evidence for a Nuclear Electric Quadrupole Moment for Sb^{123}

D. H. TOMBOULIAN AND R. F. BACHER
Cornell University, Ithaca, New York

(Received May 11, 1940)

Measurements of the hyperfine structure of the line λ5895 of Sb II by the use of a Fabry-Perot interferometer have shown that there are deviations from the interval rule in the case of the isotope with mass number 123. The hyperfine structure intervals of the $^3D_1$ level of Sb^{121} ($I=5/2$) are found to be 0.6801 and 0.4832 cm^{-1}. The corresponding intervals in Sb^{123} ($I=7/2$) are 0.4814 and 0.3603 cm^{-1}. The error in these measurements is of the order of 0.001 cm. The observed ratio of the two separations gives 1.407 and 1.336 for the light and heavy isotope, respectively, whereas the corresponding ratios on the basis of the interval rule are 1.400 and 1.286. The deviation in the case of the light isotope is within the experimental error. The deviation for the heavy isotope, however, is a real effect which cannot be accounted for on the basis of perturbing effects of neighboring levels and must therefore be ascribed to the presence of an electric quadrupole moment of the nucleus of Sb^{123}.

INVESTIGATIONS[1,2] of the hyperfine structure in the spectrum of Sb II have revealed patterns that are extremely complex. Because of the comparable relative abundance of the two isotopes (mass number 121, and 123) and because most of the intense lines involve transitions between levels of high J value, the observed patterns suffer from serious blending. In the spectral range 5000–7000A, the line λ5895 is among the few which show sufficiently simple and well resolved structure. This line has been assigned to the transition $5p6p^3D_1 \rightarrow 5p6s^3P_0$ by Krishnamurty.[3] Because of the complexity of the atomic system and particularly because of the large number of unassigned levels nearby, this assignment cannot be considered as certain. However, there is no question from the hyperfine structure of the line which shows six resolved components, that the line is a transition from a state $J=1$ to a state $J=0$. Since this is sufficient information to make a comparison of the nuclear effects produced by the two isotopes, the present investigation was undertaken for the purpose of making accurate measurements on the structure of this line.

The spectrum was excited in a hot hollow cathode tube through which purified helium was circulated. In operating the tube considerable difficulty was encountered in arriving at conditions favorable for the production of a strong, sharp spectrum. Tube currents of 100 to 200 ma were used; the pressure of the helium gas was kept as low as possible for the maintenance of a steady discharge. The sample of antimony was free from the oxide and other impurities were less than 0.03 percent. The high resolution apparatus consisted of a Fabry-Perot interferometer which was mounted in the collimated beam of a Zeiss three-prism spectrograph. A series of separators, in the 2- to 5-mm range, was employed in conjunction with heavily silvered plates. Exposure times were of the order of several minutes.

The energy level diagram and the observed line structure for λ5895 is shown in Fig. 1. The solid and dotted lines refer, respectively, to the light and heavy isotopes. The measurements on the various intervals are summarized in Table I. In the reduction of the plates 8 to 10 orders of interference were included. The largest deviation from the mean in the measurement of any one interval is 0.0019 cm^{-1}. The present results are considered more accurate than those given by previous measurements,[1,2] in which intervals 1–2, 2–3 and 3–4 show wide variations. In particular, Tolanski[2] states that the deviation in the separation of the smallest interval is 0.019 cm^{-1}. In the present data the deviation in the same interval (3–4) is of the order of 0.001 cm^{-1}.

The results obtained by Crawford and Bateson[4] from a study of Sb IV show that the nuclear spin of Sb^{121} is 5/2 and that of Sb^{123} is 7/2. Their conclusions were based upon a study of the line λ3537A($5s6p^3P_0 \rightarrow 5s6s^3S_1$) and are in agreement with the previous conclusions of Badami.[1] This

[1] J. S. Badami, Zeits. f. Physik **79**, 206 (1932).
[2] S. Tolanski, Proc. Roy. Soc. **A146**, 182 (1934).
[3] S. G. Krishnamurty, Ind. J. Phys. **10**, 90 (1937).
[4] M. F. Crawford and S. Bateson, Can. J. Research **10**, 693 (1934).

line, which they completely resolved, is free from quadrupole effects so that the nuclear spins can be determined directly from an application of the interval rule. From their values of the nuclear spins, it is possible to compare the separations of the $5p6p^3D_1$ level of Sb II with those to be expected on the basis of the interval rule (see Table II).

Since there usually is a likelihood of underestimating the separation of close components it is of importance to note the spread of the observed interval ratios. From the data of Table I it is found that for Sb^{121}, the largest and smallest values of this ratio are 1.415 and 1.395, respectively. Similar quantities for Sb^{123} are 1.344 and 1.323. For Sb^{121}, the observed deviation from the interval rule is probably within the experimental error, but for Sb^{123} the observed deviation is decidedly outside the inaccuracies of measurement and therefore is a real effect.

Deviations from the interval rule have been successfully ascribed in general either to the presence of a nuclear electric quadrupole moment or to the effect of perturbations of nearby terms. In the present case, the Sb^{121} separations obey the interval rule almost exactly while for those of Sb^{123}, the observed ratio shows a deviation of 3.9 percent. This large difference for the two isotopes indicates that the effect cannot be ascribed to perturbations by nearby levels. Furthermore, the observed deviation for Sb^{123} is quite large and would be very difficult to account for even without the above argument. On the

TABLE I. *Hyperfine structure intervals* λ5895 Sb II.

Separator (mm)	Intervals in 10^{-3} cm^{-1}				
	1–2	2–3	3–4	4–5	5–6
2.780	113.3	482.2	84.8	274.5	208.1
3.691	112.7	482.0	85.7	274.2	208.2
3.691	113.2	481.9	85.6	274.0	208.5
4.054	114.2	479.7	85.4	276.8	208.6
Averages	113.3	481.4	85.4	274.9	208.3

TABLE II. *Separations of* $^3D_1$ *level.*

Isotope	Separation of $^3D_1$		Observed Ratio	Ratio from Interval Rule
121	680.1	483.2	1.407	1.400
123	481.4	360.3	1.336	1.286

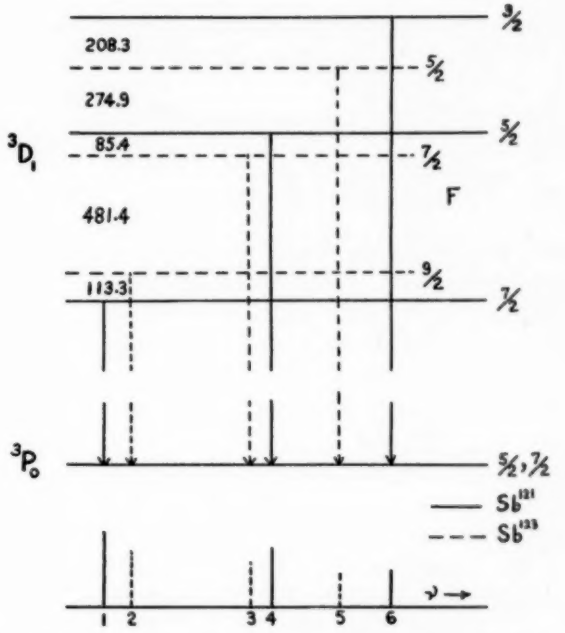

FIG. 1. Level diagram and line structure λ5895 of Sb II.

basis of observed levels the nearest neighbor is 86 cm^{-1} above. It has $J=2$ and has been ascribed to $5p6p^3D_2$ and the order of its perturbing effect can be obtained from the ratio A^2/d, where A is the h.f.s. separation factor and d the distance to the nearest level. For Sb^{123} $A=0.105$ cm^{-1}, the effect of a level 86 cm^{-1} away would be of the order of 10^{-4} cm^{-1} which is negligible. It is, of course, possible that a state as yet undiscovered lies nearer than the one we have considered. Under these circumstances the relative perturbations for the two isotopes would be given by

$$\frac{P_{121}}{P_{123}}=\frac{(A_{121})^2}{(A_{123})^2}=\left(\frac{96.9}{52.6}\right)^2=3.4.$$

A larger perturbation would be expected for Sb^{121}. This is the isotope for which the interval ratio is found to agree with the expected value. From the above considerations it appears that the observed deviation from the interval rule for Sb^{123} must be ascribed to some other cause and presumably to the presence of an electric quadrupole moment.

The atomic state which gives this quadrupole effect has been assigned to $5p6p^3D_1$. This assignment is somewhat uncertain due to the intermediate coupling between the two electrons and

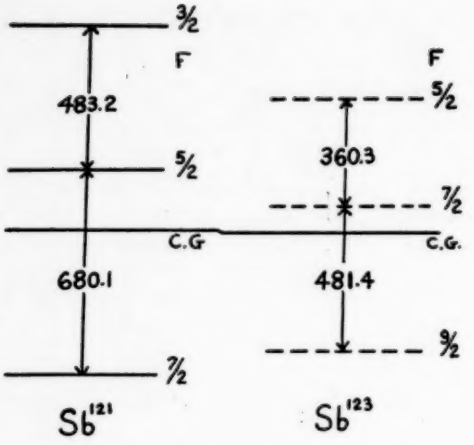

FIG. 2. Observed separations of $^3D_1$ level.

possibly also due to perturbing effects from the $5p4f$ configuration. While the quadrupole effect is definitely recognizable, it does not seem feasible to attempt a determination of the quadrupole moment from the observed deviations.

As a check on the measurements reported here the ratios of the magnetic moments for the two isotopes can be determined from the total separations of the hyperfine structures. This gives $\mu_{121}/\mu_{123}=1.316$ and is in close agreement with the value 1.32 which is obtained from the separations of the $5s6s\,^3S_1$ level of Sb IV studied by Crawford and Bateson.[4]

Finally it is of interest to see whether the observed line shows any isotope shift. This can be done by determining the center of gravity of the observed structures taking the statistical weight of each hyperfine state $(2F+1)$. As shown in Fig. 2 the centers of gravity for Sb^{121} and Sb^{123} are almost coincident. The c.g. for Sb^{121} lies 0.001 cm^{-1} above that for Sb^{123} indicating that the isotope shift in this transition is negligible.

JULY 1, 1940 PHYSICAL REVIEW VOLUME 58

Note on the Effect of Pressure on the Curie Point of Iron-Nickel Alloys

J. C. SLATER
Massachusetts Institute of Technology, Cambridge, Massachusetts
(Received April 25, 1940)

By applying Clapeyron's equation, an estimate is made of the increase of the Curie point of nickel with pressure, which comes out of the order of magnitude of 5×10^{-3} degree per atmosphere. For iron-nickel alloys, the increase of Curie point with pressure would become less as more iron is added, becoming zero with something like 70 percent of nickel, and for the alloys containing more iron the Curie point would decrease with pressure. These magnitudes are such that it seems most unlikely that pressures existing in the iron-nickel core of the earth would raise the Curie point of the material enough so that it could be ferromagnetic at the temperatures existing inside the earth. This makes any ferromagnetic explanation of the magnetism of the earth most implausible.

IT is a matter of considerable geophysical interest to know the effect of pressure on the Curie point of iron-nickel alloys such as may constitute the core of the earth. It is ordinarily supposed that the permanent magnetism of the earth cannot be explained as being of ferromagnetic origin, because at the high temperatures assumed in the interior, of the order of several thousand degrees absolute, the alloys would be far above their Curie points, and would not be ferromagnetic. On the other hand, there are presumably very high pressures, of the order of 10^6 atmospheres, in the interior of the earth, and if such a pressure should raise the Curie point enough, the interior of the earth might still be ferromagnetic. It thus becomes important to know whether pressure would be expected to raise or to lower the Curie point, and if it raises it, to know whether it could be by some such amount as $5000/10^6=5\times10^{-3}$ degree per atmosphere (taking the temperature to be 5000°), which would suffice to make the interior of the earth ferromagnetic. Not many experiments are available to settle this point, on account of the difficulty of combining high pressure and high temperature technique. It becomes important

therefore to see how much information can be given by theory. Shockley[1] has qualitatively discussed the anomaly in the thermal expansion of iron-nickel alloys at the Curie point, and the method of discussion which he uses has been extended by Bozorth[2] to the question of the effect of pressure on the Curie point. Bozorth concludes that pressure does in fact increase the Curie point of nickel, but decreases that of iron, and for alloys of intermediate composition has an intermediate effect, so that there is a certain concentration, with perhaps of the order of magnitude of 70 percent of nickel, for which the Curie point is independent of pressure. Bozorth makes no estimate of the magnitude of the change of Curie point, and it is the purpose of the present note to make such an estimate. The result is that the effect is too small to be of geophysical importance. A rough estimate of the effect of pressure on the Curie point of nickel would be an increase of 5×10^{-5} degree per atmosphere, only about one percent of that required to make the core of the earth ferromagnetic, and it is hard to see how the calculations could be in error by more than a factor of ten, to be generous. Thus our conclusion is that it remains extremely unlikely that the material of the interior of the earth is in a ferromagnetic state.

The method which we shall use is based on Clapeyron's equation. The Curie point is of course a phase change of the second order, to which Clapeyron's equation is not applicable. Nevertheless we commit no serious error if we consider only two limiting states of the metal, the completely magnetized and the completely unmagnetized states, and consider the phase change of the first order which would occur between them if states of intermediate magnetization did not exist. Actually, instead of a sharp transition between these two phases, we have a continuous transition, which becomes complete at the Curie point Θ. If there were only the two limiting phases, there would be a sharp transition at the temperature Θ' at which their free energies were the same. It is not hard to show that this temperature Θ' would be less than Θ, about 0.7Θ in some simple cases. We are now justified in supposing that the effect of pressure on the transition temperature Θ' will be similar to that on the Curie temperature Θ. It is simple to compute, however, for the assumptions of Clapeyron's equation apply to it. This equation may be written

$$d\Theta'/dP=\Delta V/\Delta S, \tag{1}$$

where ΔV is the volume difference between the magnetized and unmagnetized phases, ΔS the entropy difference between the phases, equal in the case of a phase change of the first order to the latent heat of transition divided by the absolute temperature. To estimate the variation of the temperature Θ' with pressure, then, we need the increases of volume and entropy in going from the magnetized to the unmagnetized phases.

Experimentally, there is no sharp transition, so that there is no directly measurable change of volume and latent heat. Instead, the transition is spread through a range of temperatures, and there are anomalies in the thermal expansion and specific heat throughout these regions, coming to a peak at the Curie point. The quantities which we wish in Eq. (1) are the integrated anomalies in thermal expansion and specific heat, giving estimated values of the total changes in volume and entropy between the two phases. Shockley[1] and Bozorth[2] have both given curves for thermal expansion as a function of temperature, for a series of iron-nickel alloys. From these curves it is seen that pure nickel has an increase of thermal expansion below the Curie point, falling to zero suddenly at the Curie point, meaning that the unmagnetized, high temperature phase has a larger volume than the magnetized phase, so that by Eq. (1) $d\Theta'/dP$ is positive, and increase of pressure increases the Curie point. The other alloys shown by Shockley and Bozorth, however, beginning with 66.8 percent nickel, have decreases of thermal expansion, indicating a reduced volume for the unmagnetized phase, and a negative value of $d\Theta'/dP$. A rough estimate from the figure indicates that the change of sign might come at about 70 or 75 percent nickel.

Using Shockley and Bozorth's curves, one can make a rough estimate of ΔV, for pure nickel. Very crudely, we may suppose the anomaly to be a triangle, extending through about 300° (from about 75°C to 375°C), and of height at the Curie point of 1×10^{-6}. Thus, since the area of a

[1] W. Shockley, Bell Sys. Tech. J. **18**, 645 (1939).
[2] R. M. Bozorth, Bell Sys. Tech. J. **19**, 1 (1940).

triangle is half the base times the altitude, the fractional increase in length from magnetized to unmagnetized state would be $300\times1\times10^{-6}/2 = 1.5\times10^{-4}$, and the fractional increase in volume three times this, or 4.5×10^{-4}. Next we must estimate the change in entropy. This could be done from observations on specific heat. It is perhaps simpler, however, to use a direct theoretical estimate, since it is known that theory gives an adequate interpretation of the entropy anomaly. The estimate is slightly different depending on whether we use the Weiss-Heisenberg model or the electron band model, but since we are looking for only approximate values, we may use the Weiss model for simplicity. An elementary magnet with angular momentum $lh/2\pi$ will have $(2l+1)$ orientations, so that the entropy per magnet will be $k \ln (2l+1)$, or will be $Nk \ln (2l+1)$ for N magnets. This will represent the entropy of the unmagnetized, random state; the magnetized state will have zero entropy of orientation. For nickel, we may take as far as order of magnitude is concerned $l=\frac{1}{2}$, giving two orientations (corresponding to one spin per atom), so that we have $\Delta S = Nk \ln 2$, for N atoms. If we now take N to be the number of atoms in unit volume, we may take ΔV to be 4.5×10^{-4} cc, making all calculations for unit volume. For nickel, the density is 8.6, and the atomic weight 58.7. Thus the number of atoms per unit volume is $6.03\times10^{23}\times8.6/58.7 = 0.88\times10^{23}$. Hence we have $\Delta S = 0.88\times10^{23}\times1.38\times10^{-16}\times0.6931 = 0.84\times10^{7}$. Finally, then, using Eq. (1),

$$\frac{d\Theta'}{dP} = \frac{4.5\times10^{-4}}{0.84\times10^{7}} = 5\times10^{-11} \text{ degrees per unit pressure} \qquad (2)$$

$$= 5\times10^{-5} \text{ degree per atmosphere.}$$

This is the estimate mentioned in the first paragraph. It is noteworthy that the one accurately measured value of change of Curie point with pressure, for a Ni-Cu alloy,[3] was 6×10^{-5} degree per atmosphere, just of this order of magnitude. The smallness of the effect of pressure on the Curie point is a direct result of the small volume difference between magnetized and unmagnetized states, a much smaller difference than found in the usual polymorphic transition, resulting in a correspondingly small effect of pressure. It is hard to see how this estimate can be very greatly in error. If one allows a factor of two in ΔV and ΔS, and assumes that our replacement of the phase change of the second order by one of the first order introduces an additional factor of two, and makes the unlikely assumption that all these errors work in the same direction, one could conceivably get an effect eight or ten times as large as (2), though there is no reason for expecting it. But it seems quite out of the question to understand an error by a factor of a hundred, as we should need to explain the magnetism of the earth. Furthermore, we must remember that the calculations are made for pure nickel, and that iron-nickel alloys will show a smaller, or even negative, effect.

An even stronger reason for suspecting that the effect of pressure on the Curie point is not large comes from the general point of view underlying the theory, as described for instance by Shockley and Bozorth. One can draw a curve of Curie point as a function of the ratio of the lattice spacing to the average radius of the d shell of electrons. This curve has its maximum about at cobalt, or alternatively about at a 70-percent Ni-Fe alloy, in which the iron atoms, with d shells larger than cobalt, and the nickel atoms with smaller d shells, seem to give about the same average effect. Pure nickel corresponds to a larger ratio than cobalt, pure iron to a smaller ratio. Compression decreases the lattice spacing, bringing nickel closer to the maximum of the curve and increasing its Curie point. But the most that pressure can do, according to the picture, is to change the lattice spacing enough to bring the material to the maximum of the curve, or to give it about the same Curie point as pure cobalt, or as a 70-percent Ni-Fe alloy. In other words, the only effect of pressure on the Curie points of real substances would be expected to be to change them so that they resemble other real substances. But there are no known substances with Curie points much above the 1400° Abs. which we find for cobalt. Thus it is most unlikely that pressure will raise the Curie point of any substance much above this value, so that it is most improbable that any material could be ferromagnetic in the interior of the earth, if it is as hot as usually supposed.

[3] A. Michels, A. Jaspers, J. de Boer and J. Stryland, Physica **4**, 1007 (1937).

A New Electron Microscope*

L. MARTON
RCA Manufacturing Company, Camden, New Jersey
(Received May 1, 1940)

The design of a high power electron microscope of the transmission type is described. It is constructed as a self-contained unit which may be operated by a practical microscopist who does not necessarily have training as a physicist. Microphotographs are shown which indicate that a resolving power of about 50A can be readily obtained.

IN the last few years considerable effort has been devoted to the development of the transmission-type high power electron microscope. It has been proved that such an instrument can become a very valuable tool of research because of its enormous resolving power. After devising adequate methods, research problems have recently been successfully attacked.

The microscope described in the present paper was built in the RCA laboratories and incorporates a number of new features as well as others previously described by the author.[1] In addition it is designed for operation by a practical microscopist, who does not necessarily have training as a physicist. It is free to a great extent from external disturbances. The latter feature is due partly to a new design of the objective lens, and partly to the general principles involved in the construction. A new object chamber allows easy adjustment of the specimen, and its rapid introduction into and withdrawal from the microscope. A new photographic chamber allows a larger picture size than former instruments and facilitates operation. Another advantage is a complete freedom from greased joints.

DESCRIPTION OF THE MICROSCOPE

A. Electron source

The electron source (Fig. 1) is of the single potential hot cathode type, without use of intermediate potential electrodes. A hairpin-shaped tungsten filament is surrounded by a smooth guard electrode. The filament and the guard electrode are the only parts of the microscope at high potential, the whole instrument being very carefully grounded. The filament carrier, which is easily inserted and tightened by means of a rubber gasket, is adjustable in both horizontal and vertical directions by means of a flexible bellows. Two additional gaskets allow an easy dismounting of the electron gun for cleaning. The complete gun is connected with the microscope by means of a second flexible bellows allowing the optical alignment.

B. Microscope body

All the important parts of the new microscope are built in two thick-walled brass tubes separated by the object chamber. This method of construction provides great rigidity of the microscope, a point which in recent years has been stressed also in the building of optical microscopes. Because of this rigidity, the instrument reacts as a unit to mechanical vibrations and the image quality is not impaired. The results are well illustrated by the microphotographs shown at the end of this article, which were obtained when a Megavac pump was less than two feet distant from the instrument and directly connected to it by means of a rubber hose.

Below the object chamber, the inside wall of the main tube is lined with a very efficient magnetic shielding. For 60 cycles the shielding factor can be estimated to be approximately 10^{-3} to 10^{-4}.

Two large windows allow observation of the greatly magnified image and, by means of a "periscope" system, of the intermediate image. The "periscope" consists of two surface aluminized mirrors and an achromatic lens inside of the vacuum, and an eyepiece outside. Its purpose is to observe both images from the same place, and to avoid cutting a hole in the magnetic

* Presentation at the meeting of the American Physical Society, Washington, D. C., April 26, 1940.

[1] L. Marton, Bull. Acad. Belg., Bruxelles **20**, 439 (1934); **21**, 553 (1935); **21**, 606 (1935); **22**, 1336 (1936); Physica **3**, 959 (1936).

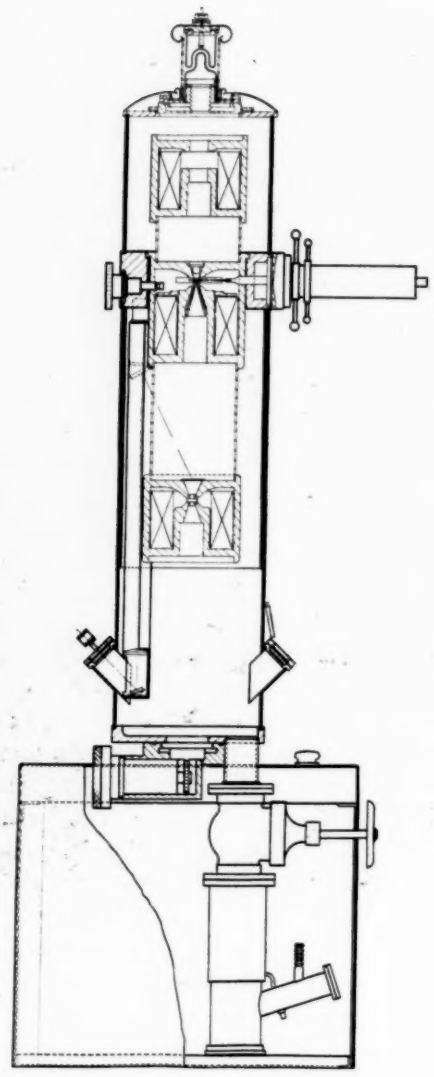

FIG. 1. Diagram of the electron microscope.

shielding at the height of the intermediate screen. It magnifies the intermediate image three times. Both windows are provided with movable red filters and black covers for taking photographs in a lighted laboratory. The complete instrument is built upon a metal pedestal of adequate size, which houses not only the vacuum pump, but also the entire control panel. The observer can thus adjust the instrument completely from his seat before the microscope.

C. Electron optical system

The electron optical system consists of a condenser coil, an objective coil, and a projection coil. Each coil is ironclad, the two latter being provided with pole pieces. The iron enclosures are made of soft iron.

Because the coils are entirely in vacuum and might give a considerable amount of gas without special precautions, it has been decided to enclose each coil in a sealed copper "can" with glass-metal seals for the leads.[2]

Whereas the designs of the condenser and the projection coil do not differ much from previous designs, the objective coil differs considerably. Preliminary experience has shown that it is possible to obtain short focal length with pole pieces of considerably greater bore diameter than has been previously accepted. Such a large inner diameter has multiple advantages: the spherical aberration for equal incident beam section is much reduced, the intensity of the image is increased, and the accuracy requirements for machining and aligning are not as high as for smaller bores.

The actual pole pieces of the objective coil show an $f_{\min}/d_p$ ratio of 0.3 instead of 0.8 which was given in an article by Ruska,[3] for equal velocity and pole piece diameter. The present distribution of magnifications is 100 in the first stage and 200 in the second stage. Further modifications of the lenses and discussions of them will be contained in a future article.

D. The object chamber

The object chamber allows introduction of specimens into the evacuated microscope and

FIG. 2. H. pertussis, electron optical magn. 9000.

[2] Joint development with Dr. V. K. Zworykin and M. C. Banca.

[3] E. Ruska, Zeits. f. Physik **89**, 120 (1934).

FIG. 3. Typhoid fever, electron optical magn. 10,000.

their withdrawal without breaking the vacuum, horizontal and vertical adjustment of the specimens, and a temperature control of the specimens —for example, cooling with liquid air. The specimens are mounted on little disks of very fine wire cloth instead of the generally used drilled apertures. Not only is this way of mounting much less expensive, but it permits exploration of a much greater area of the specimen, distributed at random over a relatively extended surface. The disks are clamped between apertures made in two "blades" fixed at the closed end of a tube, and introduced between the pole pieces of the objective coil through a lateral hole in the iron enclosure. In this way the most sensitive part of the optical system is well shielded. A ring-shaped holder for the "blades" can be moved horizontally and vertically by the required amount by means of screws and gears operated externally through vacuum-tight flexible bellows. When the specimen is withdrawn, the microscope can be closed by means of an externally operated gate. The lateral compartment, which contains the specimen holder, can be opened and pumped out separately. The tube which holds the "blades" can be filled with a liquid of a given temperature which is communicated to the "blades." The time required to change a specimen depends on the pumping speed of the auxiliary pump system; with good pumps it is about one minute. A bellows-operated two-way valve establishes the connection with the auxiliary pump or with the exterior.

E. The photographic chamber

The photographic chamber consists of a rack and pinion operated carriage, which allows either the closing of the chamber toward the microscope by means of a gate, or a substitution of the gate by a photographic plateholder with automatically removed cover. After exposure, when the

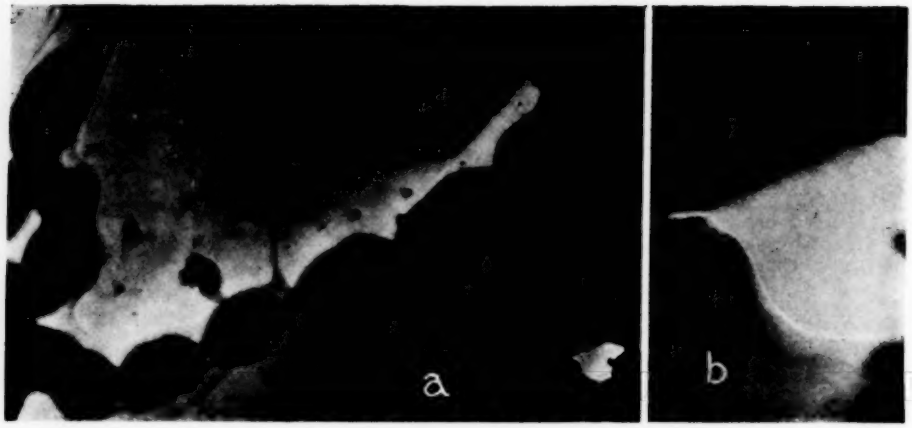

FIG. 4. Streptococcus haemolyticus, electron optical magn. 20,000.

cover is pushed back over the plate, the gate is pressed at the same time against the microscope opening, and the photographic chamber can be filled with air. Standard 9×12-cm plateholders can be exchanged through a door communicating with the exterior. An externally operated and hinged fluorescent screen permits the covering of the photographic plate in the "open" position, and observation of the highly magnified image. Series exposures can be taken on the same plate by moving the carriage by fractions of its total motion, and covering the field partially by means of the fluorescent screen. The time for exchanging one plateholder for another is again limited only by the pumping speed; with good pumps the instrument is ready for a new exposure in one minute.

RESULTS

Some of the photographs obtained by means of the new microscope are reproduced in Figs. 2, 3 and 4. The performance of the instrument can best be judged by Fig. 4(b), which is a partial enlargement of Fig. 4(a). The nitrocellulose film supporting the bacteria developed a crack, the edges of which were at a distance of 100A. Both edges are still so sharp that a resolving power of at least 50A can be safely estimated under these conditions.

Grateful acknowledgment is made to Dr. V. K. Zworykin, director of the Electronic Research Laboratory for his constant interest in this work, and to my colleagues who helped with the constructional details, in particular Mr. M. C. Banca, who executed most of them, Mr. J. F. Bender, who collaborated on many details, Mr. A. W. Vance for his contribution on some parts and his work on the electrical equipment with Mr. J. M. Morgan, and Mr. V. Goltzoff who helped with tests, as well as to the entire RCA organization for their cooperation on this project, and also to Drs. S. Mudd, E. W. Flosdorf, D. B. Lackman and K. Polevitsky of the University of Pennsylvania, who supplied the bacteriological specimens shown in this paper.

Electron Emission into Dielectric Liquids

WILBUR R. LEPAGE AND L. A. DUBRIDGE
University of Rochester, Rochester, New York

(Received May 2, 1940)

The current between polished nickel electrodes immersed in pure toluene has been measured as a function of electric field (over the range 0 to 250,000 volts/cm) and of temperature (from −15 to 70°C). The Richardson lines are straight but show a very small slope (0.05 to 0.4 ev) and a small value of the constant A (10^{-9} to 10^{-11} amp./cm² deg.²). The log i *vs.* $E^{\frac{1}{2}}$ curves show a slope about twice the value $e^{\frac{1}{2}}/D^{\frac{1}{2}}kT$ predicted by the simple Schottky theory, but in agreement with the theory of Baker and Boltz. It is found however that there are serious objections to this theory, and the agreement with it is probably accidental. The situation is in fact too complex to be handled by a simple theory. It is suggested that for the low potential barrier present at the metal-dielectric interface a combination of thermionic and field currents would be expected which would account qualitatively for the observed behavior.

THE conduction of electricity through liquid and solid dielectrics is a phenomenon which is as yet imperfectly understood as the review of the field by Nikuradse[1] shows. Even the nature and origin of the conduction currents has been, and still is, in dispute. During recent years the suggestion has been advanced that, in very pure dielectric liquids at least, the currents are caused either by thermionic emission across the metal-dielectric interface or by field emission.

This question has been recently investigated by Baker and Boltz[2] who studied the voltage dependence of the current between plane metal surfaces immersed in pure liquid toluene. At high fields they found that the log i *vs.* $V^{\frac{1}{2}}$ curves approximated straight lines whose slopes were greater by a factor $D^{\frac{1}{2}}$ (D = dielectric constant) than the Schottky lines for thermionic emission in a vacuum. This was in agreement with a theory they proposed for the effect of a dielectric on thermionic emission and they concluded that their results supported the thermionic emission theory.

We believe, however, that serious questions can be raised concerning the validity of their theory of the Schottky effect in a dielectric. In this paper we re-examine briefly the theory of the effects to be expected and present some further measurements on the temperature and field variation of the conduction currents.

THEORY

The theory of the effect of a dielectric on the thermionic emission from a metal has been sufficiently reviewed by Baker and Boltz, so that only a brief discussion need be given here.

The total potential barrier, W_a, at a metal-vacuum interface may be arbitrarily divided into two parts: W_{a1}, the work done against the rather large but short range forces very close to the metal, and W_{a2}, the work done against the smaller forces which extend from about one or two atomic diameters out to infinity. For a homogeneous surface, W_{a2} is principally the work done against the ordinary image force, but for "patchy" surfaces (far more common in ordinary experimental work) contact fields between patches cause large deviations from the image law. There is no accurate way of determining the relative magnitudes of W_{a1} and W_{a2}. However, at distances less than that for which the potential energy is equal to the maximum kinetic energy

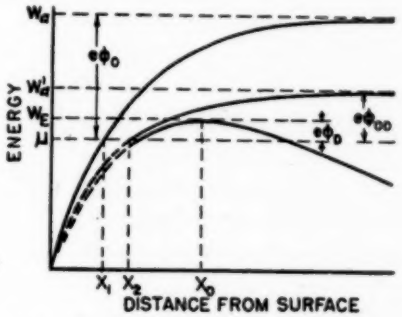

FIG. 1. Variation of potential energy of an electron near a metal surface in vacuum (upper curve), in dielectric (middle curve), and in dielectric with applied field (lower curve).

[1] A. Nikuradse, *Das Flussige Dielektrikum.*
[2] E. B. Baker and H. A. Boltz, Phys. Rev. **51**, 275 (1937). (Additional references to the literature will be found in this paper.)

(the highest Fermi level) the space charge of electrons escaping out to this point before returning to the surface will prevent the application of the image law. Beyond this point the image law may hold for uniform surfaces. Arbitrarily, then, we set $W_{a1}=\mu$, the work done against forces within the distance x_1 (Fig. 1) and $W_{a2}=W_a-\mu=\varphi_0 e$ the work done from x_1 to ∞, φ_0 being the usual thermionic work function. If $f(x)$ is the force on an electron at the distance x then

$$W_{a1}=\mu=\int_0^{x_1} f(x)dx$$

and

$$W_{a2}=\varphi_0 e=\int_{x_1}^{\infty} f(x)dx. \tag{1}$$

These equations serve to define x_1. If, for distances greater than x_1, $f(x)$ is the image force, $e^2/4x^2$, then $\varphi_0 e=e^2/4x_1$.

When a dielectric is placed in contact with the metal surface the potential barrier will be lowered because (1) the short range forces will be reduced since the outermost layer of positive ions in the metal will have a less asymmetrical position than in the absence of the dielectric atoms and (2) the long range electrostatic forces on an escaping electron (e.g., the image force) will be reduced by a factor D.

Because of the reduction in short range forces the distance at which the potential energy becomes equal to μ will be greater, x_2 in Fig. 1. We will have then in place of (1)

$$\varphi_{0D}e=\int_{x_2}^{\infty} f_D(x)dx,$$

where $f_D(x)$ is the force on an electron in the dielectric. If the image force predominates we have $\varphi_{0D}e=e^2/4Dx_2$. Thus even though the image force is reduced only by a factor D, the work function may be reduced by a much larger factor since $x_2>x_1$. In a qualitative way the picture will be similar if other long range forces in addition to the image force are present.

Effect of applied field

Suppose now a uniform electric field, E, be applied at the metal-dielectric surface. The force on an electron in the dielectric near the metal will now be

$$F=f_D(x)-Ee.$$

Very close to the metal-dielectric interface, however, there will be a layer of polarization charge, located, say, at the average distance a from the metal. At distances less than a the field will be DE when the field in the dielectric is E. The force on an electron here then will be

$$F_a=f_D(x)-DEe.$$

The total work W_E required to take an electron from the metal out to the distance x_0 where the potential energy is a maximum will be

$$\begin{aligned} W_E&=\int_0^a (f_D(x)-DEe)dx+\int_a^{x_0}(f_D(x)-Ee)dx \\ &=\int_0^{\infty} f_D(x)dx-DEea-Ee(x_0-a)-\int_{x_0}^{\infty} f_D(x)dx \\ &=W_a'-\int_{x_0}^{\infty} f_D(x)dx-Ee[x_0+(D-1)a], \end{aligned}$$

where W_a' is the potential barrier in the dielectric in the absence of the field. Since $e\varphi_D=W_E-\mu$ and since W_a' and μ do not depend on E we find

$$\begin{aligned} \frac{d\varphi_D}{dE}&=\frac{1}{e}f_D(x_0)\frac{dx_0}{dE}-[x_0+(D-1)a]-E\frac{dx_0}{dE} \\ &=-[x_0+(D-1)a], \end{aligned} \tag{2}$$

since by definition $f_D(x_0)=Ee$. For $D=1$ (vacuum) this reduces to the usual relation[3]

$$d\varphi/dE=-x_0. \tag{3}$$

We have assumed a to be independent of E which seems reasonable, since the polarization charge will always be as close to the metal as possible. Hence a will be determined by the molecular structure and should always be of the order of one molecular diameter. At the highest field used in our experiments x_0 is of the order of 20 molecular diameters, hence $(D-1)\,a$ will be much smaller than x_0. (For toluene $D=2.39$). In the case of an image field $x_0=\frac{1}{2}(e/ED)^{\frac{1}{2}}$ and we then find $\varphi_{0D}-\varphi_D=(eE/D)^{\frac{1}{2}}$. Whence

$$d\varphi_D/dE^{\frac{1}{2}}=-(e/D)^{\frac{1}{2}}. \tag{4}$$

From the Richardson equation (if A does not

[3] See J. A. Becker, Rev. Mod. Phys. 7, 95 (1935).

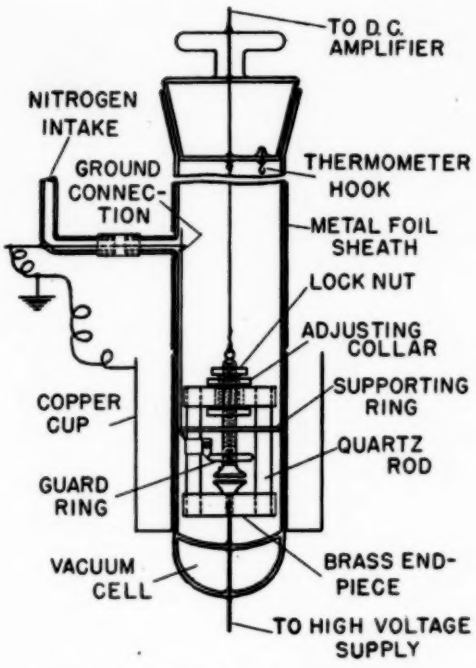

FIG. 2. Diagram of experimental tube.

depend on E) we have then

$$d(\log I)/dE^{\frac{1}{2}}=e^{\frac{1}{2}}/D^{\frac{1}{2}}kT. \tag{5}$$

These are the expected Schottky relations for a dielectric and we see that the slope of the $\log I$ *vs.* $E^{\frac{1}{2}}$ or the φ_D *vs.* $E^{\frac{1}{2}}$ lines should be $D^{\frac{1}{2}}$ times *smaller* than in vacuum.

In the theory of Baker and Boltz the assumption was apparently made that $a=x_0$. If we make this assumption and also assume an image field then Eq. (4) becomes

$$d\varphi_D/dE^{\frac{1}{2}}=-(eD)^{\frac{1}{2}} \tag{6}$$

and Eq. (5) becomes

$$d(\log I)/dE^{\frac{1}{2}}=e^{\frac{1}{2}}D^{\frac{1}{2}}/kT, \tag{7}$$

which are the Baker and Boltz relations.

However, we can see no justification for the assumption $a=x_0$. The point x_0 is *not* a position of equilibrium for positive ions when the field is such as to accelerate electrons. It seems unreasonable to suppose that for weak fields the polarization charge would be located 50 to 100 atomic diameters from the metal-dielectric interface. Hence we set $a \ll x_0$ and obtain Eqs. (4) and (5).

However it must be emphasized that the failure of experimental curves to follow Eq. (4) may not necessarily imply that the currents are not thermionic but possibly only that the field is not an image field. In this case Eq. (3) would still apply but not Eq. (4).

The situation to be expected in case field emission plays a part will be discussed later.

APPARATUS

The apparatus used was similar to that employed by Baker and Boltz except that provision was made for measuring the currents as a function of temperature. A diagram of the tube is shown in Fig. 2. The two electrodes were of nickel with carefully polished surfaces. They were first cleaned in boiling NaOH and in dilute HCl and washed in distilled water. They were then heated for several hours at 100°C in an atmosphere of hydrogen to remove oxide layers. The electrodes were mounted in a suitable adjustable support, insulated by fused quartz rods.

Pure toluene ($D=2.39$) was circulated through the tube by a distillation train not shown. C.P. Toluene was further purified by treatment with H_2SO_4 and NaOH to remove traces of thiophene. The toluene was then distilled over metallic sodium to remove most of the water while final traces of water were removed by passing the liquid into a reservoir containing two electrodes connected to a high voltage source. After about two hours the top water-free portion was drawn from this reservoir directly into the tube. The evacuated chamber at the lower end of the tube in Fig. 2 was provided to prevent condensation of moisture on the glass near the high voltage lead during the low temperature measurements.

Temperature variation was obtained over the range −15°C to 70°C by filling the copper reservoir around the tube with hot water, ice or dry-ice-alcohol mixtures. Ample time was allowed for thermal equilibrium between readings.

A kenotron rectifier furnished an adjustable voltage up to 30 kv. Control was obtained with an induction regulator in the primary circuit of the transformer. Sufficient filtering for the very low currents used was obtained with a 0.01 μf condenser across the output. A group of 39 200-megohm resistors in series with a galvanometer served as a voltmeter. A 200-megohm protective resistor was placed in the high voltage line to the tube. The currents between the two electrodes

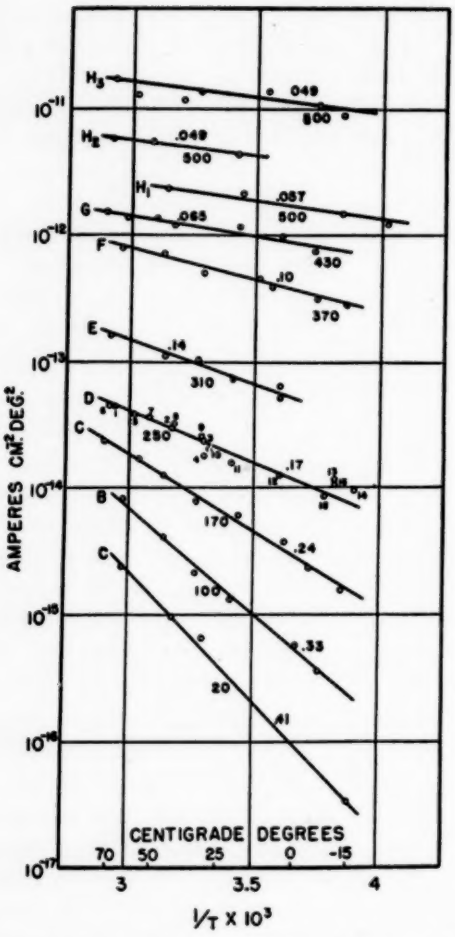

FIG. 3. Richardson plots of currents through dielectric. Figure below each curve gives the value of $E^{\frac{1}{2}}$ in (volts/cm)$^{\frac{1}{2}}$; figure above each curve gives the slope in e-volts.

were measured either directly with a galvanometer or with a DuBridge-Brown d.c. amplifier.

RESULTS

In order to determine whether the temperature variation of the current across the dielectric obeyed the Richardson equation, current-temperature runs were taken for different applied voltages. When the temperature was first increased above room temperature the current behaved erratically at high voltages, tending to decrease with time after temperature equilibrium was established. However, after reaching a given high temperature, reproducible currents could be measured at any lower temperature. There is presumably some sort of surface layer formed by heating which remains reasonably stable at lower temperatures. This type of irregularity has been found by most investigators in this field and suggests that metal-dielectric interfaces are more difficult to control than vacuum-metal surfaces. This itself suggests that one will expect a more complex behavior than is observed for clean metals in vacuum. In particular, with complex surfaces of the type present here one will hardly expect a simple image law of force on the electrons near the surface.

A series of Richardson plots for applied fields ranging from 400 to 25×10^4 volts/cm is shown in Fig. 3. The figures below each line give the values of $E^{\frac{1}{2}}$. The slope of each curve expressed in electron-volts is indicated by the number above each curve and these vary from 0.41 ev at 0.4 kv/cm to about 0.05 ev for 250 kv/cm. Since the work function of Ni in vacuum is of the order of 5 volts it is evident that even at low applied fields the work function of Ni in toluene is over 10 times smaller than in vacuum. The Richardson slopes then decrease by a factor of 8 as the field is increased to 250 kv/cm.

The three curves H_1, H_2, and H_3 all taken at the same field indicate the variations in position (but not in slope) of curves taken at different times at high fields. At low fields the curves are quite reproducible. The numbering of the points in curve D shows the order in which the readings were taken.

The data of Fig. 3 show that within the rather large errors and over this restricted temperature range, the currents follow the Richardson thermionic equation.[4] While this is in agreement with the hypothesis of thermionic emission it is not of course to be taken as final evidence since other theories also predict an exponential type of current-temperature curve. The most important result of these measurements is the very small slope exhibited by the Richardson curves and the rapid variation of slope with applied field.

If we pick off from the curves of Fig. 3 a series of points corresponding to measurements made at a single temperature but for different applied fields and plot log I *vs.* $E^{\frac{1}{2}}$ we obtain the curve shown as A in Fig. 4. It is evident that at constant temperature the currents are closely a linear function of $E^{\frac{1}{2}}$. This is just the relation to

[4] This result has also been reported by Edler and Zeier, Zeits. f. Physik **84**, 356 (1933).

be expected from the Schottky theory of an image field. However, the slope of this curve is about twice as great as that given by the Schottky theory for a dielectric, namely $e^{\frac{1}{2}}/(DkT)^{\frac{1}{2}}$. The slope is actually about $D^{\frac{1}{2}}$ times greater than for a vacuum instead of $D^{\frac{1}{2}}$ times smaller.

If, instead of plotting the log I *vs.* $E^{\frac{1}{2}}$ curves from the data of Fig. 3, one plots the data obtained in a single run at constant temperature, much less reproducible curves are obtained, one of which is reproduced as curve B of Fig. 4. Curve B is very similar to typical curves obtained by Baker and Boltz, agreeing with theirs also in the slope of the upper linear portion. Comparison with Curve A, which was reproduced at several different temperatures, shows the large effect of the "temperature conditioning" process.

The data giving the Richardson slope φ and the thermionic constant A as a function of $E^{\frac{1}{2}}$ are shown in Fig. 5. The values were deduced from the curves of Fig. 3, under the assumption that the emitting surface area is the geometrical area of the cathode. It is evident that at low fields both φ and A vary rapidly with the field but that above $E^{\frac{1}{2}}=300$ A remains constant and φ falls off linearly with $E^{\frac{1}{2}}$. Again the slope of the φ *vs.* $E^{\frac{1}{2}}$ line is over twice as great as the slope given by Eq. (4), though about equal to the slope predicted by the Baker and Boltz theory, Eq. (6). The assumption that A is independent of E made in deducing Eq. (5) is seen to hold for high fields

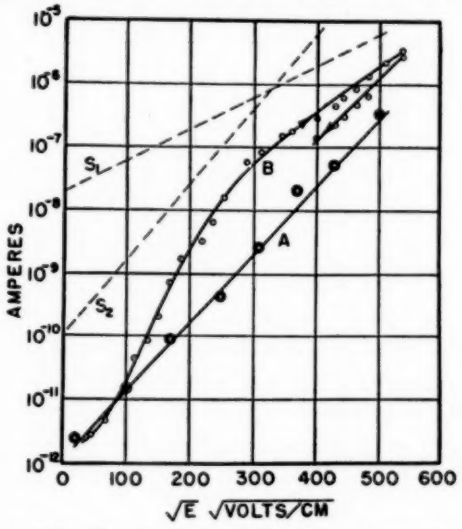

FIG. 4. Schottky plots of dielectric currents. A, data from Fig. 3 for −15°C; B, run at constant temperature, −15°C. S_1 and S_2 are the theoretical curves calculated from Eqs. (5) and (7), respectively.

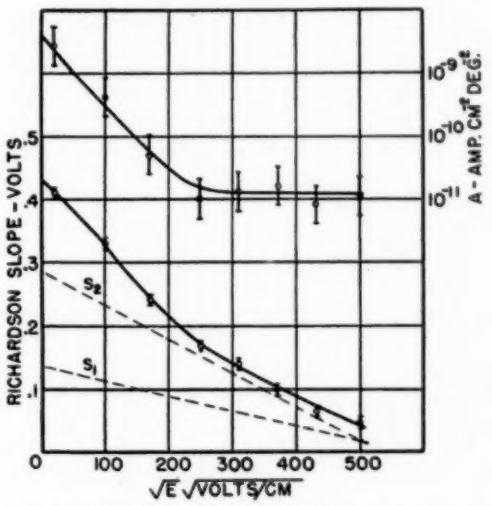

FIG. 5. Richardson slopes, φ, and thermionic constant A as function of $E^{\frac{1}{2}}$. S_1 and S_2 are theoretical curves calculated from Eqs. (4) and (6), respectively.

but to fail badly for low fields. It is therefore evident that the linearity of Curve A of Fig. 4 down to low fields is accidental, resulting from a simultaneous decrease of both A and φ in such a way as partially to compensate each other.

It will be noted that the values of the thermionic constant A are only 10^{-11} to 10^{-13} of the theoretical value 120 amp./cm² deg.². Values as small as this might be accounted for by assuming that (1) the emitting area of the cathode is much smaller than the geometrical area, (2) there is a large temperature coefficient of the work function,[5] (3) the surface potential barrier is a complex one having an exceedingly small transmission coefficient, (4) the currents are not (or are only in part) of thermionic origin.

Evidence that the emitting area is indeed smaller than the cathode area is the fact that, after a long series of runs, the *anode* is covered with small spots of wax-like material, presumably formed by chemical action of the electron stream. The cathode shows no such markings. This phenomena was also reported by Baker and Boltz and attributed to the concentration of the electron current into small pencils emanating from sensitive points or irregularities in the cathode surface. One could hardly assume, however, that the emitting area is only 10^{-13} of the total since this would require current densities up

[5] Cf. J. A. Becker and W. H. Brattain, Phys. Rev. **45**, 694 (1934).

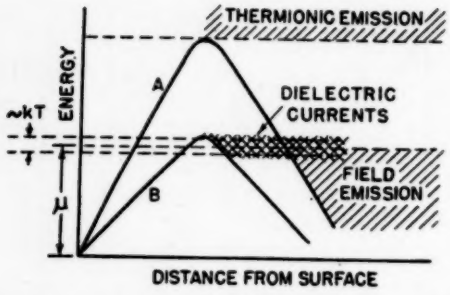

FIG. 6. Showing origin of thermionic, field and dielectric currents. *A*. Barrier in vacuum with field, thermionic electrons passing over the barrier, field currents penetrating the barrier; *B*. Barrier in dielectric indicating dielectric currents as consisting of electrons passing over as well as through the barrier.

to 10^7 amp./cm^2. A factor of 10^4 in surface area might not be ruled out leaving still a factor in A of $\sim 10^9$ to be accounted for.

There is no way of estimating the importance of the other factors, any one of which might be sufficiently important to account for the observed discrepancy.

DISCUSSION

The chief results of these experiments are: (1) The currents between Ni electrodes in toluene obey Richardson's equation, over the temperature range available, showing a very small slope and small value of A; (2) the log I *vs.* $E^{\frac{1}{2}}$ curves are linear with a slope over twice that predicted by the simple Schottky relation for a dielectric.

Neither of these is sufficient either to confirm or to rule out the hypothesis of the thermionic origin of the currents. The agreement of the Schottky slope with the Baker and Boltz equation must be regarded as accidental since the derivation of this equation is open to serious question. The failure to agree with the simple Schottky slope would be accounted for if (a) the field at the surface is not an image field or (b) if the emission came largely from surface irregularities where the actual field is higher than the "geometrical" field. Both of these possibilities find strong support in the experiments themselves so that lack of agreement with Eq. (5) is not surprising.

On the other hand the fact that our results agree approximately with those of Baker and Boltz suggests that something more fundamental is involved than either of the above-mentioned factors. This leads at once to the question of whether the observed currents are really of pure thermionic origin or whether, for example, they may not be attributed to field emission. At first sight it would appear that this could be tested experimentally, for the Fowler-Nordheim equation[6] for field emission is of the form

$$i = Ce^{-a/E},$$

where C and a are constants. However this equation is derived on the assumption that the potential barrier is so high and the temperature so low that the temperature "tail" of the Fermi distribution of electrons may be neglected. When the potential barrier is not large compared to kT, however (as in a dielectric), this equation no longer holds. In fact, in this case, the distinction between thermionic and field emission loses its significance.

Referring to Fig. 6 we may say that for a metal-vacuum interface (curve A) the thermionic currents consist of the electrons from the extreme tail of the Fermi distribution, the transmission coefficient over the barrier being large but the number of available electrons small. Field currents arise from the penetration of the barrier by the electrons from the main (temperature independent) part of the distribution (transmission coefficient small, number of electrons large). When the barrier is very low (curve B), however, there will be, even at fairly low fields, a moderately large transmission coefficient over and through the tip of the barrier and a moderately large number available electrons at the edge of the highest Fermi level. No calculations appear to have been made[6] of the current as a function of field and temperature to be expected in this case. It is easy to see, however, that if penetration of the tip of the barrier is important the currents will vary *more* rapidly with the field than the Schottky relation would predict since the transmission coefficient depends strongly on the field. Also they will vary *less* rapidly with the temperature than the Richardson equation would predict, since there is some contribution from the temperature independent part of the Fermi distribution.

This is precisely what is observed experimentally, namely, a large slope for the log i *vs.* $E^{\frac{1}{2}}$ curves and a small slope and small value of A for the Richardson curves. A quantitative test of this hypothesis, however, must await more complete theoretical calculations.

[6] R. H. Fowler and L. Nordheim, Proc. Roy. Soc. **119**, 173 (1928).

Time-Lag Analysis of the Townsend Discharge in Argon with Activated Caesium Electrodes*

R. W. ENGSTROM† AND W. S. HUXFORD
Northwestern University, Evanston, Illinois

(Received August 30, 1939)

A study of the time-lag in a photoelectric, gas amplified discharge for parallel electrodes as a function of gas pressure, plate separation, and amplification has demonstrated that diffusion of metastable argon atoms is the source of the lag and that these atoms striking the activated caesium cathode are highly efficient in liberating secondary electrons. The Townsend ionization coefficients, α and γ, have been determined in the usual manner over an extended range of values of E/p_0. Analysis of the time-lag function has made possible the separation of the number of secondary electrons released at the cathode into those due to positive ions and those produced by metastable argon atoms. A factor representing the fraction of electron energy gained in the field which is used to excite atoms to the metastable level has been determined as a function of E/p_0. The coefficient of diffusion of metastable argon atoms in argon has been computed and shown to be that expected for a metastable atom having a diameter effectively 1.74 that of the normal atom.

THE TOWNSEND DISCHARGE

ONLY in recent years has the Townsend discharge been studied with suitable gas purity to provide acceptable data on the primary ionization coefficient α. Secondary coefficients, often lumped into a single coefficient, γ, have been determined for a number of cases in which normally the cathode is a pure metal. But interpretation of γ is usually not precise since analysis of the ionization data can neither distinguish between proposed mechanisms nor separate the total γ into its parts when more than one secondary process is operative. The case of argon gas with activated caesium electrodes has been considered by W. S. Huxford[1] who shows that the most important considerations for relatively low pressures are secondary electron emission by positive ions and the action of metastable atoms in ionizing impurities or in releasing electrons from the cathode. Since separation of these factors is impossible by analysis of the static Townsend discharge some new means of investigation is necessary.

Such a new approach to the study of the Townsend discharge is suggested by the time of action expected for each of the several mechanisms. The release of a photoelectron has been shown by Lawrence and Beams[2] to occur in less than 10^{-8} second after the arrival of the exciting photon. The time of transit for electrons is very short but for positive ions is long enough to be easily detected. This time is determined by the positive ion mobility and has been observed by numerous investigators[3–5] using frequency response methods. But an even greater time-lag is evidenced in commercial types of gas photo-tubes.[5, 6, 7] Many suggestions have been made as to the probable cause of this lag, but delayed secondary emission by positive ions[8] and the natural delay time involved in the diffusion of metastable atoms are probably the most important of the proposed hypotheses. Certain impurity gases are known to destroy metastable states of argon; Campbell and Rivlin[9] have shown that the introduction of hydrogen decreases the amount of time-lag in the discharge. Similarly, a significant decrease in this lag by the introduction of argon into neon has been obtained by Kruithof[5] and taken as a strong argument in favor of the metastable atom hypothesis.

If metastable atoms are responsible for the large time-lag, the lag should increase with gas pressure and with length of the discharge path,

* Presented in part at the Chicago Meeting of the American Physical Society, December 1–2, 1939.

† Now at State Teachers College, St. Cloud, Minnesota.

[1] W. S. Huxford, Phys. Rev. **55**, 754 (1939).

[2] E. O. Lawrence and J. W. Beams, Phys. Rev. **32**, 478 (1928).

[3] A. Roggendorf, Physik. Zeits. **36**, 660 (1935).

[4] A. M. Skellett, J. App. Phys. **9**, 631 (1938).

[5] A. A. Kruithof, Philips Tech. Rev. **4**, 48 (1939).

[6] N. R. Campbell, H. R. Noble, and L. G. Stoodley, Phys. Soc. Proc. **48**, 589 (1936).

[7] F. Schroter and G. Lubszynski, Physik. Zeits. **31**, 897 (1930).

[8] K. H. Kingdon and H. E. Thompson, Physics (now J. App. Phys.) **1**, 343 (1931).

[9] N. R. Campbell and R. S. Rivlin, Phys. Soc. Proc. **49**, 12 (1937).

predictions which are contrary to those based on the hypothesis of delayed action of positive ions. Tests of the variation of time-lag with pressure have been unconvincing. Campbell, Noble, and Stoodley[6] have reported no appreciable variation with length of the discharge path. Their experiment, however, was handicapped by a narrow tube and small electrodes, a combination which does not afford a critical test. Therefore it was felt that a more thorough examination of the contrasting predictions was necessary.

In order to investigate the time-lag phenomenon more carefully, a tube with parallel plates was constructed in which gas pressure and plate separation could be varied. A critical investigation was undertaken with a new method recently developed in this laboratory[10] and particularly suited to direct measurement of the lagging current response to a periodically interrupted light beam. Combining the results of this study and the measured static coefficients for argon for the same tube, it was possible to separate the secondary mechanisms, and thus to obtain a complete analysis of the factors which contribute to gas-amplification in tubes having compound photo-cathodes.

Theory of Action of Metastable Atoms in the Discharge

Results of the experiment show that the diffusion of metastable atoms to the cathode is the source of the large time-lags observed; further, that the release of secondary electrons at the cathode by metastable atoms contributes substantially to the current amplification. An analysis of these effects is presented below for use in evaluation of the experimental data.

Amplification of the photoelectric current is accomplished by the ionization of the gas together with secondary effects at the cathode. Of these, the release of γ_p secondary electrons by each positive ion impact at the cathode is assumed instantaneous. A delayed emission is caused when γ_m secondary electrons per positive ion are released *by metastable atoms* diffusing to the cathode. We set

$$\gamma=\gamma_p+\gamma_m, \tag{1}$$

where γ is defined by the amplification equation upon which analysis of the Townsend discharge is based:

$$n_a=\frac{n_0e^{\alpha(d-d_0)}}{1-\gamma(e^{\alpha(d-d_0)}-1)}. \tag{2}$$

Here n_0 is the number of photoelectrons emitted per second, n_a is the equilibrium electron current collected at the anode, α is the number of electrons produced by each electron in traveling 1 cm in the direction of the electric field, d is the plate separation, and d_0 is the distance an electron moves in the direction of the field before gaining sufficient energy for ionization of an argon atom.

In order to obtain a more direct insight into the part played by metastable atoms as symbolized by the term γ_m, consider α_m to represent the number of metastable atoms produced per cm per electron. Since the number of positive ions created per cm per electron is α, the ratio of the number of metastable atoms produced per cm to the number of positive ions produced in the same cm is a constant, α_m/α. For simplification one may approximate the critical distance for onset of excitation of the metastable level by the corresponding distance for ionization, d_0. (Actually the ionization energy is 15.7 electron volts; the excitation energies, 11.5 and 11.7 electron volts.) It follows then that the ratio of the total number of metastable atoms created per second throughout the entire discharge to the number of positive ions created per second in the same discharge is again as above, α_m/α. However, of all the metastable atoms created in the discharge, only a fraction, f, determined by geometrical considerations, diffuse to the cathode. If each of those reaching the cathode liberates an average of ϵ electrons, the number of secondary electrons emitted from the cathode due to metastable atoms, per positive ion created, is

$$\gamma_m=\epsilon f\alpha_m/\alpha. \tag{3}$$

The ionization equation may now be written

$$n_a=n_0e^{\alpha(d-d_0)}/[1-(\gamma_p+\epsilon f\alpha_m/\alpha)(e^{\alpha(d-d_0)}-1)]. \tag{4}$$

This equation gives the equilibrium current for the case we have considered, but it does not indicate the build-up time of the discharge.

In order to introduce the element of time it is necessary to consider first the probable delay

[10] W. S. Huxford and R. W. Engstrom, Rev. Sci. Inst. **8**, 385 (1937).

time in metastable atoms diffusing to the cathode and second the effect this delay has on the measured current function. For those metastable atoms reaching the cathode by diffusion, it may be shown that the probability of arrival at time t per unit time is closely approximated by the form

$$P(t)=(1/\tau_0)e^{-t/\tau_0}, \quad t\geq 0$$
$$=0, \quad t<0. \tag{5}$$

τ_0 is taken as the average interval between creation and arrival for those metastable atoms reaching the cathode, $t=0$ denoting the time of creation of the metastable atoms in question.

In order to determine the average arrival time of metastable atoms at the cathode it is necessary to set up the differential equation for the diffusion of the metastable atoms. If infinite plane parallel electrodes are assumed, this equation is

$$\partial m(x,t)/\partial t = D\partial^2 m(x,t)/\partial x^2, \tag{6}$$

where D is the coefficient of diffusion and $m(x,t)$ is the linear density of metastable atoms at a distance x from the cathode, at time t. We assume the spacial distribution of metastable atoms when created to be

$$m(x,0)=0, \quad x<x_m,$$
$$m(x,0)\propto e^{\alpha(x-x_m)}, \quad x_m\leq x\leq d, \tag{7}$$

where x_m is the distance which an electron must traverse in the direction of the field to obtain the energy of excitation of the metastable state. A further assumption is that any metastable atom contacting either electrode loses its metastable energy. With these conditions Eq. (6) may be solved for $m(x,t)$ thus giving the distribution of metastable atoms at any time after creation. Of these, the number arriving per second at the cathode is

$$D[\partial m(x,t)/\partial x]_{x=0}.$$

The average arrival time may be obtained as follows:

$$\tau_0=\frac{\int_0^\infty tD[\partial m(x,t)/\partial x]_{x=0}dt}{\int_0^\infty D[\partial m(x,t)/\partial x]_{x=0}dt}. \tag{8}$$

Carrying out this operation, we find that τ_0 may be expressed as a series involving constants of the discharge:

$$\tau_0=(d^2/12D)\{1+(2/15)\alpha d+(1/180)\alpha^2d^2+\cdots$$
$$+(x_m/d)[2-(2/5)\alpha d-(1/45)\alpha^2d^2+\cdots]$$
$$+(x_m^2/d^2)[-1+(2/5)\alpha d+(1/36)\alpha^2d^2+\cdots]$$
$$+$$
$$\cdot$$
$$\cdot\ \cdot\ \cdot\ \cdot\ \cdot\ \cdot\ \cdot\ \cdot\}. \tag{9}$$

Knowing the probable time of delay in the arrival of metastable atoms in form [Eq. (5)] and in magnitude [Eq. (9)], we can now calculate its retarding effect on the measured current. Thus, it may be shown[11] that the form of the

[11] In order to do this and retain generality so that the method may be applicable to similar discharge problems, we proceed as follows: Let R represent the number of secondary electrons immediately produced at the cathode as a result of one primary electron leaving the cathode (R includes also the secondary emission by positive ions whose transit time is assumed to be negligible). Let L represent the delayed production of electrons per electron leaving the cathode (including those produced at the cathode by impact of metastable atoms whose diffusion time is the source of the observed time-lag). In the present case it follows that

$$R=\gamma_p(e^{\alpha(d-d_0)}-1),$$
$$L=\gamma_m(e^{\alpha(d-d_0)}-1).$$

If $n(t)$ represents the number of electrons leaving the cathode at time t, it must follow that

$$n(t)=n_0(t)+Rn(t)+L\int_0^\infty P(\tau)n(t-\tau)d\tau, \tag{A}$$

where τ represents the time variable of integration. A fundamental assumption of this equation is that the effect produced by an individual electron leaving the cathode is in no way a function of the immediate or previous current in the discharge. In this experiment the use of low current densities insured the absence of appreciable space charge. Small changes in emissivity of the cathode were found when the bombarding current was varied, as indicated in a later section. Equation A is supplemented, of course, by the normalization requirement:

$$\int_0^\infty P(t)dt=1.$$

Consider two cases corresponding to the experimental sequence in measuring the lagging current: the *rise*, where the light comes on and the current increases from zero to equilibrium; the *fall*, beginning with cessation of illumination and including the dying away of the current. Case I: The *Rise*. Take $n_0(t)=0$, $t<0$; $n_0(t)=1$, $t\geq 0$. It follows that $n(t)\equiv 0$, $t<0$. Therefore, indicating the *rise* solution by subscript r, one obtains

$$(1-R)n_r(t)-L\int_0^t P(\tau)n_r(t-\tau)d\tau=1, \quad t>0, \tag{B}$$

the general integral equation for the rising current. Case II: The *Fall*. Add the stipulation, $n_0(t)=0$, $t>T$, where T is the duration of the illumination. It follows for $t>T$, subscript f denoting the *fall* solution, that

$$(1-R)n_f(t-T)-L\int_0^{t-T}P(\tau)n_f(t-T-\tau)d\tau$$
$$-L\int_{t-T}^t P(\tau)n_r(t-\tau)d\tau=0, \tag{C}$$

where $n_f(t-T)$ has been written so that $n_f(0)$ corresponds

lagging current response to a constant photocurrent initiated at time $t=0$ is

$$i_{rise}(t)=1-(1-i_a)e^{-(i_a/\tau_0)t}, \qquad (10)$$

where the maximum equilibrium current is referred to as unity. Further, if the photoelectric source is cut off at time $t=T$ ($t'=0$), when the rising current lacked saturation by an amount i_c, the falling characteristic may be represented by the equation:

$$i_{fall}(t')=(1-i_b-i_c)e^{-(i_b/\tau_0)t}. \qquad (11)$$

In these equations, i_a and i_b represent the fraction of nonlagging current for the *rise* and for the *fall* characteristic, respectively; it can be shown that $i_a=i_b$. Eqs. (10) and (11) may now be used in the analysis and interpretation of the time lag data.

Since it is experimentally possible to measure the exponential decay constant, $\tau(\tau=\tau_0/i_a)$, and the nonlagging fraction of the current i_a, one may evaluate the fundamental time constant, τ_0. The variation of τ_0 may be studied as a function of distance and pressure as predicted by Eq. (9) wherein D varies inversely as the pressure. One may also determine D_0, the coefficient of diffusion of metastable argon atoms in normal argon for standard temperature and pressure.

Having α from static ionization measurements, we can calculate γ for each time-lag curve since the current amplification is known to be

$$A=n_a/n_0=e^{\alpha(d-d_0)}/[1-\gamma(e^{\alpha(d-d_0)}-1)]. \qquad (12)$$

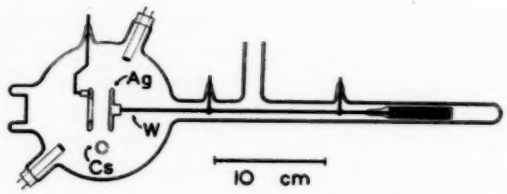

FIG. 1. The experimental tube, side view, showing arrangement for adjusting the plate separation of the plane parallel electrodes. A side arm is indicated which contained capsulated metallic caesium for activation of the electrodes.

In addition, having determined the amount of nonlagging current, one may find γ_p from the fact that the instantaneous amplification is independent of the metastable atom contribution in the term γ_m. Thus,

$$i_aA=\frac{e^{\alpha(d-d_0)}}{1-\gamma_p(e^{\alpha(d-d_0)}-1)}. \qquad (13)$$

Having both γ and γ_p, one may now determine $\gamma_m=\gamma-\gamma_p$. Furthermore, since f may be calculated from the geometry of the tube and a knowledge of the particular values of α, d, and d_0, one has a measure of $\epsilon\cdot\alpha_m$ [Eq. (3)], and, since ϵ is independent of the field strength, a function proportional to α_m. However, it is more convenient to discuss a number proportional to the fractional electron energy being delivered to excitation of metastable states. Therefore, write

$$\epsilon\cdot(\alpha_m/E)=(\alpha/E)(\gamma_m/f), \qquad (14)$$

where E is the magnitude of the electric field. Comparing this function with the maximum excitation possible if all the energy available to the electron in the field were used for this purpose $[(\alpha_m/E)_{max}=1/V_m$, where V_m is the critical energy of excitation (11.5 and 11.7 electron volts for argon)], we can obtain an estimate at least of the lower limit of ϵ.

Thus, an analysis of the time-lag current function, while significant as a means of testing the metastable atom theory of the lag, also allows a separation of the secondary emission into positive ion and metastable atom sources, provides a measure of the fraction of electron energy used to excite atoms to the metastable state, and permits an estimate of the efficiency of liberation of electrons at the cathode by metastable atom contact.

---

to the beginning of the *fall* current at $t=T$. Throughout this discussion $n_r(t)$ is considered to maintain its form independent of the condition imposed by interruption of the light. By direct substitution in Eq. (C) and comparison with Eq. (B) it is easily shown shat

$$n_f(t')\equiv n_r(t'+T)-n_r(t'),\ t'>0, \qquad (D)$$

where $t'=t-T$. *Therefore it is only necessary to solve Eq. B for $n_r(t)$ and obtain $n_f(t')$ by Eq. (D).* When T is sufficiently large, as may or may not be the case, the solution for the *fall* is simply the *rise* solution inverted with the maximum value as zero. Using $P(t)$ of Eq. (5) in integral Eq. (B), one obtains:

$$n_r(t)=[1/(1-R-L)][1-(L/(1-R))\times\exp-\{[(1-R-L)/(1-R)]t/\tau_0\}]. \qquad (E)$$

From Eq. (D):

$$n_f(t')=\frac{L}{1-R-L}\times\left[\frac{1-\exp-\{[(1-R-L)/(1-R)]T/\tau_0\}}{1-R}\right]\times\exp\{-[(1-R-L)/(1-R)]t'/\tau_0\}. \qquad (F)$$

Eqs. (E) and (F) represent the form of the time-lagging current for the *rise* and for the *fall*, respectively. From these two it is only necessary to make the proper interpretations of symbols to obtain forms (10) and (11).

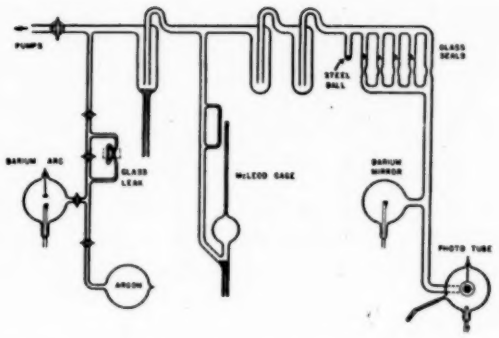

FIG. 2. The vacuum system iucluding the experimental photo-tube, end view.

EXPERIMENTAL PROCEDURE

The essential parts of the tube are the two parallel electrodes. These were made of cast silver, 4 cm in diameter, turned into shape with an approximate Rogowski contour,[12] polished to plane surfaces and supported by tungsten rods as shown in Fig. 1. A circular hole 2 cm in diameter was cut in the anode and across it a mesh was woven flush with the flat plate. The mesh was made of 0.005-inch silver wire spaced at 1-mm intervals; its transparency to light was about 80 percent. The cathode was mounted axially on a tungsten rod supported by nickel eyelets. At the other end of the tungsten rod an iron bar was welded and enveloped in glass. This arrangement provided external magnetic control of the position of the cathode, separation of the plates being measured within an error of approximately 0.003 cm. The plates were parallel to within an error of 0.5° of arc. For plate separations up to a maximum of 1.5 cm the spacing of electrodes and side walls was such as to prevent wall charges from distorting the electric field in the region of the discharge. Light from an incandescent filament was admitted through the anode mesh to the cathode by means of a plane Corex window in one end of the Pyrex envelope. Tungsten filaments were provided for degassing the metal parts by electron bombardment.

The vacuum system of Fig. 2 shows the arrangement used for admitting argon to the photo-tube. Spiral tungsten filaments were used to hold pieces of barium metal in both the arc chamber and in the barium mirror tube. The arc discharge in argon was controlled by carefully adjusting the temperature of the hot tungsten-barium cathode and was run many hours in the purification of the gas. Satisfactory purity of the argon was judged not only by the absence of impurity lines in the spectrum but also by the observation of no change in photo-sensitivity of the caesium surface when the gas entered the photo-tube. After the gas had been slowly admitted to the tube chamber and the pressure measured, one of the series of glass seals was closed by means of a small flame so that photo-tube and barium mirror were completely isolated from the rest of the system. When the measurements at one pressure were completed the fore-system was baked and evacuated, one of the inner seals broken by means of a magnetically controlled steel ball, and the entire purification and filling process repeated. If small amounts of gas impurities were released in closing the seals they were effectively removed by the barium mirror surface in the side tube, since no change of photo-sensitivity was observed during the series of measurements at four different pressures.[13] The processing of the caesium-oxide surface was carried out prior to admission of argon. The cathode had the usual sensitivity of commercial photo-tubes with a threshold at about 10,000A.

MEASURING CIRCUITS

The method used in measuring the time variation in the photo-tube has been described in a previous paper.[10] The circuit shown in Fig. 3, with switches in the *solid line* positions, is an improved arrangement having a current sensitivity some ten times that of the earlier circuit. Light from a tungsten filament entering the photo-tube was interrupted by means of a 45° sector in a disk driven by synchronous motor M_1. Instantaneous values of current were measured by potentiometer, P, by a null method using a highly insulated electrometer tube, T_3. The limit of accuracy of the readings was 0.0001 volt, corresponding to a current sensitivity of 5×10^{-10}

[12] W. Rogowski and H. Rengier, Archiv f. Elektrot. **16**, 73 (1926).

[13] Experience shows that great care must be exercised in degassing the metal parts and in applying a flame in sealing off the photo-tube if contaminations arising from chemically active gases and vapors are to be avoided. We are indebted to Professor Robert J. Cashman for valuable suggestions concerning vacuum technique and use of the barium mirror surface for removing impurity gases and vapors.

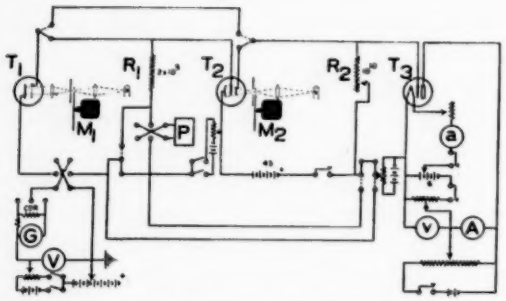

FIG. 3. Electrical circuit. T_1, the experimental tube; T_2, photoelectric triode; T_3, a three-element electrometer tube; M_1 and M_2, synchronous motors; P, potentiometer. The time-lag measuring circuit is shown with switches in the *solid line* position; the ionization measuring circuit with switches in the *dotted line* position.

amp. The arrangement shown with the switches in the *dotted line* positions, eliminating the photoelectric triode, T_2, from the circuit, was used for measuring static ionization currents.

IONIZATION COEFFICIENTS

The usual method for obtaining the Townsend ionization coefficients requires a knowledge of the current as a function of plate separation at constant field. However, fatigue effects common to the type of surface used made it expedient to measure current-voltage characteristics at a number of plate separations and from these to obtain current-distance data by interpolation. Effects of back diffusion of electrons, of change of photo-sensitivity with field, and of variation of scattered light with plate separation were accurately measured and corrections suitably applied to the data. In these measurements the density of the initiating photo-current was of the order of 1×10^{-10} ampere cm^{-2}; smaller currents were not feasible because of the magnitude of the thermionic emission at room temperature.

Data were obtained for four pressures, p_0 (reduced to a temperature of 0°C) = 0.0983, 0.1933, 0.407 and 0.815 mm of Hg. In Fig. 4, the results are shown in the form α/p_0 plotted as a function of E/p_0, with the curve of Kruithof and Penning[14] for argon dotted in for comparison. Two tendencies are observed: for successively lower pressures the data are lower; for the higher pressures the points are high with reference to the Kruithof and Penning curve. Accuracy of analysis decreases with decrease in pressure; for the lowest pressure the inaccuracy is so large that the points are of little value; (this is again apparent in the trend of the secondary coefficient, γ). However it is believed that the downward trend of the points for lower pressures was the unfortunate result of using an open mesh which undoubtedly distorted the field besides allowing penetration of electrons and possibly ionization behind the anode. In general the trend of the data agrees with that of Kruithof and Penning. It is possible that the apparently larger α/p_0 values are the result of ionization of caesium vapor which may be present in the gas. For very large values of E/p_0 there is no tendency to reach a maximum value of α/p_0 as was observed by Huxford.[1]

Values of the secondary coefficient γ obtained from the ionization analysis are shown in Fig. 5 (solid points). The order of magnitude agrees very well with that reported by Huxford[1] for similar cathodes. The data for the three highest pressures are fairly consistent but those for the lowest show a divergence, as anticipated. The solid line has been drawn disregarding the points for the lowest pressure used.

TIME-LAG DATA

It was not possible to measure the trend of the current with time for currents of the low order of magnitude used in the measurement of the ionization coefficients. However, the maximum

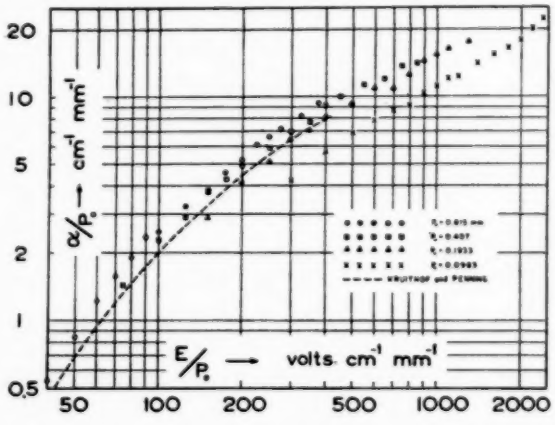

FIG. 4. Results for the first Townsend coefficient, for argon, compared with those of Kruithof and Penning. The errors were so large in the determinations at the lowest pressure (crosses) that these values are disregarded in the analysis.

[14] A. A. Kruithof and F. M. Penning, Physica **3**, 515 (1936).

gas amplified current densities used never exceeded 1×10^{-7} ampere cm^{-2}. When currents of the order 10 to 100 times this were used serious distortion of the time-lag function resulted as judged by the asymmetry of rising and falling current functions. Even for the currents used there was some evidence of asymmetry, but in general the distortion was negligible.

Figure 6 shows a characteristic time-lag curve at a pressure of 0.815 mm of Hg as compared with the current observed for a discharge in vacuum. Since the photoelectric response is instantaneous[2] the curve for a vacuum represents quite accurately the illumination function. From the time-lag currents plotted on a logarithmic current scale, Fig. 7, we see that the currents are indeed exponential as predicted. Measurement of the slope allowed a determination of the time constant τ. The values of i_a, i_b, and i_c were also obtained from the logarithmic plot as indicated.

Table I shows the tabulated constants for the curves analyzed. A comparison of $(\tau)_r$ and $(\tau)_f$ as well as i_a and i_b shows fairly good agreement between the rising and falling characteristics, confirming the assumption that the effects produced by an individual electron leaving the cathode are independent of the immediate or previous discharge current. However, for the lowest pressure, besides the regular time-lag attributable to metastable atoms, a very much longer time-lag was found. This lagging current had a time constant of the order 0.01 sec. and amounted in some cases to a few percent of the

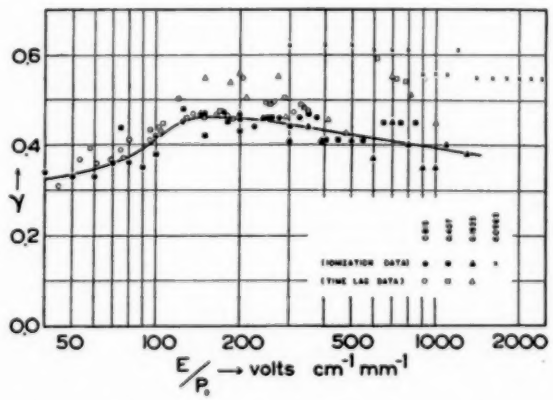

FIG. 5. Values of the second Townsend coefficient, γ *vs.* E/p_0 for the ionization data (solid points), and for the time-lag data (open points). The points for the lowest pressure (crosses) were disregarded in drawing the line through the solid points.

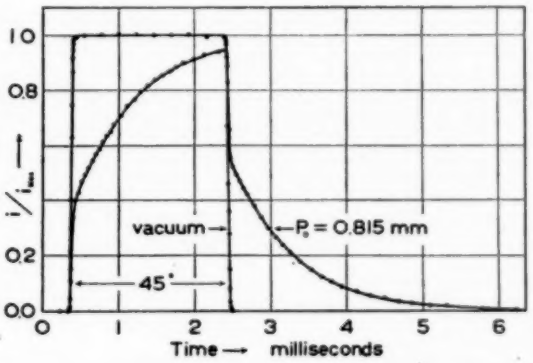

FIG. 6. Samples of the time-lag curves as measured, i/i_{max} *vs.* time in milliseconds, for vacuum and for argon with $p_0=0.815$ mm of Hg, $d=0.399$ cm, $V=57$ volts, current amplification, 29.6. The period of illumination was 45° a.c. cycle as indicated.

total current. The probable cause is a slow change in the cathode surface with bombarding current. In all cases where this lag appeared it was subtracted from the main data which could then be satisfactorily analyzed in terms of the action of metastable atoms.

The values of τ show a very decided increase with current amplification, but the fundamental constant, τ_0, shows very little trend. Values of τ_0 for the *rise* and for the *fall* are given in Table I for the separate corresponding values of i_a and i_b. The data for the falling current are more accurate since measurement of the time constant was direct and did not involve inverting the curve about the maximum value.

Since the variation of τ_0 with amplification is small and uncertain, it was disregarded and an average value, obtained by weighting according to accuracy of measurement at a given distance and pressure, was used. The variation of these average time constants with pressure and distance furnishes the major confirmation of the metastable atom theory of the time-lag. A weighting equivalent to that of the time constants applied to the averaging of the constants of Eq. (9) yielded values of $(\alpha\cdot d)_{Av}=1.25$, and $(x_m/d)_{Av}=0.20$. Substituting these average values in Eq. (9) and dropping insignificant terms, we approximate

$$\tau_0=1.36d^2/12D=k\cdot p_0\cdot d^2, \qquad (15)$$

where

$$k=1.36/12\cdot D_1 \qquad (16)$$

and D_1 is numerically equal to the coefficient of

TABLE I. *Tabulation of constants for the time-lag curves.*

p_0	d	V	A	i_a	i_b	i_c	$(\tau)_r$	$(\tau)_f$	$(\tau_0)_r$	$(\tau_0)_f$
0.815	0.210	25.0	1.64	0.940	0.950	0.000	0.137	0.201	0.129	0.191
		35.0	2.57	0.877	0.896	0.000	0.124	0.141	0.109	0.126
		45.0	4.90	0.826	0.836	0.000	0.152	0.159	0.125	0.133
		53.0	10.1	0.63	0.692	0.000	0.137	0.170	0.086	0.118
		59.0	38.2	0.31	0.408	0.000	0.269	0.244	0.083	0.099
	0.399	35.0	2.32	0.875	0.877	0.001	0.402	0.419	0.352	0.367
		45.0	4.45	0.762	0.787	0.001	0.426	0.444	0.325	0.349
		53.0	10.7	0.585	0.624	0.009	0.551	0.559	0.322	0.348
		57.0	25.4	0.361	0.382	0.048	0.800	0.815	0.289	0.311
	0.715	30.0	1.44	0.955	0.917	0.009	1.27*	1.19	1.21*	1.09
		43.0	2.73	0.819	0.807	0.037	1.20*	1.20	0.98*	0.97
		55.0	7.20	0.624	0.598	0.099	1.40	1.51	0.873	0.903
		60.0	16.3	0.421	0.422	0.220	2.16*	2.18	0.910*	0.920
	1.107	45.0	2.08	0.851	0.833	0.064	2.46	2.41	2.09	2.00
		55.0	3.74	0.728	0.717	0.130	2.84*	2.88	2.06*	2.06
		62.0	7.00	0.594	0.585	0.210	3.18*	3.28	1.89*	1.92
		68.0	19.5	0.360	0.348	0.412	5.24*	5.19	1.88*	1.80
	1.604	45.0	1.53	0.897	0.855	0.091	—	4.20	—	3.59
		58.0	2.57	0.780	0.760	0.151	5.8	4.43	4.5	3.36
		68.0	5.10	0.627	0.633	0.252	5.6	5.60	3.5	3.54
		75.0	13.2	0.420	0.434	0.429	7.9	7.30	3.3	3.16
0.407	0.221	35.0	2.31	0.948	0.958	0.000	0.24	0.155	0.23*	0.148
		55.0	6.31	0.67	0.87	0.000	0.105	0.131	0.070	0.114
		65.0	12.1	0.55	0.83	0.000	0.167	0.103	0.092	0.085
		70.0	20.2	0.37	0.85	0.000	0.193	0.211	0.071	0.179
	0.450	30.0	1.78	0.907	0.923	0.000	0.232	0.272	0.210	0.251
		45.0	4.00	0.824	0.845	0.000	0.274	0.298	0.226	0.252
		53.0	7.21	0.718	0.798	0.001	0.328	0.324	0.236	0.258
		60.0	15.9	0.519	0.664	0.002	0.382	0.360	0.198	0.228
	0.822	40.0	2.71	0.850	0.854	0.009	0.769	0.780	0.652	0.665
		50.0	5.12	0.732	0.762	0.021	0.835	0.867	0.610	0.660
		55.0	8.65	0.628	0.646	0.047	1.00	0.990	0.628	0.640
		62.0	35.4	0.328	0.347	0.242	2.1	1.74	0.67	0.604
	1.157	30.0	1.42	0.916	0.921	0.022	1.6	1.37	1.5	1.26
		40.0	2.29	0.842	0.861	0.037	1.5	1.40	1.3	1.21
		50.0	4.24	0.748	0.755	0.068	1.60	1.47	1.20	1.11
		60.0	13.4	0.514	0.514	0.202	2.5	2.08	1.0	1.07
	1.530	35.0	1.52	0.908	0.908	0.037	2.4	2.68	2.2	2.43
		50.0	3.14	0.778	0.780	0.100	2.7	2.54	2.1	1.98
		60.0	7.42	0.601	0.604	0.205	3.4	3.06	2.0	1.85
		65.0	16.6	0.435	0.442	0.332	4.7	4.04	2.0	1.78
0.1933	0.194	25.0	1.47	0.924	0.948	0.000	0.230	0.201	0.212	0.190
		40.0	2.31	0.89	0.86	0.000	0.161	0.167	0.143	0.144
		65.0	4.69	0.67	0.81	0.000	0.147	0.175	0.098	0.142
		80.0	8.72	0.61	0.75	0.000	0.208	0.314	0.127	0.236
	0.443	40.0	2.41	0.889	0.901	0.000	0.224	0.167	0.199	0.150
		60.0	4.85	0.75	0.85	0.000	0.165	0.191	0.124	0.162
		70.0	7.28	0.65	0.81	0.000	0.145	0.226	0.094	0.183
		85.0	19.5	0.60	0.70	0.000	0.195	0.258	0.117	0.180
	0.762	40.0	2.54	0.869	0.892	0.000	0.282	0.296	0.245	0.264
		50.0	3.84	0.820	0.853	0.000	0.268	0.322	0.220	0.274
		60.0	6.48	0.754	0.815	0.001	0.370	0.330	0.278	0.269
		70.0	12.2	0.66	0.748	0.002	0.402	0.334	0.265	0.250
	1.167	35.0	1.97	0.917	0.920	0.001	0.390	0.665	0.358	0.612
		45.0	3.18	0.885	0.870	0.006	0.725	0.649	0.640	0.565
		55.0	5.64	0.808	0.819	0.004	0.550	0.716	0.444	0.586
		65.0	14.1	0.64	0.672	0.040	0.960	0.885	0.61	0.595
	1.556	35.0	1.74	0.912	0.920	0.018	1.31	1.13	1.19	1.04
		45.0	2.89	0.857	0.869	0.020	1.07	1.04	0.92	0.90
		55.0	5.64	0.77	0.791	0.048	1.33	1.15	1.02	0.91
		62.0	11.4	0.66	0.65	0.11	1.93	1.38	1.27	0.90

EXPLANATION OF SYMBOLS: p_0 = pressure of argon in mm of Hg reduced to 0°C. d = plate separation in cm.
V = potential in volts applied to the electrodes.
A = current amplification = ratio of the current collected to the initiating photo-current (corrections having been made to account for back diffusion and change in emission with field, so that A may be inserted directly in Eqs. (12) and (13)).
i_a = nonlagging fraction of the current as measured in the *rise* of the time-lag current function.
i_b = nonlagging fraction of the current as measured in the *fall*.
i_c = ratio of the difference between the equilibrium current and the current at the end of the light period, to the equilibrium current.
$(\tau)_r$ = $1/e$th life of the exponential current for the *rise* in milliseconds.
$(\tau)_f$ = $1/e$th life of the exponential current for the *fall* in milliseconds.
$(\tau_0)_r$ = fundamental time constant obtained from the *rise*, in milliseconds, $= i_a \cdot (\tau)_r$ = average time of arrival of metastable atoms at the cathode [see Eq. (10)].
$(\tau_0)_f$ = fundamental time constant obtained from the *fall*, in milliseconds, $= i_b (\tau)_f$ [see Eq. (11)].

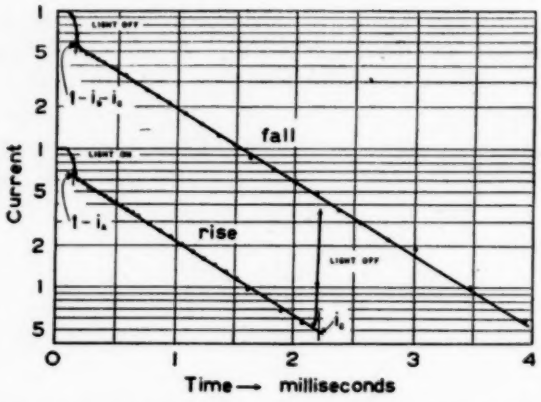

FIG. 7. The time-lag curve of Fig. 6 for argon is here plotted on a logarithmic current scale. The slope of the line determines the time constant. Intercepts of the lines with those lines indicating the time of light on and light off are measures of i_a, i_b, and i_c.

diffusion of metastable argon atoms in argon at 1 mm Hg reduced pressure.

Preliminary graphing indicated that at the lower pressures there is an apparent elongation of the discharge region. This suggests that metastable atoms may diffuse back and forth through the mesh thus allowing more diffusion space than was assumed. Since the transparency of the mesh was about 80 percent, this apparent elongation of the discharge may amount to several free paths. Therefore one may write

$$\tau_0 = k \cdot p_0 (d + c\lambda)^2, \tag{17}$$

where λ is the mean free path of a metastable argon atom and c is a constant. Since $\lambda = \lambda_1/p_0$ where λ_1 is numerically the mean free path at 1 mm Hg,

$$\tau_0 = k \cdot p_0 (d + c\lambda_1/p_0)^2; \tag{18}$$

and by algebraic manipulation,

$$\tau_0^{\frac{1}{2}} p_0^{\frac{1}{2}} = k^{\frac{1}{2}} (p_0 d + c\lambda_1). \tag{19}$$

If $\tau_0^{\frac{1}{2}} p_0^{\frac{1}{2}}$ is plotted against $p_0 \cdot d$ a straight line of slope $k^{\frac{1}{2}}$ should result regardless of the correction due to the mesh. In addition, by measuring the negative intercept on the $p_0 \cdot d$ axis, the term $c\lambda_1$ may be evaluated.

The averaged data are portrayed graphically as suggested by Eq. (19) in Fig. 8, showing satisfactory conformity to the predicted relationship. Since the data cover a considerable range of pressures and distances we may say that, qualitatively, the theory of release of electrons from the cathode by metastable atoms is confirmed.

Again it may be noted that while there are slight differences in the points obtained from the *rise* and from the *fall*, the agreement is satisfactory.

The data were evaluated by a least squares method to obtain the best values for the slope of the line and for the intercept on the p_0d axis. The following are the values so determined:

$$k^{\frac{1}{2}}=0.0410 \text{ mm}^{\frac{1}{2}} \text{ sec.}^{\frac{1}{2}} \text{ mm}^{-1} \text{ cm}^{-1},$$
$$c\lambda_1=0.047 \text{ mm cm}.$$

Since for argon λ_1 is very nearly 0.0076 mm (of Hg) cm, c is approximately 6 free paths, a reasonable figure. Computing by use of Eq. (16), we find the coefficient of diffusion of metastable argon atoms in argon for $p_0=1$ mm Hg at room temperature to be $D_1=67.5$ cm^2 sec.$^{-1}$ mm.

From the experimental law,

$$D=D_0(T/273)^n(760/p)=D_0(T/273)^{n-1}(760/p_0)$$

and taking $n=1.75$,[15] we obtain: $D_0=0.084$ cm^2 sec.$^{-1}$ at standard temperature and pressure.

There are no experimental values for the coefficient of self-diffusion of argon atoms or for excited argon atoms in argon. However, D_0 may be obtained with fair accuracy from the expression involving the coefficient of viscosity, η, and the density of the gas, ρ, both of which are known. Thus,[16] $D_0=1.336\eta/\rho$. Taking the value $\eta=2196\times10^{-7}$ dyne sec. cm^{-2},[17] we obtain $D_0=0.157$ for argon atoms in argon.

However, we are dealing with excited atoms diffusing in a gas composed of normal atoms. Undoubtedly the kinetic cross section of the excited atoms is larger than that of the normal atoms. Just how much, it is difficult to predict. Coulliette[18] concluded, in an experiment with metastable mercury atoms diffusing into mercury vapor and subsequently striking a nickel hemisphere where secondary electrons were ejected, that the effective diameter of the excited mercury atom is 1.5 normal.

The normal argon state is a $3p^6\,{}^1S$ configuration; the excited metastable levels are $3p^5(^2P_{1\frac{1}{2}})4s$, $J=2$; $3p^5(^2P_{\frac{1}{2}})4s$, $J=0$. The electron involved in each case has moved from a $3p$ to a $4s$ level. Since the average distance of the electron from the nucleus increases as the square of the principal quantum number, the average diameter would be increased by a factor $\frac{16}{9}=1.78$. This of course, does not necessarily approximate the kinetic diameter but it gives strong evidence that the diameter is larger.

According to Jeans[19] the coefficient of interdiffusion varies inversely as the square of the arithmetical mean of the diameters. If we assume the difference in diameters as the explanation of the discrepancy in the experimental and calculated values above, we obtain for the ratio of the excited atom diameter to the normal atom diameter the value 1.74. This very close agreement of the metastable atom diameter as observed and predicted, while fortuitous in view of the various assumptions involved, is significant in that the correction is the right order of magnitude and thus lends strong support to the whole theory of action of metastable atoms in the discharge.

Evaluation of Secondary Mechanisms

From the values of α calculated from the ionization data at each pressure and the measured amplification factor, A, γ may be computed for each of the time-lag curves by means of Eq. (12). For low amplifications, the errors were quite large; hence only results for amplifications greater than 2.5 are shown in Fig. 5 (open

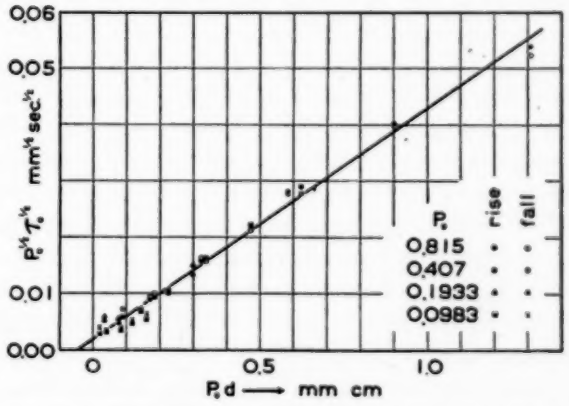

FIG. 8. Experimental verification of Eq. (19) $[\tau_0^{\frac{1}{2}}P_0^{\frac{1}{2}}=k^{\frac{1}{2}}(P_0d+c\lambda_1)]$ which is based on considerations of the diffusion time of metastable argon atoms and their subsequent release of electrons at the cathode.

[15] Int. Crit. Tab. **5**, p. 62.
[16] L. B. Loeb, *The Kinetic Theory of Gases* (McGraw-Hill, second edition, 1934), p. 273.
[17] E. H. Kennard, *Kinetic Theory of Gases*, (McGraw-Hill, first edition, 1938), p. 149.
[18] J. H. Coulliette, Phys. Rev. **32**, 636 (1928).
[19] J. H. Jeans, *The Dynamic Theory of Gases* (Cambridge University Press, second edition, 1921), p. 332.

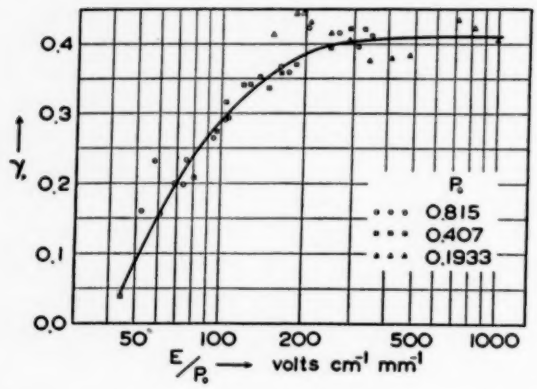

FIG. 9. γ_p, the number of secondary electrons emitted per positive argon ion at the activated caesium cathode, *vs.* E/p_0. These values were obtained from the time-lag data by eliminating the contribution of the metastable atoms to the Townsend γ.

points). The trend of γ values so obtained is somewhat higher than that for the ionization data, again indicating increased surface sensitivity for larger bombarding currents.[20]

Values of γ_p, the secondary coefficient for positive ions may now be determined by the use of Eq. (16). These values, corrected for back diffusion to yield the total emission, are plotted in Fig. 9. It is interesting to note that while the γ values showed no appreciable decrease for low E/p_0, the values of γ_p do show this trend with a tendency to level out at higher E/p_0 values. The difference between γ and γ_p gives an indication of the contribution of metastable atoms to the discharge. This is seen to be most important in the lower range of E/p_0.

Now, following Eq. (14), it is possible to calculate $\epsilon\alpha_m/E$ which is proportional to the fractional energy being used in the excitation of metastable atoms. The curve, Fig. 10, showing $\epsilon\alpha_m/E$ as a function of E/p_0, was drawn to fit the more reliable points. By comparing this curve with the energy balance curves of Penning[21] and with the maximum possible value of $\alpha_m/E=1/V_m=0.086$, it has been determined that the *minimum efficiency* for the production of secondary electrons by metastable argon atoms from an activated caesium surface is $\epsilon=0.4$ secondary electron per metastable atom.

[20] Increased gas amplification and photo-sensitivity of the cathode with rise of current has previously been noted. See reference 1, p. 756.

[21] F. M. Penning, Physica **5**, 286 (1938).

OTHER EVIDENCE

Time-lag curves obtained from measurements made with the caesium-activated, mesh-centered electrode as cathode show that the order of the time-delay was the same as for the solid cathode, but the fraction of lag current was less. Analysis shows nearly the same γ_p but considerably smaller γ_m. One possible explanation is that the surfaces differ in activation, but the obvious interpretation is that many of the metastable atoms pass through the mesh cathode and fail to contribute to the discharge.

In connection with work already reported on ionization coefficients for argon with a pure barium cathode,[22] time-lag measurements were also taken. There was no measureable lag of the order found in the present experiment with caesium. At a pressure of 1.51 mm Hg, a plate separation of 2.96 cm, an applied potential of 186 volts, and a gas amplification of 18.9, the $1/e$th life of the barely observable lag was approximately 7×10^{-5} second which agrees very closely with the time of transit of positive ions. Since metastable atoms certainly are present, the obvious conclusion is that the efficiency of release of electrons by metastable atoms, ϵ, is very small for pure barium.

After the main data had been taken with the barium tube, the surface was contaminated with hydrogen and an attempt was made to produce an activated surface having a higher sensitivity. Although the increased photo-sensitivity was not of the magnitude found in the case of the caesium surface, there was considerable increase in photo-emission and the surface no doubt had a complex structure. Time-lag measurements were again taken and at a pressure of 0.219 mm, a plate separation of 0.24 cm, a potential of 238 volts and an amplification of about 49, the $1/e$th life was 0.17 millisecond, the fraction of the lagging current being about 62 percent. Calculating, we find $\tau_0=0.067$ millisecond, which is in good agreement with the value 0.076 millisecond, computed from the assumption of metastable atom action. It would seem that activation of the barium surface greatly increased the efficiency of release of electrons by metastable atoms. Undoubtedly many of the conflicting results of

[22] R. W. Engstrom, Phys. Rev. **55**, 239(A) (1939).

previous investigations of the efficiency of metastable atoms in releasing electrons are due to wide variations in surface contamination of the electrodes used.

Interesting in this connection is the experiment of Skellett[4] in which the frequency response of photo-currents was measured in an argon-filled spherical tube having a carbon cathode on the walls. Skellett reported no time-lag that could not be explained by mobility of positive ions. Low efficiency of the carbon to release of electrons by metastable atoms no doubt accounts for the nonappearance of the long time-lag.

Ionization of Impurities

Before concluding, we must consider the other possible effect of metastable atoms. As shown by Penning,[23] gas impurities with an ionization potential below the metastable excitation potential of the main gas may be ionized by collisions with metastable atoms. The rate of disappearance of metastable atoms would in this case be proportional to the impurity present.

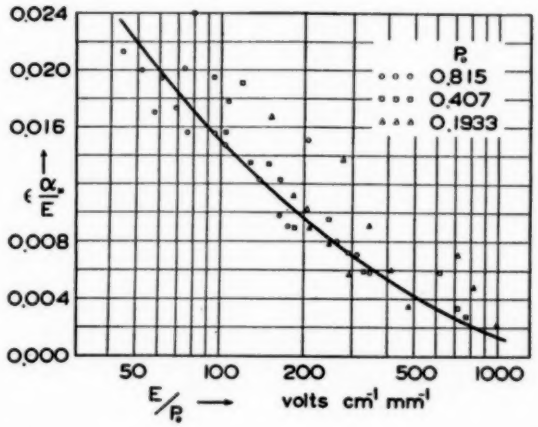

FIG. 10. $\epsilon \cdot \alpha_m/E$ *vs.* E/p_0 where ϵ is the number of electrons liberated from the cathode per impacting metastable atom and α_m is the number of metastable atoms produced per electron in traveling one cm in the direction of the electric field. $\epsilon \cdot \alpha_m/E$ is proportional to the fractional energy dissipation of the electrons in exciting atoms to the metastable state. It is estimated that ϵ is greater than 0.4.

[23] F. M. Penning, Zeits. f. Physik **46**, 335 (1928).

A study of Fig. 8 shows a slight tendency of the data toward a negative curvature. This is what would be expected if there were ionization of caesium vapor by metastable atoms. When a least square evaluation of the curvature tendency was made it was found that the pressure of caesium necessary to account for the result is slightly more than 10 times the vapor pressure of free caesium at room temperature, 1.7×10^{-6} mm of Hg (if every collision of a metastable argon atom with a caesium atom resulted in ionization). Nevertheless, although ionization of impurities may occur, it cannot account for the entire action of the metastable atoms, and the evidence suggests that the Penning effect is of minor importance in this experiment. Moreover, the curvature (Fig. 8) may also be explained on the assumption that there is a small but finite probability of a metastable atom losing its energy in a collision with a normal argon atom; one destructive collision in about 10^4 would suffice. Of course any loss of metastable atoms by collision of the second kind with electrons would be negligible since the current density is so small.

Conclusion

In the Townsend discharge for argon gas and an activated caesium cathode, the important auxiliary mechanisms are the secondary electron emission by positive ions and the liberation of cathode electrons by the impact of metastable argon atoms. The diffusion time of the latter remarkably efficient agent is the source of the long time-lag observed in this type of discharge.

Acknowledgment

The writers wish to acknowledge the valued assistance of Mr. George Olewin and Mr. Howard S. Martin of the Northwestern University staff. Mr. Olewin designed and built the motor housings and phase shifting mechanism used in taking the time-lag data; Mr. Martin was responsible for the glass blowing involved in the vacuum system and experimental tube.

Note on Thin Quartz Crystals as Used in the Cauchois Focusing X-Ray Spectrograph

F. R. HIRSH, JR.
California Institute of Technology, Pasadena, California
(Received February 29, 1940)

Doubled x-ray lines, produced by the Cauchois focusing spectrograph, have their origin as a result of double curvature of the crystal which causes defocusing of strong surface layer reflections. At the center of the lines shown in this paper, is a single portion, where the surface layer reflections are superimposed as a result of Cauchois exact focusing, showing that the surface layers share in the uniform strain of the crystal. Calculated separation of doubled lines, on the assumption of parallelism of surface layer reflections, shows poor agreement with the actual separations, adding support to the idea of the origin of the doubled lines as a result of crystal warping. The breaking of bent crystals is attributed to the presence of this double curvature. Broadened lines due to light etching are the result of poor resolving power of the thinned surface layers which still do the bulk of reflection.

INTRODUCTION

FINCH[1] first demonstrated that the surface layers of quartz (and other crystals), formed by grinding and polishing, are crystalline and integral with the body of the crystal. DuMond and Bollman[2] and D. L. Webster[3] have commented on the existence of doubled x-ray lines, observing that the two lines came from the two surfaces of the crystal. Watson[4] has observed doubled lines with the Cauchois spectrograph. Recently, a more detailed study[5] was made of these doubled lines. It is the purpose of the present paper to offer explanations for certain unexplained phenomena which exist in these studies[1–5] of crystals. They are: (1) Why are doubled lines, produced by the Cauchois focusing spectrograph, sometimes observed to be single lines at their center? (2) May we account for the separation of the doubled lines in terms of crystal thickness? (3) Why does light etching greatly broaden lines?

DISCUSSION

1. Doubled x-ray lines formed by the Cauchois spectrograph

In Fig. 1 is shown an enlargement (10×) of half of the length of the $K\alpha_{1,2}$ lines in a typical molybdenum K spectrum[6] taken with the Cauchois focusing spectrograph. In Fig. 1 the reader may assume that the missing half of the line is the mirror image of the half reproduced, the mirror being placed at right angles to the end of the single portion, to produce *a line doubled at the ends, and single at and near the center*. This is a new observation for which the following explanation is presented.

The fact that the line is single at the center, shows that Cauchois exact focusing exists for the center portion of the crystal: at the outside of the crystal the grating space of the crystal lattice is increased by tension; at the inside (next to the convex warping cylinder) the grating space is decreased by compression, the resulting alteration in Bragg angles being just exactly right for the two portions so that they will focus along with the radiation from the "zero strain surface" where the grating space is unaltered. Thus we have focusing from the thickness of the crystal, as well as along the arc of the crystal. Although the crystal has been ground and polished, *at the center of the line the reflections from the two disturbed surfaces are superimposed* (Cauchois exact focusing) *showing that the surface layers, at the center of the crystal at least, share in the uniform radial strain of the crystal.* This is in accord with the findings of Finch.[1]

We must now concern ourselves with the doubled ends of the x-ray line. Unmistakably, the two components of the doubled line are due to

[1] G. I. Finch, Nature **138**, 1010 (1936); Science Progress (April, 1937).
[2] J. W. M. DuMond and V. L. Bollman, Phys. Rev. **50**, 524 (1936).
[3] Unpublished data.
[4] B. B. Watson, Rev. Sci. Inst. **8**, 480 (1937).
[5] F. R. Hirsh, Jr. and J. W. M. DuMond, Phys. Rev. **54**, 789 (1938).
[6] This is the same line whose photometric profile is shown in reference 5, Fig. 1.

the two disturbed surface layers of the crystal: this was clearly shown in reference 5. But why are not the two components exactly focused near the ends as at the center? The following explanation is offered. In bending an elastic quartz crystal between two rigid cylindrical surfaces, such as are employed in the Cauchois focusing spectrograph, the crystal does not assume a true cylindrical shape. The behavior of a simple elastic body such as rubber eraser will remind us that bending develops one curvature, while as a result of tension and lateral contraction on the outside of the eraser arc, and compression and lateral swelling on the inside arc, a second curvature develops at right angles to the primary curvature (see Fig. 2). The result of the curvature shown in the horizontal section of Fig. 2 is the curvature (shown exaggerated) in the vertical section of Fig. 2. As a consequence, the quartz crystal pulls back from the inside (convex) warping cylinder of the spectrograph at the top and bottom of the window aperture, while at the center the crystal should be roughly tangent to the convex warping cylinder and coincident with the focal circle. Thus the x-radiation from the top and bottom of the window comes to the photographic film on the focal circle "out of focus," being focused in front of the film and re-divergent at the film (see doubled ends of spectral lines in Fig. 1). The x-radiation from the horizontal central zone of the crystal at the window, where the crystal is approximately tangent to the convex warping cylinder, will be in quite sharp focus. (See single part of lines in Fig. 1.) (If, however, the crystal is not bent so as to be roughly tangent to the convex warping cylinder at the center of the window, we could not expect a single line at the center of the recording film. For a probable example of this see Fig. 3, reference 4. Here the warping cylinders must not have been tightened enough to bring the center zone of the crystal into tangency with the convex cylinder, i.e. coincident with the focal circle.)

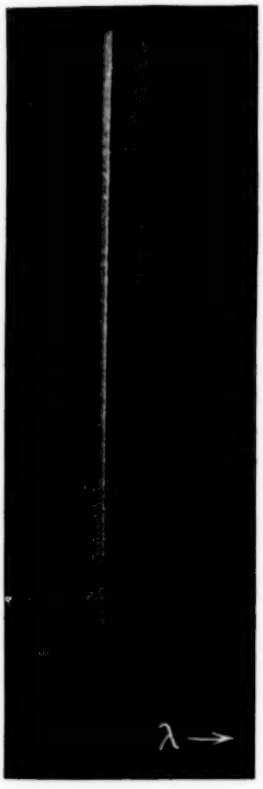

FIG. 1. Tenfold enlargement of half of the Mo $K\alpha_1$, α_2 lines secured in Cauchois spectrograph with thin quartz crystal. The lines are doubled near the ends, and in good focus (single) at center.

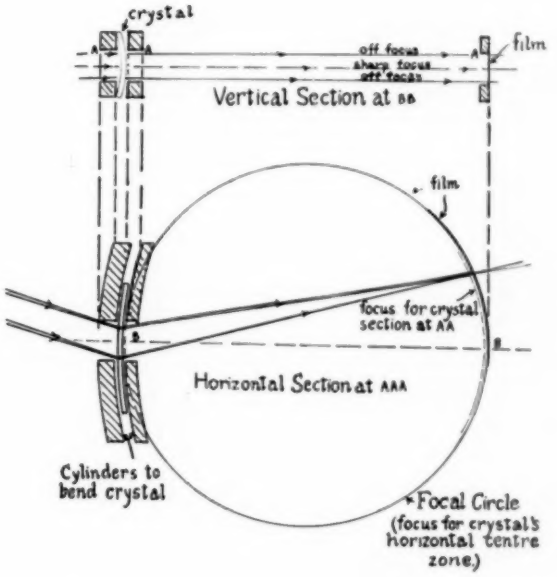

FIG. 2. Idealized sections of Cauchois spectrograph to demonstrate effects of double curvature of crystal.

The beauty of this explanation of de-focusing of the two components (due to the disturbed surfaces) as a result of the double curvature of the crystal, is that the fact, discovered by Finch,[1] is not contradicted. The two surface layers are crystalline and integral with the crystal body as they share in the uniform crystal strain.

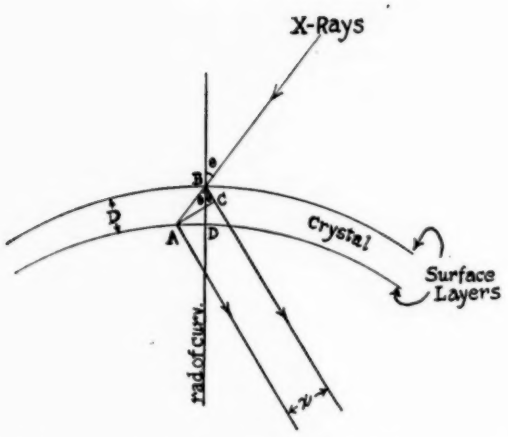

FIG. 3. Diagram to explain separation of doubled x-ray lines on assumptions of reference 5.

2. Separation of doubled lines in relation to crystal thickness

If we assume, as was done in reference 5, that the two surface reflections come from the two crystal surfaces parallel to each other, and that the two surface layers do not share in the uniform strain of the crystal, the linear separation of the two components of the doubled lines should be simply related to the thickness of the crystal. (Fig. 1 shows that such a simple relation does not hold.) However for the sake of argument, making the assumptions of reference 5, in Fig. 3, in triangle ABD, the side AB is equal to $D \sec \theta$. In triangle ABC

$$x/D \sec \theta = \cos(\pi - \pi/2 - 2\theta)$$

or the linear separation of the two components of the doubled line

$$x = D \sec \theta \cos(\pi/2 - 2\theta),$$
$$x = D \sec \theta \sin 2\theta$$

or

$$x = 2D \sin \theta,$$

where x is the distance between the two components of the doubled line, D is the perpendicular distance between the two surface layers on the quartz crystal, and θ is the Bragg angle of diffraction.

Taking Watson's[4] value of d for the basal planes of quartz as equal to 5.393A, and knowing that $n=3$ for the first order of reflection by quartz, we have (using the Bragg relation):

$$\sin \theta = n\lambda/2d = (3 \times 0.7076)/(2 \times 5.393) = 0.1968, \text{ for MoK}.$$

Substituting in the expression for the double line separation, and knowing that the crystal used to obtain Fig. 1 was slightly under fifteen thousandths of an inch in thickness, we have:

$$x = 2 \times 2.54 \times 0.015 \times 0.1968 = 0.015 \text{ cm}.$$

With a comparator, on the original film of Fig. 1 the doubled lines were found to be separated by 0.009 cm about halfway from the single center portion to the end of the line where the doubling was clearest. When the observed separation, 0.009 cm, is compared with the separation calculated on the assumptions of reference 5 (0.015 cm), it seems clear that the reflection from the two crystal surfaces did not leave the crystal parallel to each other, but have been focused in front of the film and are now redivergent, the position of actual focus depending on the second curvature of the crystal.

3. Breakage of crystals in holder due to secondary curvature

While working at the Cornell x-ray laboratory, the present author had considerable difficulty in bending calcite crystals without breakage, in a focusing spectrograph crystal holder. Much of this difficulty must have been due to the crushing effect of the warping cylinders on the doubly-curved crystal. Even quartz crystals show this tendency to fracture, which is easily explained by this view of the warped crystal shape. The calculation of the actual crystal shape will be a task of much interest.

4. Broadened lines caused by light etching of the crystal surface

Light etching will decrease the thickness of the disturbed surface layers which do the main amount of the x-ray reflection. Hence a very short (radially) imperfect grating is left. In Wood's *Physical Optics*[7] is this statement: "it to be specially noted that the resolving power of the grating does not depend on the closeness of the ruling, but merely on the number of lines." The radial grating of the disturbed surface layers of

[7] R. W. Wood, *Physical Optics* (second edition, 1929), p. 216.

the bent quartz crystal, is thinned down by light etching until we have relatively few lines in our imperfect grating: the net result being that the doubled lines are un-resolved and even blurred (see Fig. 3(b), reference 5) by the scanty grating available.

ACKNOWLEDGMENTS

The author wishes to thank Dr. Arne Sandström of Uppsala for a discussion which revived the author's interest in this subject. In conclusion, the writer wishes to thank Professor Millikan for extending research privileges.

JULY 1, 1940 PHYSICAL REVIEW VOLUME 58

The Fundamental Relation Between Lattice Constants and Density*

FRANK FOOTE, *Cooper Union, New York, New York*

AND

ERIC R. JETTE, *School of Mines, Columbia University, New York, New York*

(Received September 21, 1939)

Lattice constants have for many years been based on Siegbahn's crystal wave-lengths which are now known to be different from true wave-lengths. It is proposed that a unit called the "crystal angstrom" be defined as follows: 1 crystal angstrom $=1A_{cr}=10^3$ X units, and be used in crystal structure work where "crystal wave-lengths" are used. $1A_{cr}$ is not equal to 10^{-8} cm. To place the calculation of the density from lattice constant measurements on a sound and uniform basis it is proposed that the fundamental density equation be rewritten in the form $\rho=K(nM/V')$ where $n=$No. of atoms or molecules in the unit cell, $M=$atomic or molecular weight and $V'=$volume of the unit cell in crystal angstroms. The constant K is evaluated empirically from data on calcite and is found to be equal to $1.650_{23}\pm0.00015$ where 0.00015 is the calculated value of the standard deviation. This is the only value which is consistent with (1) the basis for the crystal wave-length scale adopted by Siegbahn, namely $d_{100}=3.02945$ $A_{cr}=3029.45$ X units at 18°C for the cleavage cell of calcite, and (2) the best available values for the atomic weight, density and rhombohedral angle of calcite. This value of K must be used in calculating densities from lattice constants if crystal wave-lengths are used. Density calculations are made for five metals and compared with directly measured densities. The error in the calculated density attributable to errors in lattice constant measurements is generally smaller than those due to the atomic weights and to K. For Al, Mg and Ni excellent agreement is obtained between the calculated and measured densities. For Cu and Ag there is marked disagreement but since the directly measured densities are far from concordant while the lattice constants of various investigators agree closely, it is concluded that the main source of the discrepancy lies in the directly measured values.

FOR many years, the scale of wave-lengths for x-rays proposed by Siegbahn and the relative wave-lengths tabulated by him have been the basis for the evaluation of lattice constants. Densities calculated from such lattice constant data have frequently not agreed well with directly measured densities and much speculation has arisen as to the reason for the disagreement. Fundamentally, the Siegbahn wave-length scale may be considered to be based on the measured density of calcite. This may be seen from the agreement between the calculated and measured calcite spacings which Siegbahn[1] himself discussed and considered as fortuitous. It seems unnecessary to enter into the detailed arguments at this point as to why calcite turns out to be the ultimate standard rather than sodium chloride. As far as density calculations are concerned we may state simply that if the value for Avogadro's number used by Siegbahn ($N=6.0594\times10^{23}$) had been used consistently in subsequent calculations of density from lattice constants based on the Siegbahn wave-length scale, the accuracy of densities would have been limited only by (1) the accuracy of the density and rhombohedral angle values of calcite used by Siegbahn, (2) the accuracy of the determinations of the lattice constants and (3) the relative accuracy of the molecular weight of calcite compared with that of

* Publication assisted by the Ernest Kempton Adams Fund for Physical Research of Columbia University.

[1] M. Siegbahn, *Spectroskopic der Roentgenstrahlen* (Springer, Berlin, 2nd Ed., 1931).

the substance being considered. In recent years, new determinations of Avogadro's number have been made, the relation between the Siegbahn wave-length scale and the absolute scale has been investigated,* and new experimental data on other fundamental values involved in calculating the calcite spacing have been available. These changes have obvious bearing on density calculations.

The main objectives of this article are: (1) To indicate a way by which immediate decision on the choice of the wave-length scale and on the true value of Avogadro's number becomes unnecessary. (2) To put the calculation of density from lattice constants on as thoroughly sound a basis as the experimental data available at present will permit. (3) To demonstrate that the main source of discrepancy between densities calculated from lattice constants and directly measured densities does not lie in lack of precision in determining lattice constants.

In order to minimize the confusion which is certain to arise until there is a general agreement to use absolute wave-lengths rather than crystal wave-lengths, we propose the adoption of a unit which we shall call the "crystal angstrom," a term suggestive of "crystal wave-lengths," and which we shall define by the equation:

$$1 \text{ crystal angstrom} = 1\text{A}_{cr} = 10^3 \ (X \text{ units}).$$

This unit would apply to all measurements made in terms of Siegbahn's crystal wave-lengths. If we represent "absolute angstroms" by A and define the ratio

$$f = \frac{(\text{wave-length in centimeters})}{(\text{wave-length in } X \text{ units}) \times 10^{-11}},$$

we may also write our definition of the "crystal angstrom" in the form

$$1 \text{ cm} = 10^8 \text{ A} = \frac{10^8}{f} \text{A}_{cr} = \frac{10^{11}}{f} (X \text{ units}).$$

It is to be emphasized that all previously reported lattice constants have actually been given in crystal angstroms and not in centimeters $\times 10^{-8}$.

The fundamental relation used for calculating densities from x-ray measurements is

$$\rho = \frac{\text{mass}}{\text{vol.}} = \frac{nM}{N} \cdot \frac{1}{V}, \qquad (1)$$

* Concerning the use of absolute wave-lengths, we shall not attempt to answer the question of whether in the long run it would be better to retain the Siegbahn scale for crystal structure work, making the conversions to the absolute scale for those few problems were it is important, or to recalculate more than 25 years of crystal structure determinations to the absolute scale.

TABLE I. *Values of the density of calcite.*

AUTHOR	ORIGIN	T	ρ	PROB. ERROR	ρ_{18}
Defoe and Compton[1]	Missouri	0°	2.7114	0.0001	2.7107
	U.S.A.	0°	2.7110	0.0001	2.7103
	Iceland	0°	2.7111	0.0001	2.7104
	Iceland	0°	2.7098	0.0001	2.7091
	Unknown	0°	2.7109	0.0001	2.7102
	Unknown	0°	2.7112	0.0001	2.7105
Bearden[2]	Iceland	20°	2.7104	0.00002	2.7105
	Iceland	20°	2.71035	0.00002	2.71043
	Montana	20°	2.7102	0.00008	2.7103
	Montana	20°	2.7102	0.00002	2.7103
	Argentina	20°	2.7102	0.00004	2.7103
	Spain	20°	2.7102	0.00004	2.7103
Tu[3]	Unknown	18°	2.71003	0.00005	2.71003
DuMond and Bollman[4]	Unknown, powdered	20°(?)	2.71022	0.00035	2.71030
	Macroscopic	20°(?)	2.71085	0.00019	2.71093
Batuecas and Casado[5]	Unknown, powder, 1.2 mm	0°	2.71123	0.00011	2.71055

Stand. Dev. $= \Delta\rho = [\Sigma(v_i)^2/n(n-1)]^{\frac{1}{2}} = 9.7 \times 10^{-5}$; Av. $\rho_{18} = 2.71032 \pm 0.00010$.

[1] O. K. Defoe and A. H. Compton, Phys. Rev. **25**, 618 (1925).
[2] J. A. Bearden, Phys. Rev. **38**, 2089 (1931); **48**, 385 (1935).
[3] Y. C. Tu, Phys. Rev. **40**, 662 (1932).
[4] J. W. M. DuMond and V. L. Bollman, Phys. Rev. **50**, 524 (1936).
[5] T. Batuecas and F. L. Casado, Zeits. f. physik. Chemie **181A**, 197 (1937).

TABLE II. *Values of the dihedral angle of calcite; calculation of* $\phi(\beta)$.

AUTHOR[1]	ORIGIN	T	α	α_{18}
Bearden	Iceland	20°	105° 3′ 29″	105° 3′ 39″
	Montana	20°	105° 3′ 31″	105° 3′ 41″
	Argentina	20°	105° 3′ 28″	105° 3′ 38″
	Spain	20°	105° 3′ 29″	105° 3′ 39″
Tu	Unknown	18°		105° 3′ 23.7″
DuMond and Bollman	Unknown	Recalculated by authors		105° 3′ 34″

Stand. Dev. $=\Delta\alpha=\pm 2.6''$ Av. $\alpha_{18}=105°\ 3'\ 35.8''\pm 2.6''$

$\beta_{18}=101°\ 54'\ 7.7''\pm 1.6''$; Av. at 18°C $\phi(\beta)=\dfrac{(1+\cos\beta)^2}{(1+2\cos\beta)\cdot(1-\cos^2\beta)^{\frac{1}{2}}}=1.09595_6\pm 0.0000093.$

[1] See references to authors given in Table I.

where n = No. of atoms (or molecules) in the unit cell, M = atomic (or molecular) weight in grams, N = Avogadro's number—No. atoms in gram atomic weight or the corresponding molecular quantity—and V = *true* volume of unit cell in cubic centimeters.

In order to retain the Siegbahn scale, we shall write Eq. (1) in the form

$$\rho=nM\cdot 10^{24}/f^3NV', \qquad (2)$$

where V' = volume in crystal angstroms. We propose that at present the values of both f and N be considered as not fully established and that Eq. (2) be modified to

$$\rho=KnM/V', \qquad (3)$$

where

$$K=10^{24}/f^3N. \qquad (4)$$

The value of K can be obtained directly from (4). It may also be found empirically from suitable data by means of (3). For the present it seems best to resort to the latter alternative using data for the reference substance on which the crystal wave-length scale itself is based, namely calcite. The required values have been determined repeatedly by various investigators with, generally, excellent agreement.

The experimental values of the density of calcite are given in Table I which includes the value originally reported, the value corrected to 18°C by means of Benoit's[2] data on the expansion coefficients, and the probable errors of the determinations given by the original investigators. The number of significant figures for each value in these tables is the same as that given in the original source. It is important to notice that in each case where an investigator used different samples of calcite for the measurements, the range or "spread" of the values is well beyond the stated probable errors.

The three factors which can give rise to density differences among the several calcites are (1) differences in chemical composition, (2) differences in physical imperfections, voids, fissures, inclusions, lattice irregularities, etc., and (3) the presence of systematic errors in the determinations. Bearden[3] is the only one to report chemical analyses; the results were closely similar showing about 99.98 mol. percent $CaCO_3$. Nothing is known concerning the other two factors but it cannot be assumed that the samples were all identical with respect to the second or that the systematic errors were the same for all investigators. We shall, therefore, treat each value given in Table I as an individual value. The character of the information available also makes it necessary to give equal weights to all the values. At the bottom of Table I we give the mean value of ρ and the *standard deviation of the listed values*, calculated as indicated.

Calculation of the density of calcite is usually made in terms of the cleavage rhombohedron for which $\phi(\beta)$ is a function of the characteristic rhombohedral angle β and d_{100} is the spacing of the cleavage cell. In terms of crystal angstroms we have $V'=\phi(\beta)\cdot d^3_{100}$. The angle usually measured is the dihedral angle α which is related to β by the equation $\cos\frac{1}{2}\beta=1/(2\sin\frac{1}{2}\alpha)$. The measured values of α are given in Table II, together with the values calculated to 18° which again

[2] Benoit, Int. Crit. Tab. III, 44.

[3] J. A. Bearden, Phys. Rev. **38**, 2089 (1931); **48**, 385 (1935).

involve Benoit's data on expansion coefficients.[4] As in the case of the density data, each value in Table II was considered as an individual determination and given the same weight. Again the *standard deviation* of the listed values of α is given. At the bottom of the table the calculated values of β and $\phi(\beta)$ with their respective *standard deviations* are given.

For the molecular weight of $CaCO_3$ several different estimates are possible. We have adopted the value suggested by Birge[5] but have multiplied the probable error of 0.0054 by 1.5 to secure the standard deviations. The value on the chemical scale is $M=100.09_0\pm0.0081$.

For d_{100} we use the arbitrary value adopted by Siegbahn as the basis of the crystal wave-length scale $d_{100}=3.02945A_{cr}$ at 18°C.

In Table III we give the value of K calculated from the preceding data and Eq. (3).

This value of K is the only one consistent with the measured density and crystallographic data on calcite and the adopted basis of the crystal wave-lengths used in lattice constant measurements. It is, therefore, this value of K which must be used in calculating densities from lattice constants so long as (1) the Siegbahn crystal wave-lengths are used, (2) the molecular weight of calcium carbonate is unchanged and (3) no better values for the density and $\phi(\beta)$ of calcite are available.* It must be emphasized that for any comparison of the calculated densities with directly measured values to be valid, ***the material which is used for the direct measurement must enable the investigator to obtain the true density rather than the apparent density and must have the same composition as the solid phase to which the lattice constant determinations apply.*** These requirements go far deeper than might at first be supposed. The direct density measurements are influenced by cracks, holes, solid or liquid inclusion, surface films of oxides or adsorbed gas, etc., which do not influence the lattice constant determinations at all. Both types of method of measuring densities are affected by internal strain such as arises from cold work or quenching. Finally, the interpretation of any density, however measured, is dependent upon the chemical analysis of the material and this is particularly important in the case of the x-ray methods where the mass per unit cell must be computed with the aid of the analysis of the particular solid phase under investigation.

TABLE III. *Calculation of K.*

$n=0.5$	
$M=100.09_0\pm0.0081$	$\Delta M/M=8.1\times10^{-5}$
$\rho=2.710_{32}\pm0.00010$	$\Delta\rho/\rho=3.7\times10^{-5}$
$d_{100}=3.02945$	$\Delta d/d=0$ (reference length)
$\phi(\beta)=1.09595_6\pm0.0000093$	$\Delta\phi(\beta)/\phi(\beta)=0.8\times10^{-5}$
$K=\frac{\rho d^3_{100}\phi(\beta)}{nM}=1.65023$	
$\frac{\Delta K}{K}=\pm\left[\left(\frac{\Delta\rho}{\rho}\right)^2+\left(\frac{\Delta\phi(\beta)}{\phi(\beta)}\right)^2+\left(\frac{\Delta M}{M}\right)^2\right]^{\frac{1}{2}}=8.94\times10^{-5}$ (cf. Eq. (6))	
Stand. Dev. $=\Delta K=14.7\times10^{-5}$, $K=1.650_{23}\pm0.00015$.	

Following the conventional methods used by physicists in computing errors, the standard deviations of K in Table III and of V' and ρ in Table IV have been obtained by means of the equation[6]

$$(\Delta c)^2=(\partial c/\partial x)^2\langle\Delta x\rangle_{Av}^2+(\partial c/\partial y)^2\langle\Delta y\rangle_{Av}^2+\cdots. \quad (5)$$

For the constant K in Table III this becomes

$$\Delta K/K=\pm[(\Delta\rho/\rho)^2+(\Delta\phi(\beta)/\phi(\beta))^2+(\Delta M/M)^2]^{\frac{1}{2}}. \quad (6)$$

In calculating the densities in Table IV, we have used

$$\Delta\rho/\rho=\pm[(\Delta M/M)^2+(\Delta K/K)^2+(\Delta V'/V')^2]^{\frac{1}{2}}, \quad (7)$$

where $\Delta V'/V'=3(\Delta a_0/a_0)$ for cubic crystals and

[4] Of Bearden's results (reference 3) the values from his methods 1 and 2 were used and the mean for each calcite is given in Table II. Bearden also discarded the results of his third method. The x-ray results of DuMond and Bollman (reference 4, Table I) were subject to a considerable systematic error which we were able to eliminate by methods previously used in this laboratory (reference 7). These authors unfortunately do not state the temperature at which any of their measurements were made; from internal evidence it was inferred that the results were reported at 20°C. The results of Beets (H. N. Beets, Phys. Rev. **25**, 621 (1925)) seemed definitely too high by about 90 seconds in comparison with those of three later investigations and have been omitted entirely.

[5] R. T. Birge, "A consistent set of values of the general physical constants." Mimeographed letter, August 1939, page 5.

* The value of $10^{24}/K=6.0598\times10^{23}$ is very close to the Avogadro number used by Siegbahn, reference 1.

[6] R. T. Birge, Am. Phys. Teacher **7**, 351 (1939).

TABLE IV. *Calculation of ρ and $\Delta\rho$ from lattice constants ($T=25°C$).*

	Al	Mg	Ni	Cu	Ag
a_0	4.0413_9	(*)	3.5168_4	3.6077_8	4.0778_7
V'	66.00_{74}	46.20_{35}	43.49_{69}	46.95_{91}	67.81_{10}
M	26.97	24.32	58.69	63.57	107.880
K	1.650_{23}	1.650_{23}	1.650_{23}	1.650_{23}	1.650_{23}
n	4	2	4	4	4
ρ	2.69_{71}	1.737_3	8.90_{65}	8.93_{65}	10.50_{13}
Δa_0	0.00004	(*)	0.00004	0.00004	0.00004
$(\Delta V'/V')\times 10^5$	3.0	5.2	3.4	3.3	2.9
$(\Delta M/M)\times 10^5$	37.1	41.1	17.0	15.7	0.9
$(\Delta K/K)\times 10^5$ (Eq. (6))	8.9	8.9	8.9	8.9	8.9
$\Delta\rho/\rho\times 10^5$ (Eq. (7))	38.3	42.4	19.5	18.3	9.4
$\Delta\rho$	0.0010	0.0007	0.0017	0.0016	0.0010

* $a=3.2030_0\pm 0.00008$; $c=5.2002_1\pm 0.00007$.

$\Delta V'/V'=\pm[(2\Delta a/a)^2+(\Delta c/c)^2]^{\frac{1}{2}}$ for hexagonal crystals.

We shall illustrate the application of Eq. (3) and the calculations of the errors with several specific cases. We should mention at this point that the important question regarding the necessity of applying a refraction correction in the calculation of lattice constants has not yet been finally decided. However, in only one of the cases to be discussed below does this correction reach a value which will sensibly affect the result. This case is silver and the omission of the correction increases the calculated density by about one or two parts in 10,000.

In Table IV we give the results of calculations of the densities for five metals. The lattice constants were taken from measurements made by the authors and all, except the value for copper have been previously reported.[7] These values were corrected for refraction. For the standard deviation of the atomic weight we have assumed plus or minus one unit in the last significant figure quoted for the element in the 1939 table of "International Atomic Weights." This appears to be a safe assumption and one not likely to affect our main conclusions significantly. As will be seen, should the chosen standard deviation prove to be too large, the calculated densities would become even more reliable.

The values of $\Delta\rho/\rho$ in Table IV were found from Eq. (7). A study of these results shows that for these measurements the part of the error in the density attributable to errors in the lattice constants are in every case much less than at least one of the other two errors. In only one case (Ag) is this error greater than that due to the uncertainty in the atomic weight. Since it is possible by modern methods for any competent investigator to obtain lattice constants with the same order of accuracy as those quoted, the main source of the discrepancy between the calculated and measured densities must be sought in the other quantities including, of course, the measured densities themselves.

In Table V we compare the calculated densities found in Table IV with densities directly measured by various investigators. It will be seen that the agreements in the cases of aluminum, magnesium and nickel are excellent. For copper and silver the situation is quite different. The calculated and measured densities show wide discrepancies. In an investigation in this laboratory with copper from four different sources, including a "spectroscopic" copper, with samples heat treated in various ways to yield a total of 16 different measurements, the lowest value of a_0 secured was 3.6076_3 and the highest $3.6081_5 A_{cr}$. This range will include all the precision measurements on copper recently published and the "spread" of the density values calculated from such measurements will at the most be about ± 2 parts in 10,000, a trifle more than $\Delta\rho/\rho$ given in Table IV. The same degree of agreement is found for silver. The source of the disagreement in densities must, therefore, be sought either in the direct density measurements, or, what is the far more probable source, in the samples used in the direct measurements. In this connection we may mention the extensive work of Ruer and

[7] E. R. Jette and F. Foote, J. Chem. Phys. **3**, 605 (1935). In this paper fiduciary limits with $P=0.05$ were used in reporting the errors. These have been converted to standard deviations in Table IV.

TABLE V. *Comparison of calculated and measured densities at 25°C.*

	ρ_{CALC}	ρ_{MEAS}	SOURCE OF ρ_{MEAS}
Al	2.6971±0.0010	2.6978	Taylor[1] *et al.*
		2.6967±0.0003	Batuecas and Casado[2]
Mg	1.7373±0.0007	1.7373±0.0002	Batuaecas and Casado[2]
		1.738	Elchardus[3]
		1.736	F. Foote (unpublished)
Ni	8.9065±0.0017	8.901–8.903	Jordan and Swanger[4]
Cu	8.9358±0.0016	8.9154	Ruer and Kuschmann[5]
		8.94126	Maier,[6] vac. melted and solidified
		8.94304	Maier,[6] vac. melted and solidified under He
		8.95231	Maier,[6] single crystal
		8.94±0.01	Int. Crit. Tab. II, 456
Ag	10.5013±0.0010	10.4936	Ruer and Kuschmann[5]
		10.492	Jette and Foote[7]
		10.50	Phelps and Davey[8]
		10.438–10.535	Int. Crit. Tab. II, 456
		10.489	Kahlbaum,[9] *et al.* (vac. distilled)

[1] C. S. Taylor, L. A. Willey, D. W. Smith and J. D. Edwards, Metals and Alloys **8**, 183 (1938).
[2] See reference 5, Table I.
[3] E. Elchardus, Value reported by van Arkel, *Reine Metalle* (Springer, Berlin, 1939), p. 119.
[4] L. Jordan and W. H. Swanger, Bur. Stand. J. Research **5**, 1291 (1930).
[5] R. Ruer and J. Kuschmann, Zeits. f. anorg. allgem. Chemie **173**, 233, 262 (1928).
[6] C. G. Maier, Trans. Am. Inst. Min. Met. Eng. **123**, 121 (1936).
[7] See reference 7 in text.
[8] R. T. Phelps and W. P. Davey, Trans. Am. Inst. Min. Met. Eng. **99**, 234 (1932).
[9] G. W. A. Kahlbaum, K. Roth and P. Seider, Zeits. f. anorg. allgem. Chemie **29**, 177 (1902).

Kuschmann,[8] who have shown the effects of chemical treatment and of annealing under various conditions upon the densities, and of Maier,[9] who investigated the effects of various mechanical and heat treatments on the densities. The remarkably high value for a large single crystal of copper (cf. Table V) is entirely beyond the range of any normal errors and has not been explained.

It is interesting to calculate K from Eq. (4) with data given by Birge[5] recognizing, of course, that Birge does not intend these values to be final ones.

$$N=(6.0227_4\pm0.0014)\times10^{23}$$

$$\text{Stand. Dev.}=\Delta N=\pm0.0021$$

$$f=1.002034\pm0.00006$$

$$\text{Stand. Dev.}=\Delta f=\pm0.00009.$$

From Eq. (4) we obtain

$$K=10^{24}/f^3N=1.650_{28}\pm0.00074,$$

where ΔK the standard deviation is obtained by means of

$$\Delta K/K=\pm[(3\Delta f/f)^2+(\Delta N/N)^2]^{\frac{1}{2}}=\pm0.00045.$$

A similar calculation but with Bearden's[3] estimate that the probable error in f is 0.000016 with a corresponding standard deviation $\Delta f=0.000024$ gives $K=1.650_{28}\pm0.00059$. When these values of K are compared with the one in Table III, it will be seen that the values differ by only 3 parts per 100,000 and the main difference lies in the standard deviations.

[8] R. Ruer and J. Kuschmann, Zeit. f. anorg. allgem. Chemie **173**, 233, 262 (1928).
[9] C. G. Maier, Trans. Am. Inst. Min. Met. Engrs. **123**, 121 (1936).

LETTERS TO THE EDITOR

Prompt publication of brief reports of important discoveries in phyiscs may be secured by addressing them to this department. Closing dates for this department are, for the first issue of the month, the eighteenth of the preceding month, for the second issue, the third of the month. Because of the late closing dates for the section no proof can be shown to authors. The Board of Editors does not hold itself responsible for the opinions expressed by the correspondents.

Communications should not in general exceed 600 words in length.

Internal Friction at High Temperatures*

The internal friction of metals is known to increase rapidly at high temperatures.[1-3] The only type of internal friction which has been thoroughly investigated is that associated with thermal currents flowing back and forth between stress inhomogeneities,[4-8] and this can be shown to vary only comparatively slowly with temperature. Thus a new type of internal friction is apparently introduced at high temperatures. Before one can profitably speculate as to the origin of this internal friction, it is necessary to find how it depends upon certain parameters. In this letter the dependence upon temperature and grain size is given.

In order to reduce the temperature range necessary to obtain a large variation of internal friction, a metal with a low melting point was chosen, namely zinc. The specimens (dimensions $30\times1\times0.45$ cm^3) were from a set of zinc samples furnished by Gerald Edmunds of the New Jersey Zinc Company. They contained less than 0.5 percent of alloying elements. Their approximate grain sizes of 0.04 mm, 0.04 mm, 0.06 mm and 0.4 mm were obtained by annealing at 175°C, 225°C, 275°C and 400°C, respectively. A complete description of this set will be given elsewhere, together with a detailed analysis of their internal friction. Measurements were made at the lowest frequency for transverse vibration, 180 cycles per second, in order to eliminate as far as possible the effects of intercrystalline thermal currents. The temperature was measured by letting the two supports, placed at nodes of vibration, and the specimen form the hot junction of a thermocouple.

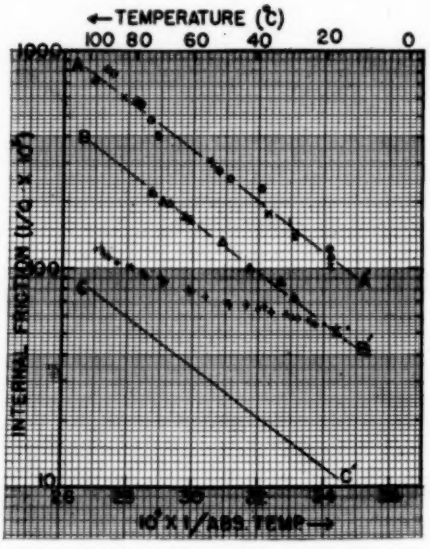

FIG. 1. *Variation of internal friction of zinc with temperature.* All measurements were made at a frequency of 180 cycles per second. 0, X, Δ, + refer to specimens with the approximate grain sizes 0.04 mm, 0.04 mm, 0.07 mm and 0.4 mm, respectively. The three straight lines AA', BB' and CC' are parallel to each other. The dots lie a constant value of 44×10^{-5} above CC'. This coincidence with the experimental points + shows that the internal friction of the 0.4-mm grain size specimen is given by CC' plus the constant value 44×10^{-5}.

* This research was supported by a grant from the Penrose Fund of the American Philosophical Society, and by a grant from the Rumford Fund of the American Academy of Arts and Sciences.

The measurements are plotted in Fig. 1 on semilog paper against $1/T$. The measurements on the three smallest grain size specimens lie upon a straight line, indicating that the internal friction has a heat of activation. For all three specimens this is 5200 calories per gram atom.

The measurements for the largest grain size specimen do not lie upon a straight line. For this specimen the adiabaticity parameter[6]

$$\frac{\text{frequency}\times(\text{grain size})^2}{\text{thermal diffusion constant}}$$

is 0.8, as against 0.008, 0.008, 0.02 for the other three specimens. Since the intercrystalline thermal currents have a maximum effect when this parameter is of the order of magnitude of unity, it is to be expected that their contribution to the internal friction of this specimen be not negligible. Our measurements are consistent with the assumption that this contribution is 44×10^{-5} over the temperature range studied, and that the temperature dependent part of the internal friction has the same heat of activation as have the other three specimens.

To within experimental error in grain size estimates, the temperature-dependent part of the internal friction varies inversely with grain size. Now the area of the grain boundaries per unit volume is also inversely proportional to grain size. Hence this experiment indicates that the source of this high temperature internal friction lies on the grain boundaries, rather than in the interior of the grains.

ARTHUR H. BARNES
CLARENCE ZENER†

College of the City of New York,
New York, New York,
June 10, 1940.

† Now at the State College of Washington, Pullman, Washington.

[1] K. Iokibe and S. Salai, Phil. Mag. (6) **42**, 307 (1921).
[2] F. Förster and W. Köster, Zeits. f. Metallkunde **29**, 116 (1937).
[3] W. Köster and K. Rosenthal, Zeits. f. Metallkunde **30**, 345 (1938).
[4] C. Zener, Phys. Rev. **53**, 90 (1938).
[5] C. Zener, W. Otis, and R. Nuckolls, Phys. Rev. **53**, 100 (1938).
[6] R. H. Randall, F. C. Rose and C. Zener, Phys. Rev. **56**, 343 (1939).
[7] C. Zener and R. H. Randall, Metals Tech. **7**, Jan. (1940).
[8] C. Zener, Proc. Phys. Soc. **52**, 152 (1940).

The Induced Radioactivity of Krypton

An investigation has been made of the induced radioactivity of krypton. The gas was irradiated in a glass chamber, one end of which was closed by an aluminum window one mil in thickness. A molybdenum cup at the other end of the chamber served to prevent the bombarding particles from striking the glass. Activities were measured by introducing the gas into an ionization chamber which was connected to a d.c. amplifier with an automatic recording mechanism.

Irradiation of krypton with deuterons of 11 Mev energy from the Harvard cyclotron produced strong activities with periods of 102 minutes and 4.0 hours, and a weak activity of about 35 hours. To obtain further information, selenium was irradiated with alpha-particles of 22 Mev energy. At the end of the bombardment, the selenium was placed in a tube which was then evacuated. After boiling the selenium to drive out the active krypton, the tube was cooled in CO_2-acetone slush, and then the krypton was allowed to flow into the ionization chamber. A strong activity with a period of 114 minutes was observed, and also a weak activity of about 33 hours. The former may be assigned to Kr^{83*}, since the period coincides with that reported for this isotope by Langsdorf and Segrè.[1] These investigators found a radioactive Kr^{83}, of 113-minute period, growing out of Br^{83*}. Tests are now being made to determine to what extent the Kr^{83*} in the present work is formed directly from Se^{80}, by an (α, n) reaction, and indirectly from the decay of Br^{83*} produced by an (α, p) reaction.

The 102-minute period observed in deuteron irradiation of krypton is obtained upon the second subtraction from the decay curve, and the margin of error is therefore likely to be large. It is probable that this activity is really that of Kr^{82*}, formed by a (d, p) or (d, d) reaction. The 4.0-hour period is not observed in the alpha-particle bombardment of selenium, and hence must be assigned to Kr^{87*}, an isotope which cannot be formed from alpha-particle reactions with selenium.

Barkas, Creutz, Delsasso, and Sutton[2] irradiated bromine with protons, separated the krypton product, and observed a long period of about 23 hours due to Kr^{79*} or Kr^{81*}. The weak 35-hour period found in the present investigation can probably be assigned to the same isotopes.

In the alpha-particle irradiation of selenium, Kr^{85} ought to appear from Se^{82} as a result of an (α, n) reaction. Since no third activity appeared in this bombardment, the period of Kr^{85} is presumably long or very short.

Attempts to produce krypton activities by irradiating rubidium and strontium with fast neutrons were unsuccessful.

The author is greatly indebted to Professor K. T. Bainbridge for his ready guidance during the course of this work.

EDWARD P. CLANCY

Department of Physics,
Harvard University,
Cambridge, Massachusetts,
June 5, 1940.

[1] Alexander Langsdorf, Jr. and Emilio Segrè, Phys. Rev. **57**, 105 (1940).
[2] W. H. Barkas, E. C. Creutz, L. A. Delsasso, and R. A. Sutton, Phys. Rev. **57**, 1087 (1940).

Comparative Efficiencies of Radioactive Neutron Sources

We have measured the comparative neutron-producing efficiencies of several radium-beryllium and radon-beryllium neutron sources in order to determine whether these efficiencies are proportional to the gamma-ray activities of the sources. Neutron production from such sources has been customarily assumed proportional to the gamma-ray intensity, and furthermore it has been stated that radon-beryllium sources are more efficient than radium-beryllium sources.

Four radium-beryllium and two radon-beryllium sources were compared by placing the sources successively in a paraffin block, near which was located a boron-trifluoride-filled detecting chamber connected to a linear amplifier. Care was taken that the geometry should be the same in each measurement. The counting rate of the chamber, with and without a half-millimeter-thick cadmium shield, gave a measure of the slow neutron intensity. By establishing that there was no observable change in counting rate when 200 milligrams of radium without beryllium were brought up, it was ascertained that the strong gamma-ray intensity from these sources did not influence the detecting efficiency. The gamma-ray strengths of the several sources had been previously determined by standard procedures.

TABLE I. *Observed yields of neutrons per millicurie of gamma-ray activity in the source.*

TYPE	APPROXIMATE STRENGTH (GAMMA-RAY)	NEUTRONS/MG-EQUIV. (RELATIVE)
Ra-Be	200 mg	1
Ra-Be	200 mg	0.97
Ra-Be	200 mg	0.85
Ra-Be	9.87 mg	0.88
Rn-Be	60 mC	0.55
Rn-Be	30 mC	0.76

Table I shows the relative neutron yield per milligram-equivalent for the various sources. It will be observed that the yield is different for each of the five sources, and furthermore that the radon sources are considerably less efficient than the radium-beryllium sources. It is therefore evident that serious error may be made by assuming the neutron yield to be proportional to the gamma-ray intensity. The beryllium content of the above sources varies between 0.1 gram and 5 grams, the large radium sources containing the greater quantities of beryllium. More details of these measurements and a discussion of the efficiency variations will be published in a forthcoming issue of the *Journal of the Franklin Institute.*

EDGAR J. MURPHY
WILLIAM C. BRIGHT
MARTIN D. WHITAKER

New York University,
University Heights,
New York, New York,

S. A. KORFF
E. T. CLARKE

Bartol Research Foundation of the Franklin Institute,
Swarthmore, Pennsylvania,
June 14, 1940.

Scattering Cross Section of Protons for 900-Kev Neutrons

A number of experimental data[1-3] for the scattering cross section of hydrogen for neutrons of energies between 2 and 16 Mev are available, which agree comparatively well with Wigner's "two level formula" corrected for the finite range of the nuclear forces.[4] For lower neutron energies the cross section depends more sensitively on energy, and the singlet scattering becomes more important. Since no attempt has yet been made to check this formula between 400 kev[5] and 2 Mev, it seemed interesting to measure the cross section for an intermediate energy. For this purpose we used the neutrons produced in beryllium by the 2.62-Mev gamma-rays of ThC″. It is very likely that these neutrons are mainly due to the reaction $Be^9+h\nu \rightarrow Be^8+n^1$ and that they are consequently monokinetic. In this case, according to various determinations of the threshold energy[6-8] of the reaction, their energy is about 900 kev.

The arrangement used is shown in Fig. 1. The source consisting of about 13 mC RdTh, contained in a platinum tube of 1 cm length and 2 mm diameter, was surrounded by a cylinder of beryllium metal. The individual fast neutrons were detected by means of an ionization chamber filled with 5 atmos. of hydrogen, which was connected to a four-stage linear amplifier and a scaling circuit. The pulses could be visually observed by means of an oscilloscope. Recoil protons of more than 350 kev energy were recorded. The gamma-ray background reduced by a lead cone mounted in front of the source was well below this limit. The natural background of the chamber was 0.40 ± 0.03 count per min. The RdTh+Be source if placed in the position indicated in Fig. 1 yielded a count I_0 of 7.69 ± 0.19 pulses per min. The RdTh source itself was "neutron free." The scatterers consisted of paraffin cylinders of lengths varying between 1 and 9 cm. They were placed halfway between source and ionization chamber.

In Fig. 2 the logarithm of the ratio I/I_0 of the numbers of counts obtained per min. with and without scatterer is plotted (open circles) against the thickness in g/cm² of the scatterer. The points corresponding to smaller thicknesses lie well on a straight line indicating that at least the majority of the neutrons are monokinetic. From this straight line we obtain a value of 2.43 g/cm² for the mean free path of the RdTh+Be neutrons in paraffin. The deviation from the straight line for the points corresponding to the thickest scatterers is due partly to multiple scattering and partly to the neutrons scattered under a small angle which are still detected by the ionization chamber.

The neutron absorption in carbon was determined in the same way as that in paraffin by using graphite cylinders as absorbers. The full circles in Fig. 2 show the results from which a scattering cross section for carbon of $(2.63\pm0.25)\times10^{-24}$ cm² follows.

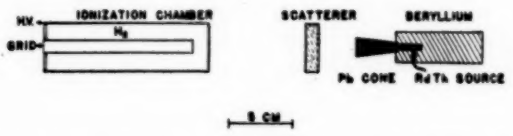

FIG. 1. Arrangement for absorption measurements of RdTh+Be photo-neutrons in paraffin and carbon.

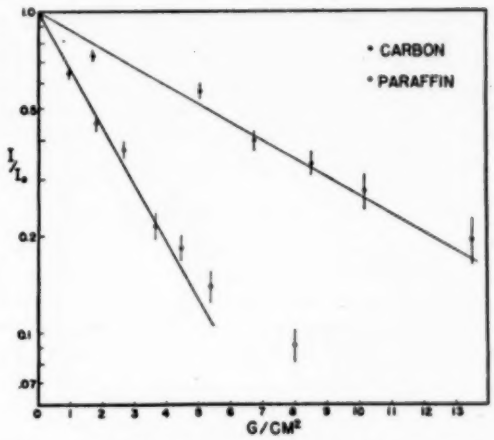

FIG. 2. Logarithmic absorption curves of RdTh+Be photo-neutrons in paraffin (○) and carbon (●).

The correction for the obliqueness of the neutron paths within the scatterer is negligible. An estimate of the effect of small angle scattering was made assuming the scattering to be spherically symmetrical in the center of gravity system. This yielded an "ideal" mean free path of 2.28 g/cm² in paraffin. The average composition of the paraffin we used corresponded to the formula $C_{28}H_{62}$. From this we obtain a proton-neutron cross section of $(3.70\pm0.35)\times10^{-24}$ cm², which lies somewhat below the value 4.65×10^{-24} cm² calculated from Kittel and Breit's[4] expression for 900-kev neutrons, and closer to the value given by Wigner's "zero range formula."

WILLIAM E. GOOD
GERTRUD SCHARFF-GOLDHABER

Department of Physics,
University of Illinois,
Urbana, Illinois,
June 6, 1940.

[1] H. Aoki, Phys. Rev. **55**, 795 (1939).
[2] W. H. Zinn, S. Seely and V. W. Cohen, Phys. Rev. **56**, 260 (1939).
[3] E. O. Salant, R. B. Roberts and P. Wang, Phys. Rev. **55**, 984 (1939).
[4] C. Kittel and G. Breit, Phys. Rev. **56**, 744 (1939).
[5] E. Amaldi, D. Bocciarelli, G. C. Trabacchi, Ricerca Scient. **9**, 121 (1940).
[6] I. Chadwick and M. Goldhaber, Proc. Roy. Soc. **A151**, 479 (1935).
[7] G. B. Collins, P. Waldman and E. Guth, Phys. Rev. **56**, 876 (1939).
[8] S. K. Allison, L. S. Skaggs, N. M. Smith, Jr., Phys. Rev. **55**, 550 (1939).

Spontaneous Fission of Uranium

With 15 plates ionization chambers adjusted for detection of uranium fission products we observed 6 pulses per hour which we ascribe to spontaneous fission of uranium. A series of control experiments seem to exclude other possible explanations. Energy of pulses and absorption properties coincide with fission products of uranium bombarded by neutrons. No pulses were found with UX and Th. Mean lifetime of uranium follows ten to sixteen or seventeen years.

FLEROV
PETRJAK

Physico Technical Institute (F),
Radium Institute (P),
Leningrad, U. S. S. R.,
June 14, 1940 (by cable).

Electron Path Lengths in Multiple Scattering

An approximate solution of the problem of multiple scattering of electrons has been given by Goudsmit and Saunderson.[1] For an initially collimated beam incident normally on a foil of thickness t the angular distribution, per unit solid angle, was given by

$$f(\vartheta, t)=\frac{1}{4\pi}\sum(2l+1)e^{-\nu Q_l}P_l(\cos\vartheta), \tag{1}$$

where Q_l, which is given explicitly in reference 1, is $[1-P_l(\cos\vartheta)]_{Av}$, averaged over the angular distribution for single (elastic) scattering. ν is the average number of collisions which the electrons undergo in traversing the foil and was given by

$$\nu=\sigma Nt, \tag{1a}$$

where σ is the total scattering cross section for single scattering and N is the number of scattering atoms per unit volume.

A more exact value for the average number of collisions would be

$$\nu=\sigma N s_{Av}, \tag{2}$$

where s_{Av} is the average length of path for the electrons traversing the foil. The approximation involved in (1) is therefore equivalent to the assumption of linearity of the electron paths and the Goudsmit-Saunderson result is thus valid only for thin foils or for very fast electrons for which the scattering of the beam is small. Stated otherwise, the assumption of linear paths is equivalent to replacing $\cos\vartheta$ by unity in the convection term of the Boltzmann equation which describes the variation in the angular distribution with penetration into the foil.[2]

A calculation of the average path length of electrons which have penetrated a given distance into the scattering foil is of importance not only for the angular distribution but also for the evaluation of experiments on energy loss.[3] The following is an attempt to make such a calculation. The restriction will be made to the case of foils thin enough, or electrons fast enough, so that back scattering is negligible. Thus, while the region of validity of (1) is to be extended, the extension is not to be made beyond the region of prediffusion. The average path is approximately given by

$$s_{Av}=\int_0^t dx\int f(\vartheta, x)\,|\sec\vartheta|\,d\Omega. \tag{3}$$

In order to avoid divergence difficulties in the angular integration $\sec\vartheta$ is expanded in a series containing a *finite* number of Legendre polynomials. This is of course equivalent to limiting the series

$$\sec\vartheta=\sum\xi^n,\quad \xi\equiv 1-\cos\vartheta<1 \tag{4}$$

to a like number of terms. By comparing the series

$$\sec\vartheta\cong\sum_0^n\xi^l=\sum_0^n a_l P_l(\cos\vartheta) \tag{5}$$

the coefficients are readily evaluated as shown in Table I. The relative error in $\sec\vartheta$ is ξ^{n+1} so that a series of six terms represents $\sec\vartheta$ with an error of only 2 percent for angles as large as 60°.

TABLE I.

n	a_0	a_1	a_2	a_3	a_4	a_5
0	1					
1	2	−1				
2	10/3	−3	2/3			
3	16/3	−33/5	8/3	−2/5		
4	128/15	−13	152/21	−2	8/35	
5	208/15	−171/7	352/21	−58/9	48/35	−8/63

From (3) and (5) the path length-thickness ratio is

$$s_{Av}/t=1+\sum_1^n a_l(n)\left(\frac{1-e^{-\nu Q_l}}{\nu Q_l}-1\right) \tag{6}$$

with ν given by (1a). As an indication of the consistency of the above procedure s_{Av}/t may be evaluated for various special cases for different values of n. For example, for medium fast electrons (∼1 Mev) traversing Al foils of thicknesses about 0.05 cm the path length-thickness ratio for various values of n (2 to 5) shows an extreme variation of only 2 percent.

The above result for the average path length may be compared with the "first approximation" result of Goudsmit and Saunderson.[1] According to these authors one may take

$$s_{Av}/t=1/\langle\cos\vartheta\rangle_{Av}\cong 1+\xi_{Av}=e^{\nu Q_1}.$$

This is equivalent to limiting the series (5) to two terms and in addition the average cosine is evaluated only at the end of the path whereas a summation over the entire trajectory should be taken (cf. 3). For a given n this latter approximation overestimates the mean path length. Thus for very thin foils, for which the Goudsmit-Saunderson result is most nearly valid, (6) gives ($n=1$)

$$s_{Av}/t=1+\tfrac{1}{2}\nu Q_1$$

instead of $1+\nu Q_1$.

Numerical applications of the above will appear in a subsequent issue of the *Physical Review*.

M. E. ROSE*

Sloane Physics Laboratory,
Yale University,
New Haven, Connecticut,
May 20, 1940.

* Sterling Fellow.

[1] S. A. Goudsmit and J. L. Saunderson, Phys. Rev. **57**, 24 (1940); Phys. Rev. **57**, 552 (1940).
[2] W. Bothe, Zeits. f. Physik **54**, 161 (1929). H. A. Bethe, M. E. Rose and L. P. Smith, Proc. Am. Phil. Soc. **78**, 573 (1938).
[3] E.g. see A. J. Ruhlig and H. R. Crane, Phys. Rev. **53**, 618 (1938); M. M. Slawsky and H. R. Crane, Phys. Rev. **56**, 1203 (1939).

Effect of the Nuclear Coulomb Field on the Capture of Slow Mesons

In their note on the absorption of slow mesons in matter Yukawa and Okayama[1] have shown, that (a) the majority of slow mesons are captured by atomic nuclei only after having been stopped by losing their energy through ionization, and (b), if the material is dense, the capture takes place nearly always before they disintegrate spontaneously. In deriving these conclusions they assumed mesons to be free. But for slow mesons, especially for those which have been stopped by ionization, the Coulomb force of the atomic nuclei plays an important part in the problem.

In consequence of the Coulomb attraction the capture probability will increase for negative mesons, while for positives it will be greatly reduced by the potential barrier. The competition between nuclear capture and spontaneous disintegration must in this way be different for mesons of different signs.

The effect of the Coulomb force on the capture of mesons in motion can roughly be taken into account by multiplying the capture probability, which was derived by various authors on the assumption of free mesons, by the factor

$$\frac{2\pi\alpha Zc/v}{1-e^{-2\pi\alpha Zc/v}} \quad \text{or} \quad \frac{2\pi\alpha Zc/v}{e^{2\pi\alpha Zc/v}-1} \tag{1}$$

for negative or positive mesons respectively, where Z is the atomic number of the material, and v is the velocity of the incident meson.

We have thus calculated the probability for a meson of an incident energy E, being captured along its path before it is brought to rest. The results for various values of E and Z are given in Table I.

TABLE I. *Capture probabilities along the path.*

	$E=10^8$	10^7	10^6	10^5 (VOLTS)	SIGN OF THE MESON
Pb	0.001	2×10^{-6}	5×10^{-15}	7×10^{-39}	+
	0.1	0.01	10^{-3}	10^{-4}	−
Al	0.017	6×10^{-4}	3×10^{-6}	4×10^{-11}	+
	0.032	2×10^{-3}	2×10^{-4}	2×10^{-5}	−
Air	0.013	5×10^{-4}	6×10^{-6}	6×10^{-9}	+
	0.019	10^{-3}	6×10^{-5}	6×10^{-6}	−

One sees from the table that this probability is, notwithstanding the Coulomb attraction, very small for slow negative mesons, and still less for positives. Consequently the capture in almost all cases does not take place before mesons come to rest. We have therefore calculated the probability per unit time for mesons being absorbed by nuclei after having come to rest. In this calculation one must realize that the factor (1) does not apply to such slow mesons as have their wave-length larger than the atomic radius. The capture cross section for mesons, the energy of which is smaller than about 1 volt, will show a very complicated dependence on v, because the screening of the nuclear Coulomb field begins now to come in (Ramsauer effect). The general feature, however, would roughly be given by assuming the cross section to vary in this energy range according to the $1/v$ law. The results obtained with this simplifying assumption are tabulated in Table II.

Since the probability for negative mesons being captured is seen always to be larger than the probability of disintegration, which is of the order of 10^6 sec.$^{-1}$, the negative mesons will be much more likely captured by nuclei than

TABLE II. *Capture probabilities per sec. for negative and positive mesons.*

	NEGATIVE MESONS	POSITIVE MESONS
Pb	2.5×10^{12}	—
Al	1.2×10^{11}	—
Air	3×10^{7}	10^{-800}

disintegrate spontaneously, not only in dense materials but also in gases. On the other hand, practically all positive mesons will disintegrate spontaneously because of the extremely small capture probability due to the existence of the potential barrier. Practically all positive mesons, which come to rest, should therefore be necessarily accompanied by a disintegration electron at the end of their range.

Experimental materials are now rather scanty, but it does not seem to us merely accidental that all the Wilson tracks, which could so far be definitely identified as disintegration electrons, are positives,[2] and none of the photographs, in which a negative meson track terminates within the cloud chamber, shows such a disintegration electron.[3]

If our theory is right, the experiments of Montgomery and others,[4] who could not find disintegration electrons, seem hardly to be understood, unless we assume that slow mesons they observed are not identical with the ordinary cosmic-ray mesons and have much smaller lifetime.

The detailed calculation and discussions will shortly appear elsewhere.

S. TOMONAGA
G. ARAKI

Institute of Physical and Chemical Research,
Tokyo, Japan,
May 24, 1940.

[1] H. Yukawa and T. Okayama, Sci. Papers Inst. Phys. and Chem. Research **36**, 385 (1939).
[2] P. Kunze, Zeits. f. Physik **83**, 1 (1933); S. H. Neddermeyer and C. D. Anderson, Phys. Rev. **54**, 88 (1938); P. Ehrenfest, Comptes rendus **206**, 428 (1938); E. J. Williams and F. R. S. Roberts, Nature **145**, 102 (1940).
[3] Y. Nishina, M. Takeuchi and T. Ichimiya, Phys. Rev. **52**, 1198 (1937); H. Maier-Leibnitz, Zeits. f. Physik **112**, 569 (1939).
[4] C. G. Montgomery, W. E. Ramsey, D. H. Cowie and D. D. Montgomery, Phys. Rev. **56**, 635 (1939).

Radio-Isotopes of Ba and Cs

With the 37-inch Berkeley cyclotron as a neutron source for irradiating Ba, a chemically identified Ba isotope of half-life 30 ± 1 hour was found.[1] The emitted radiations consisted of a "monochromatic" group of electrons at 250 KV, x-rays of approximately the characteristic energy for Ba K x-rays, and strong gamma-rays of about 250 KV, in addition to a soft complex spectrum of gamma-rays. This soft spectrum made it impossible to identify the x-rays definitely by using critical absorbers. Paraffin shielding decreased the yield of this activity, and Li was found to be a less effective source of neutrons than Be. This would seem to indicate that it is a neutron loss reaction, but that extremely high energy neutrons are not required. Deuteron bombardment of Ba metal did not give this period at all.

The 2.5-minute Ba period[2] was prepared by irradiating Ba with Li+H^2 neutrons and was proved to be chemically Ba.

The 87 ± 1-minute Ba period[3] was strongly activated by deuteron bombardment of Ba and gave a β-ray upper limit of about 1 MV and a gamma-ray of about 0.6 MV according to absorption coefficients in lead and copper. There are no very strong soft "monochromatic" electrons with this period.

Cs bombarded with deuterons or neutrons consistently gave a 3-hour$\pm$10-minute period rather than the previously reported period[4,5,6] of 1.5 hours. The normal

β-ray absorption spectrum indicates an upper limit of about 1 MV. Little if any gamma-radiation is associated with this period. It is more strongly activated with slow than with fast neutrons, and was proved to be chemically Cs.

A long period (20 ± 1 month) isotope,[7] chemically identified as Cs and apparently isomeric with the 3-hour Cs^{134}, was prepared by neutron or deuteron bombardment of Cs. Its normal β-ray spectrum has an upper limit of 0.9 MV, and there is fairly strong gamma-radiation.

Cs^{132} evidently has a very short period, a very long period, or one close to three hours, as nothing new appeared with fast neutron bombardment.

We are grateful to Professor E. O. Lawrence for his cooperation in these experiments, and to the Research Corporation and the Rockefeller Foundation for financial assistance.

D. C. KALBFELL

Radiation Laboratory,
University of California,
Berkeley, California,

R. A. COOLEY

Gates and Crellin Laboratories,
California Institute of Technology,
Pasadena, California,
June 3, 1940.

[1] D. C. Kalbfell, Phys. Rev. **54**, 543 (1938).
[2] Pool, Cork and Thornton, Phys. Rev. **52**, 239 (1937).
[3] M. L. Pool and J. M. Cork, Phys. Rev. **51**, 1010 (1937).
[4] E. Amaldi *et al.*, Proc. Roy. Soc. **A149**, 522 (1935).
[5] McLennan, Grimmet, and Read, Nature **135**, 505 (1935).
[6] Latimer, Hull and Libby, J. Am. Chem. Soc. **57**, 781 (1935).
[7] Alexeeva, Comptes rendus USSR **18**, 553 (1938).

Photo-Fission of Uranium and Thorium

We have observed fission recoils from uranium and thorium produced by γ-rays from CaF_2 and AlF_3 targets bombarded with protons. A rough estimate of the cross section, based on our data, gives 10^{-26} cm^2 for the photo-fission cross section in comparison with the theoretical estimate of 10^{-27} cm^2 given by Bohr and Wheeler.[1]

A beam of 0.5 microampere of analyzed protons of 2 to 3 Mev energy was used to bombard CaF_2 and AlF_3. With Ca and Al targets, no fissions were observed, indicating the absence of neutron fissions. Although a few neutrons are obtained when Ca is bombarded with protons, these were found to be too few to give fissions. Even fewer neutrons were found from proton bombardment of CaF_2 when a BF_3-filled ionization chamber was used to detect the neutrons. No appreciable decrease in the fission rate was observed with 4 cm of paraffin between the target (γ-ray source) and the ionization chamber containing uranium. This amount of paraffin was shown to cut down the fission rate by one-half when neutrons from $Li(p,n)$ were used instead of γ-rays. The fission rate was cut down by a lead absorber by roughly the right amount for high energy γ-rays. Further indication that the fissions are due to γ-rays is the observed proportionality of fission rate to high energy γ-ray intensity as this is increased by a factor of 5 on raising the proton beam energy from 2 to 3.2 Mev. Below 2 Mev the fission rate was too low for observation.

With 2.9-Mev protons, the observed fission rate in uranium was about one fission per 3×10^{13} protons hitting CaF_2. The γ-ray intensity measured by a Geiger counter 5 feet away and shielded with 1 inch of lead was about 150 counts per fission. Assuming the counter efficiency to be 2 percent[2] and allowing for scattering and absorption in the lead shield around the counter, we estimate a high energy γ-ray yield from CaF_2 of 10^8 γ-quanta per 3×10^{13} protons or per fission. It is to be noted that this estimate of 3 quanta per 10^6 protons at 2.9 Mev is higher than is obtained by taking the value of 1.2 γ-quanta per 10^9 protons[3] at 1.0 Mev and multiplying by 60, our observed factor of increase in intensity from 1 Mev to 2.9 Mev. This suggests that the above value for $F(p,\gamma)$ yield at 1.0 Mev and also the $Li(p,\gamma)$ cross section from which it was derived may be too low.

The fractional solid angle subtended by the uranium is 0.07, which gives about 7×10^6 γ-quanta passing through the uranium per fission. Assuming an effective thickness of 3 mg/cm^2 for the uranium whose fission recoils would be counted in the ionization chamber, we obtain about 2×10^{-26} cm^2 for the photo-fission cross section for fluorine γ-rays. The effect in thorium is roughly equal in intensity. Previous attempts[4] to observe photo-fission have not given positive results.

It has been suggested that photo-fission be referred to as "phission" to distinguish it from neutron fission.

R. O. HAXBY*
W. E. SHOUPP*
W. E. STEPHENS*
W. H. WELLS

Westinghouse Research Laboratories,
East Pittsburgh, Pennsylvania,
May 28, 1940.

* Westinghouse Research Fellow.

[1] N. Bohr and J. A. Wheeler, Phys. Rev. **56**, 426 (1939).
[2] J. V. Dunworth, Rev. Sci. Inst. **11**, 167 (1940).
[3] M. S. Livingston and H. A. Bethe, Rev. Mod. Phys. **9**, 316 (1937).
[4] Roberts, Meyer and Hafstad, Phys. Rev. **55**, 417 (1939); Heyn, Aten and Bakker, Nature **143**, 516 (1939).

Accurate Solution of the Thomas-Fermi-Dirac Equation.

The Thomas-Fermi-Dirac equation

$$d^2\psi/dx^2 = x[\beta+(\psi/x)^{\frac{1}{2}}]^3,$$

$\beta=(3/32\pi^2)^{\frac{1}{3}}Z^{-\frac{1}{3}}$ with the boundary condition $\psi(0)=1$, has been hitherto solved for $Li(Z=3)$, $Na(Z=11)$, $Ar(Z=18)$, $Cu(Z=29)$, $Kr(Z=36)$ and $Xe(Z=54)$,[1] expanding ψ in series for small values of x with an assumed value of the initial slope, and integrating numerically from there out. The most important case is that where ψ curve becomes tangent to the x axis. In this case, however, the numerical integration is very sensitive to small errors, as well as to small changes in the initial slope, so that it is very difficult to determine accurately the tangent point X_0 and consequently the value of the initial slope $-B_0$. By carrying out the calculation in the reversed direction to the above we were able to determine the relation of the tangent point X_0 to the atomic number Z as follows. We expanded for a chosen element whose atomic number is Z' in a series in the neighborhood of an assumed tangent point X_0', and integrated numerically from there out towards the ψ axis. This integration curve meets the ψ axis with a finite angle, not tangentially nor rectangularly, so that the

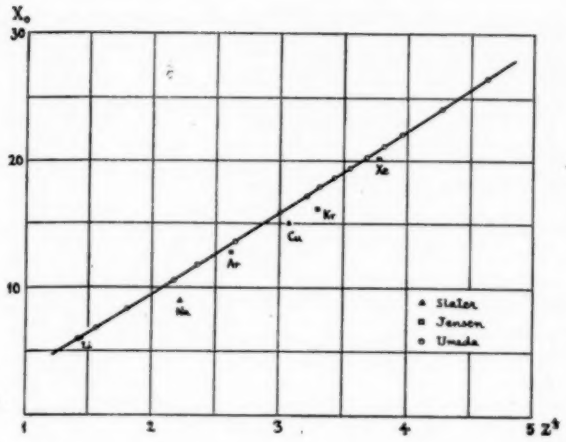

FIG. 1. Tangent point X_0 as function of cube root of atomic number Z.

initial point ψ_0 as well as the initial slope ψ_0' can be determined accurately as desired. Of course, this integration curve does not satisfy the condition $\psi(0)=1$. Dimensional consideration shows that the equation admits the following substitution with any constant parameter a:

$$\psi \to \frac{\psi}{a}, \quad x \to a^{\frac{1}{3}}x, \quad \psi' \to \frac{\psi'}{a^{4/3}}, \quad \beta \to \frac{\beta}{a^{\frac{1}{3}}}, \quad Z \to aZ.$$

Putting $a=\psi_0$ we get an exact solution satisfying the condition $\psi(0)=1$ for the element of the atomic number $Z=\psi_0 Z'$ which has the tangent point at the distance $X_0=\psi_0^{\frac{1}{3}}X_0'$ and the initial slope of the exact value $-B_0=\psi_0'/\psi_0^{4/3}$. The tangent point X_0 is plotted in Fig. 1 as the function of $Z^{\frac{1}{3}}$. The curve is approximately a straight line. Fortunately, the initial slope $-B_0$ satisfies the practically linear dependency to the parameter β, as stated by Slater and Krutter.[2] But, both curves deviate slightly from a straight line for small values of Z.

We will publish shortly in *Journal of the Faculty of Science of the Hokkaido Imperial University* the detailed numerical table of the solution for every existing element and the values of various physical quantities, computed by the use of the obtained accurate solutions.

In conclusion the author wishes to express his sincere thanks to Professor Slater and Professor Jensen for the kindness to send him the detailed numerical tables of their results. He is also grateful to Dr. Nishina in Tokyo and to Professor Matsukuma in Sendai for their continued interest and much valuable advice. Further, he is much indebted to Mr. T. Sato in Fukuoka and to Mr. S. Nagai in Muroran for their kind help in the calculation. The financial support of The Japan Society for Promotion of Scientific Research and of The Department of Education is gratefully acknowledged.

KWAI UMEDA

Department of Physics,
Hokkaido Imperial University,
Sapporo, Japan,
May 17, 1940.

[1] Li, Na, Cu: J. C. Slater and H. M. Krutter, Phys. Rev. **47**, 559 (1935). Ar: H. Jensen, Zeits. f. Physik **110**, 277 (1938); K. Umeda, unpublished. Kr, Xe: H. Jensen, Zeits. f. Physik **110**, 277 (1938).
[2] J. C. Slater and H. M. Krutter, reference 1.

Photographic Reversal

The interesting letter from J. E. Nafe and G. E. M. Jauncey[1] "The Cause and Removal of Photographic Reversal" cites N. F. Mott[2] as propounding the hypothesis that "photographic reversal (or solarization) produced by light is due to the reaction of bromine atoms released from the crystal lattice during the process of latent image formation with the silver of the concentration specks which makes a coating over the grain." The view that bromine released from relatively interior parts of the grain causes reversal by recombination with external latent image silver is known in photographic theory as the "regression theory of reversal" and was first definitely formulated by Lüppo-Cramer.[3] This "regression" theory long antedates the Gurney-Mott theory of latent image formation, and does not appear either to support this latter—whether reversal be effected by blue light or by x-rays—nor to contradict it, although the x-ray reversal curve shown by Baltzer and Nafe[4] does not exhibit the retardation which Mott[2] anticipated.

S. E. SHEPPARD

Research Laboratories,
Eastman Kodak Company,
Rochester, New York,
June 14, 1940.

[1] J. E. Nafe and G. E. M. Jauncey, Phys. Rev. **57**, 1048–49 (1940).
[2] N. F. Mott, Phot. J. **78**, 286 (1938).
[3] Lüppo-Cramer, Phot. Korr. (1905), p. 259; *Photogr. Probleme* (Halle, 1907), p. 338, *et seq.*; cf. also J. M. Eder, *Ausführl. Handbuch d. Phot.* **2**, Part 1, 586 (1927).
[4] O. J. Baltzer and J. E. Nafe, Phys. Rev. **57**, 1048 (1940).

Spectra of Highly Ionized Argon

Previous attempts to excite the spectra of high stages of ionization in the rare gases, either by electrodeless or condensed discharges, have failed to produce results beyond the fourth or fifth stage of ionization. Boyce[1] has located two multiplets in A V near 710A and 830A, but states that lines from A VI were definitely absent. One multiplet in Kr IV near 840A has been identified.[2] Paul[3] has reported the excitation of Ne III and IV (previously observed by Boyce[4]) and has tentatively identified two multiplets as radiations from Ne V.

A very simple and effective method for the excitation of the higher stages of ionization of the rare gases has recently been developed in this laboratory. It is particularly convenient in that it requires only slight modifications of the source chamber regularly used for solid or cored electrodes. A small hole is drilled centrally into the aluminum or carbon lower electrode. A fine bronze capillary connected to a gas reservoir feeds into this hole through the base of the electrode. In this way the gas can be fed directly into the spark gap. The gas in the reservoir is kept at a pressure of from 20 to 50 mm of Hg, and the flow is adjusted to a convenient rate (in the case of argon this was roughly one cc per minute) by means of a needle valve. The pumping speed is adjusted so as to remove the gas rapidly enough to prevent the formation of an arc discharge.

The spectra were photographed in the 21-foot, grazing-incidence vacuum spectrograph, which covers the range

TABLE I. *Classified argon lines.*

INT.	λ(VAC.)	ν(CM⁻¹)	STAGE OF IONIZ.	CLASSIFICATION
3	596.69	167,590	VI	$3s^23p\ {}^2P_{3/2}-3s3p^2\ {}^2S_{1/2}$
2	588.93	169,800	VI	${}^2P_{1/2}\quad {}^2S_{1/2}$
2	555.65	179,970	VI	${}^2P_{3/2}\quad {}^2P_{1/2}$
10	551.36	181,370	VI	${}^2P_{3/2}\quad {}^2P_{3/2}$
6	548.91	182,180	VI	${}^2P_{1/2}\quad {}^2P_{1/2}$
3	544.72	183,580	VI	${}^2P_{1/2}\quad {}^2P_{3/2}$
4	527.70	189,500	V	$3s^23p^2\ {}^3P_2\ -3s3p^3\ {}^3S_1$
0	526.87	189,800	VIII	$3p\ {}^2P_{3/2}-\ 3d\ {}^2D_{3/2}$
4	526.45	189,950	VIII	${}^2P_{3/2}\quad D_{5/2}$
2	524.19	190,770	V	$3s^23p^2\ {}^3P_1\ -3s3p^3\ {}^3S_1$
1	522.08	191,540	V	${}^3P_0\quad {}^3S_1$
3	519.43	192,520	VIII	$3p\ {}^2P_{1/2}-\ 3d\ {}^2D_{3/2}$
10	479.39	208,600	VII	$3s3p\ {}^3P_2\ -3s3d\ {}^3D_3$
6	475.65	210,240	VII	${}^3P_1\quad {}^3D_2$
3	473.93	211,000	VII	${}^3P_0\quad {}^3D_1$
4	260.33	384,130	VIII	$3d\ {}^2D_{5/2}-\ 3f\ {}^2F_{7/2}$
2	260.25	384,250	VIII	${}^2D_{3/2}\quad {}^2F_{5/2}$
4	250.95	398,480	VII	$3s3p\ {}^3P_2\ -3s4s\ {}^3S_1$
2	249.89	400,170	VII	${}^3P_1\quad {}^3S_1$
1	249.38	401,000	VII	${}^3P_0\quad {}^3S_0$
4	230.86	433,160	VIII	$3p\ {}^2P_{3/2}-\ 4s\ {}^2S_{1/2}$
2	229.43	435,860	VIII	${}^2P_{1/2}\quad {}^2S_{1/2}$
5	192.63	519,120	VII	$3s3p\ {}^3P_2\ -3s4d\ {}^3D_3$
3	192.04	520,720	VII	${}^3P_1\quad {}^3D_2$
2	191.76	521,490	VII	${}^3P_0\quad {}^3D_1$

from 30A to 680A. Twenty thousand sparks (at the rate of about 100 sparks per minute) gave a very satisfactory spectrogram.

In the argon spectra lines arising from argon IV, V, VI, VII, and VIII have been identified. Preliminary results for some of the stronger lines in the spectra are listed in Table I. In all cases the frequencies agree very closely with those predicted from the laws governing isoelectronic sequences.

A more complete report on the argon spectra and one on the neon and krypton spectra will be ready soon.

W. L. PARKER
L. W. PHILLIPS

Department of Physics,
University of Illinois,
Urbana, Illinois,
May 31, 1940.

[1] J. C. Boyce, Phys. Rev. **48**, 396 (1935).
[2] J. C. Boyce, Phys. Rev. **47**, 718 (1935).
[3] F. W. Paul, Phys. Rev. **56**, 1067 (1939).
[4] J. C. Boyce, Phys. Rev. **46**, 378 (1934).

Concentration of Isotopes by Thermal Diffusion: Rate of Approach to Equilibrium

The purpose of this note is to make some additions and corrections to an article[1] of the same title which appeared in a recent issue of this journal. The equation numbers given below refer to this article.

(1). In Eq. (10) we used the expression for the transport, τ_1, which was derived by Furry, Jones and Onsager[2] for the stationary condition. The detailed justification for its use in the nonequilibrium case follows. We want a solution of Eq. (4), which may be written in the form

$$\frac{\partial(\rho c_1)}{\partial t}=-\rho v\frac{\partial c_1}{\partial z}+\rho D\frac{\partial^2 c_1}{\partial z^2}+\frac{\partial}{\partial x}\left[\rho D\left(\frac{\partial c_1}{\partial x}-\frac{\alpha c_1 c_2}{T}\frac{\partial T}{\partial x}\right)\right], \quad (4')$$

subject to the boundary conditions (5) and (6):

$$c_1 v_{1x}=-D\left[\frac{\partial c_1}{\partial x}-\frac{\alpha c_1 c_2}{T}\frac{\partial T}{\partial x}\right]=0 \quad (5')$$

at $x=0$ and $x=d$, and

$$\int_0^d \rho v(x)dx=0. \quad (6)$$

Let us integrate Eq. (4) with respect to x from $x=0$ to $x=d$. Making use of (5), we find:

$$\int_0^d \rho\frac{\partial c_1}{\partial t}dx=\int_0^d \rho D\frac{\partial^2 c_1}{\partial z^2}dx-\int_0^d \rho v\frac{\partial c_1}{\partial z}dx. \quad (a)$$

In the integral on the left-hand side and in the first integral on the right-hand side we may replace c_1 by its mean value across the column without appreciable error. The fractional variation of c_1 with respect to x is of the order $\alpha\Delta T/T$, so that the error involved is certainly less than this amount. The last integral would vanish on account of (6) if c_1 were independent of x, so that it is not possible to use the mean value here. It is, of course, just the variation of the concentration across the column which gives rise to the transport.

The integral may be evaluated as follows. Let[3]

$$G(x)=\int_0^x \rho v dx; \quad (b)$$

then

$$G(o)=G(d)=0. \quad (c)$$

An integration by parts gives:

$$-\int_0^d \rho v\frac{\partial c_1}{\partial z}dx=\int_0^d G(x)\frac{\partial^2 c_1}{\partial x\partial z}dx. \quad (d)$$

The value of $\partial^2 c_1/\partial x\partial z$ may be obtained from Eq. (4) which, after integration with respect to x, may be written

$$\rho D\frac{\partial c_1}{\partial x}=\rho D\frac{\alpha c_1 c_2}{T}\frac{\partial T}{\partial x}+\int_0^x\left\{\rho' v'\frac{\partial c_1'}{\partial z}+\rho'\frac{\partial c_1'}{\partial t}-\rho' D'\frac{\partial^2 c_1'}{\partial z^2}\right\}dx'. \quad (e)$$

The prime indicates that the various quantities in the integrand are functions of x'. Differentiating (e) with respect to z, we find

$$\frac{\partial^2 c_1}{\partial x\partial z}=\frac{\alpha}{T}\frac{\partial T}{\partial x}\frac{\partial}{\partial z}(c_1c_2)+\frac{1}{\rho D}\int_0^x\left\{\rho' v'\frac{\partial^2 c_1'}{\partial z^2}+\rho'\frac{\partial^2 c_1'}{\partial z\partial t}-\rho' D'\frac{\partial^3 c_1'}{\partial z^3}\right\}dx'. \quad (f)$$

The transport equation is obtained by substituting (f) into (d) and then (d) into (a). After multiplying through by the mean circumference, B, the resulting equation may be expressed in the following form:

$$B\int_0^d \rho\left(\frac{\partial}{\partial t}-D\frac{\partial^2}{\partial z^2}\right)\left(1-I(x)\frac{\partial}{\partial z}\right)c_1 dx=-\frac{\partial}{\partial z}\left(Hc_1c_2-K\frac{\partial c_1}{\partial z}\right), \quad (g)$$

where $I(x)$ is introduced by an integration by parts;

$$I(x)=\int_0^x\frac{G(x')}{\rho' D'}dx', \quad (h)$$

and H and K are the constants designated by the same letters by Furry, Jones and Onsager.[4]

$$H=-B\int_0^d \alpha\frac{G(x)}{T}\frac{\partial T}{\partial x}dx, \qquad \text{(i)}$$

$$K=B\int_0^d \frac{[G(x)]^2}{\rho D}dx. \qquad \text{(j)}$$

Eq. (g) is the same as Eq. (10) except for the term $I(x)\partial/\partial z$. We will now estimate the magnitude of this term. In the actual operaion of the column, the maximum value of $\partial \log c_1/\partial z$ will be of the order H/K. The fractional error involved in the neglect of the term will therefore be of the order

$$(H/Kd)\int_0^d I(x)dx=(H/Kd)\int_0^d [\times G(x)/\rho D]dx. \qquad \text{(k)}$$

With the substitution of the expressions (i) and (j) for H and K, it can be seen that the error is of the order $\alpha\Delta T/T$. In most cases this will be a fraction of one percent.

Strictly, we have shown only that the derivative

$$\frac{\partial \tau_1}{\partial z}\leqq\frac{\partial}{\partial z}(\tau_1)_{\text{FJO}}.$$

By an analysis similar to that given above it can be shown that the error involved in the use of the stationary value for τ_1 itself is of the same order of magnitude.

(2). The discussion of the roots of the equation $F(p)=0$ (Eq. (38)) is not very clear in the article. The roots are most easily obtained in terms of γ:

$$p_k=-(AH/2\rho a)(1-\gamma_k^2),$$

where the γ_k are roots of Eq. (47). In deriving (47) from (38) we have, among other things, multiplied through by γ. The root $\gamma=0$ is therefore not to be included. If γ_k is a root of (47), so is $-\gamma_k$. These two roots correspond to a *single* root p_k of Eq. (38). Only one of them should be included in the sum in Eq. (49).

(3). There are two misprints in Eq. (49). The correct equation is:

$$c_1/c_1^0=Ke^{2Az}+\sum_k \frac{2(R+(H/Mp_k))(e^{AL}-\gamma_k\sinh\gamma_kAL-\cosh\gamma_kAL)-4\cosh\gamma_kAL}{(1-\gamma_k^2)(\gamma_k^{-1}R\sinh\gamma_kAL+\gamma_k^{-2}\cosh\gamma_kAL-AL\gamma_k^{-1}\operatorname{csch}\gamma_kAL)}$$
$$\times[\gamma_k^{-1}\sinh\gamma_kA(z-L)+\cosh\gamma_kA(z-L)]\exp[A(z-L)+p_kt]. \qquad (49)$$

The author wishes to thank Professor W. H. Furry for helpful correspondence about some of the above points.

J. BARDEEN

Department of Physics,
University of Minnesota,
Minneapolis, Minnesota,
June 13, 1940.

[1] J. Bardeen, Phys. Rev. **57**, 35 (1940).
[2] W. H. Furry, R. C. Jones, and L. Onsager, Phys. Rev. **55**, 1083 (1939). This paper will be referred to as FJO.
[3] Our $G(x)$ differs from the function G introduced by FJO by a factor $\rho D/Q^2\lambda$.
[4] Cf. Eqs. (24) and (25) of FJO. Their expression for the transport, τ_1, is given by (23). Our treatment justifies the method used by FJO for the inclusion of the effect of longitudinal diffusion.

Proceedings of The Ohio Section of the American Physical Society

Minutes of the Ohio State University Meeting, May 9–11, 1940

THE second meeting of the Ohio Section of the American Physical Society was held at Ohio State University, Columbus, Ohio, on May 9–11, 1940, as a joint meeting with the Ohio Academy of Science, which was celebrating its founding. There was a program of invited papers representing all branches of science. The addresses of particular interest to the physics section were:

Sound Patterns.—Harvey Fletcher, *Bell Telephone Laboratories.*
The Development of High Voltage for the Production of Neutrons and Artificial Radioactivity.—E. U. Condon, *Westinghouse Research Laboratories.*
Comparative Study of Neutron- and X-Radiation upon Biological Tissues in the Cancer Problem.—Isadore Lampe, *University of Michigan.*
Industry and Science.—Charles F. Kettering, *General Motors Research Corporation.*
Protein Molecule Structure.—Edward Mack, *Battelle Memorial Institute.*
Cancer-Producing Hydrocarbons.—M. S. Newman, *Ohio State University.*
Chemistry Through the Microscope.—H. S. Booth, *Western Reserve University.*

In addition to the invited papers, a centralized exhibit of ninety-nine projects, numerous fixed exhibits by the various science and engineering departments at Ohio State University and a tour of a neighboring industrial institution were available to members during the three-day program.

At the annual business meeting of the Ohio Section, held following a luncheon on May 10th, the following officers were elected for the year: Chairman, Paul E. Martin, Muskingum College; Vice Chairman, W. E. Forsythe, General Electric Company; Secretary-Treasurer, Richard H. Howe, Denison University.

It was announced that a symposium on "Rubber" will be held at Akron, Ohio, on October 12, 1940. This is to be the first symposium of a series based on Ohio's industries, one of which will be arranged each year by the Ohio Section.

Richard H. Howe, *Secretary-Treasurer*